SURFACE MONOLAYER INITIATED POLYMERIZATION (SMIP): A NOVEL MEANS OF FABRICATING SUB - 100 NM FEATURES

A Thesis
Presented to
The Academic Faculty

by

Kendra M. McCoy

In Partial Fulfillment
of the Requirements for the Degree
Doctor of Philosophy in Chemical Engineering

Georgia Institute of Technology
April 2004

SURFACE MONOLAYER INITIATED POLYMERIZATION (SMIP): A NOVEL MEANS OF FABRICATING SUB 100-NM FEATURES

Approved by:

Clifford L. Henderson, Chair

W. Brent Carter

Dennis W. Hess

Peter J. Ludovice

Laren M. Tolbert

DATE APPROVED: 12 April 2004

ACKNOWLEDGEMENTS

I would like to thank all the people that have contributed to the information presented in this dissertation and to those who have made the past 5 years, 6 months, and 21 days so enjoyable. I would like to express sincere gratitude to my advisor Professor Clifford L. Henderson for his guidance. His extensive knowledge and drive has served as a constant source of inspiration (and sometimes perspiration) throughout my stay at Georgia Tech. I would also like to thank the other members of my thesis committee: Professor W. Brent Carter, Professor Dennis Hess, Professor Peter Ludovice, and Professor Laren Tolbert for their support and useful advice. I must also acknowledge Patrik Dahlqvist and Patrick Bjöörn (also known as Patrik^2) for their helpful advice with evaluating QCM-D data. Without their collaboration, much of this work would not have been possible.

I am fortunate to have worked with a wonderful group of graduate students, and I would like to thank all the past and present members of the Henderson, Hess, and Tolbert Research Groups for their helpful discussions and advice. Many thanks are due to Dr. Xiaohua Chen, a former member of the Tolbert Research Group, for showing me how to synthesize the initiators used in this study. I would also like to thank Dr. Kristi Chavez, former member of the Hess research group, for showing me how to use the XPS system. Finally, I would like to thank Augustin Jeyakumar who worked with me on generating electron beam patterns.

I would like to thank all of the other friends I have made in Atlanta. In addition to those people I've met at Georgia Tech, I am truly blessed to have met so many

delightfully interesting people while practicing Tang Soo Do, attending book signings, and eating at vegetarian restaurants. I appreciate all of the interesting conversations we've had, and I know I will miss them very much. I would especially like to thank Sonja and Rico Blakely, Ellen and Jason Byrdsell, Oluwafemi Ogunşola, and Asha Rodney for their wonderful friendship. I would also like to thank my good friends from Fort Washington, Maryland with whom our bond becomes stronger as our physical distance becomes more and more separated. While living in Atlanta, Fort Washington, New Haven, Portland, and San Diego, we've maintained a bond that has continually grown since we were in the 9th grade. I am truly grateful for that. I'm never afraid to live in a city in which I don't know anyone because I know that they will be visiting, calling, or writing me sometime soon. I would also like to my family for their support, love, and encouragement. I would especially like to thank my Aunt Theresa for being my number one fan. Even when I feel I've failed a task, she is always there to make me feel like a superstar. Finally I would like to thank my parents for their unending support, love, friendship, and encouragement. Sometimes, I reflect on my near perfect childhood and am amazed by the sacrifices they made on my behalf. I pray that I will be half the parents they are, and I hope that I am living a life of which they are proud.

TABLE OF CONTENTS

LIST OF TABLES

LIST OF FIGURES

LIST OF ABBREVIATIONS

AFM	Atomic Force Microscopy
ATR-IR	Attenuated Total Reflectance Infrared Spectroscopy
C_0	Bulk Concentration
C_f	Quartz Crystal Constant
CD	Critical Dimension
D_f	Depth of Focus
DESIRE	Diffusion Enhanced Silylated Resist
DNQ	Diazonaphthoquinone
DRAM	Dynamic Random Access Memory
DUV	Deep Ultraviolet
E	Energy
Ea	Activation Energy
E_F	Fermi Level
ESCA	Electron Spectroscopy for Chemical Analysis
E_V	Vacuum Energy Level
FWHM	Full Width Half Maximum
ϕ	Work Function
Γ	Graft Density
HMDS	Hexamethyldisilazane
IC	Integrated Circuit
ITRS	International Technology Roadmap for Semiconductors
k	Process/rate Constant
λ	Wavelength
n	Overtone Number
NA	Numerical Aperture
NGL	Next Generation Lithography
NMR	Nuclear Magnetic Resonance
ODS	Octadecylmethyldichlorosilane
OMS	Octadecyldimethylchlorosilane
OTS	Octadecyltrichlorosilane
PCM	Portable Conformal Mask
PHI	Physical Electronics
QCM-D	Quartz Crystal Microbalance with Dissipation
R	Resolution
RIE	Reactive Ion Etching
SAM	Self-Assembled Monolayer
Si-CARL	Silicon Chemical Amplification of Resist Lines
SMIP	Surface Monolayer Initiated Polymerization
TLI	Thin Layer Imaging
TSI	Top Surface Imaging
UV	Ultraviolet
XPS	X-ray Photoelectron Spectroscopy

SUMMARY

The speed of microelectronic devices is controlled largely by the size of the smallest feature in the device, which is the transistor gate. In order to create faster devices, the size of this transistor gate must shrink. Microlithography is the method used to define patterns in semiconductor devices, and it is optimized periodically to create smaller feature sizes. It is a subtractive process that relies on the selective removal of material from a photosensitive polymeric film called photoresist. This photoresist is exposed to patterned ultraviolet radiation that changes the local solubility of the film which allows for the creation of relief patterns in the resist using an appropriate developing solvent. Decreasing the wavelength of the ultraviolet light used to expose the patterns is the primary method for increasing the resolution of (i.e. decreasing the minimum feature size that can be printed by) the process and advancing microlithography . There are a number of challenges associated with decreasing the exposure wavelength for conventional lithographic processes. First of all, the polymeric films must be relatively transparent at the exposure wavelength in order to allow light to propagate through the entire thickness of the film. Secondly, there is a limit in the thickness of the photoresist films that can be used which in turn limits the etch resistance of the film. In fact, the issues concerning etch resistance and transparency are generally in opposition. This makes the design of photoresist platforms for future lithographic applications very difficult. Therefore, to overcome these limitations, we are developing an unconventional approach to microlithography. In our approach, entitled Surface Monolayer Initiated Polymerization (SMIP), polymer structures are formed on a surface by polymerizing a monomer in a patterned fashion using a self-assembled monolayer that can be locally activated to

initiate the reaction. This process has been demonstrated by creating patterned polystyrene films on native silicon dioxide surfaces. In these initial studies, it took more than one day to create these features. This is unacceptable for a lithographic application. The kinetics of all the processes involved in making these patterned layers is described. Along with these rate constants, means of optimizing these rates are also presented. Additionally, the patterns grown in these initial studies exhibited poor uniformity at small feature sizes. Methods of optimizing the patterns formed are also presented.

CHAPTER 1

A BRIEF INTRODUCTION TO MICROLITHOGRAPHY

1.1 Introduction

Jack Kilby invented the integrated circuit (IC) in 1959. When commenting on the widespread use and impact of his Nobel Prize winning invention, he said that "the reality of what people have done with integrated circuits has gone far beyond what anyone, including myself, imagined possible at the time."[1] No one thought there would be such an explosion in the use of the integrated circuit (IC) over the past 45 years. ICs are an integral part of modern society. Automobiles emit fewer pollutants because of IC systems. Millions of people are connected via the internet, and wireless communication gives people easy access to each other and to vital information all over on the planet. The pace of growth of ICs has been phenomenal over the past 40 years. The early ICs that were invented in late 1950s were comprised of about one dozen electrical components. By 1970, ICs had around 10,000 components, and more than 100 million components are on a chip today. This pace of growth has been strictly following Moore's Law. Moore's Law was stated in 1965 when Gordon Moore, future chairman and chief executive of Intel Corporation at the time, stated that the number of devices on a chip would double every year.[2] This law was later revised to predict that the number of devices per chip would double every 18 to 24 months. Today the size of integrated circuits have continued to shrink according to Moore's Law; however, fundamental physical limits are being reached in which conventional means of creating small devices can no longer support this progression. For example, about 1000 electrons are needed to switch a single transistor

today. It is projected that in 2010, only 100 electrons will be needed to accomplish this task. The 2010 projection assumes higher dielectric constant materials will be used in the production of transistors. If this does not happen, then geometric scaling of devices would reduce the count to 10 electrons in 2010 and 1 electron will be needed to switch a transistor by 2020.[1] This 1 electron device obviously represents a fundamental physical limit for classical transistors. To reach this point, routes to overcoming other physical limits imposed by the materials and processes used to fabricate such a transistor must be developed.

It is easy to see how quickly this industry is approaching fundamental physical limits by charting the progression of one type of chip. Since memory chips have essentially had the same functionality for many years, the simplest means of analyzing the progression of ICs is to chart the progression of memory devices. The progression of dynamic random access memory (DRAM) devices is shown on the next page.[3] This progression begins with the 4 kilobit DRAM devices built since the mid 1970s and projects to the 16 gigabit DRAM that will be manufactured within the next few years. Each navy blue box represents a DRAM device. There are two numbers in the box that describe the device. The first is the size of the device. The second is the minimum feature size that was used to print each device. For example, the upper left corner shows the details of the 4 kilobit DRAM. To make this device, printing a 7000 nanometer (nm) transistor gate was required. This second number highlights the impact microlithography has had on this progression. Microlithography is the process of producing patterns on semiconductors for use as integrated circuits.[4] The process involves creating physical relief patterns in a photochemically active film called a photoresist using ultraviolet (UV)

light, and subsequently using this photoresist relief pattern as a protective stencil for creating patterns in the underlying substrate using various etch methods.

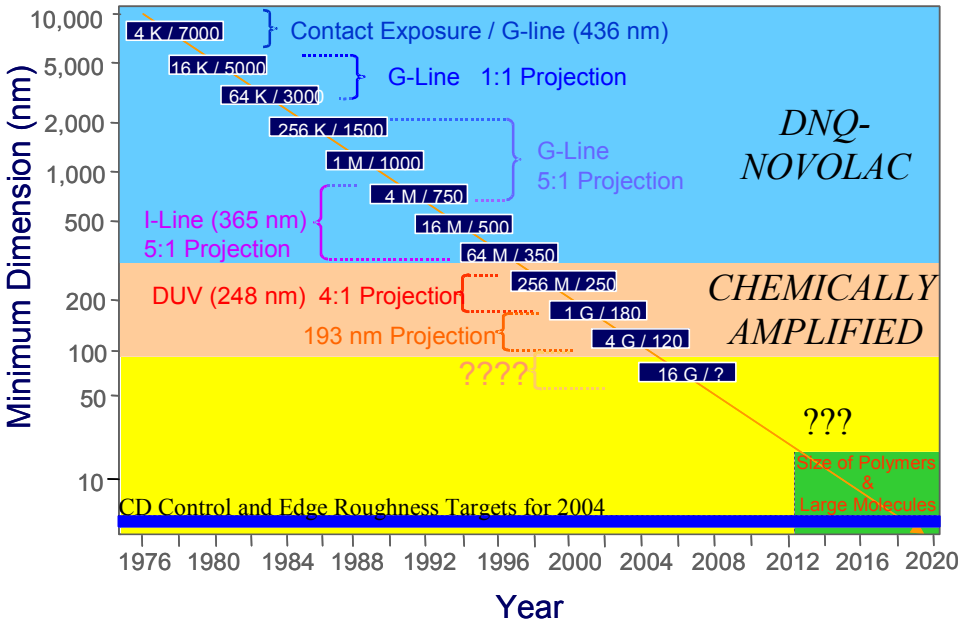

Figure 1.1: DRAM technology progression

The bracketed sections of the graph show the exposure technologies that were used to create a particular DRAM device. For example, contact exposure of mask with 436 nanometer (nm) radiation was used to create a 4 kilobit DRAM. Historically, the chemistry of the resist was specifically designed for the exposure technology used. The colored panels display the types of resist that were coupled with the exposure technology to create minimum features in particular DRAM devices. This graph also shows that the minimum features (also called critical dimensions) are rapidly approaching molecular length scales. These length scales present a fundamental limit in producing minimum features via conventional microlithography. In fact, 2004 targets for control of the critical dimension (CD) lie within molecular length scales. It is highly uncertain whether

conventional means of creating these features will be amenable to making ICs in the near future.

1.2 Microlithography

The details of creating patterns in substrates via microlithography are pictured below. The process involves first spinning a photoresist onto a substrate. While single component resist materials are possible (e.g. poly(methyl methacrylate) as an electron beam resist), current commercial photoresists are typically a multi-component mixture of a polymer, a photoactive compound, and perhaps small amounts of other additives. The polymer, which makes up the vast majority of the resist (typically 65-98 wt% of dry film is polymer), serves to provide the photoresist with good film forming ability and etch resistance. The polymer however is not generally sensitive to radiation. The photoactive compound alternatively reacts upon exposure to radiation and creates a chemical change in the resist that permits formation of relief images.

The resist is then soft baked to remove casting solvent. Next, the resist is exposed to patterned UV light. Depending on the photochemistry of the resist, the exposed areas either become more soluble (positive tone) or less soluble (negative tone) in the developer - the solution used in the next step of the process to wash off the undesired areas of the resist film. Depending on the type of chemical change that occurred, either the exposed or unexposed areas of the photoresist wash away. The resulting patterned polymer is used as a protective stencil for subsequent etch. After etch, the resist is thoroughly removed from the surface, or stripped.

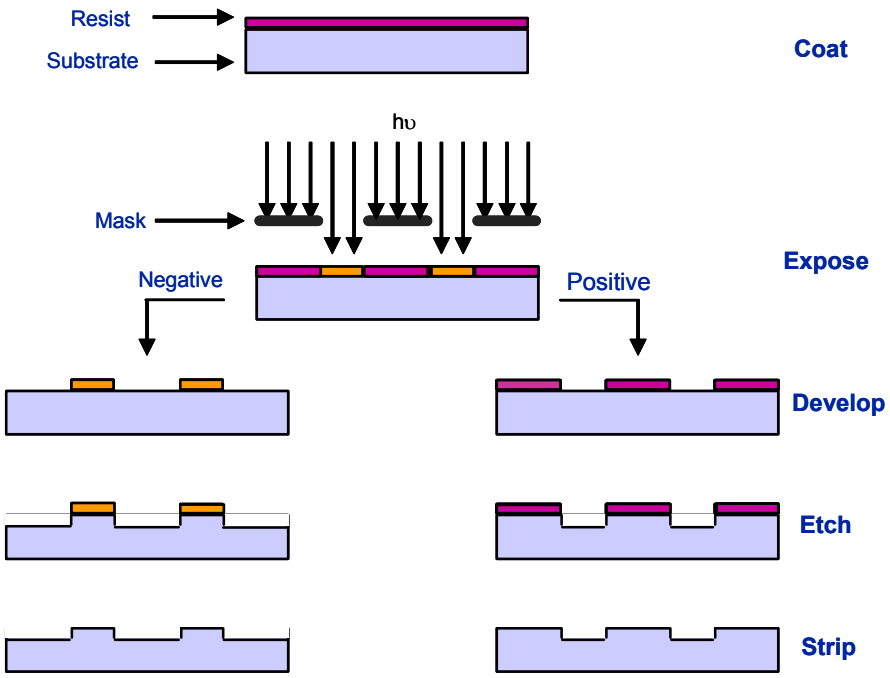

Figure 1.2: Schematic of conventional lithographic process

Improvements are made in microlithography primarily by shrinking the wavelength of light that is used to pattern the photoresist. By shrinking the wavelength of light used, the resolution of the process is improved. The resolution is the minimum feature size that can be printed in a photoresist with a given exposure technology. After a new exposure technology has been created, a resist is formulated to give the best resolution for the particular wavelength of light used. Currently, many exposure technologies are being evaluated to create features that are smaller than 100 nm.[5-10] These Next Generation Lithography (NGL) approaches involve using extreme ultraviolet radiation (wavelengths from 157 down to 13 nm)[6-8], x-ray radiation[7, 9], and electron beam radiation stemming from both high energy[5, 7] and low energy[7, 10] sources. These NGL technologies comprise the orange question mark region in the center of figure 1.1. Since it has not been decided which exposure technology will be used to produce the

critical features sizes for 16 gigabit DRAM devices, it is difficult to design the high resolution resists that are needed to make future devices. In addition to being amenable to producing high resolution features, resist materials must also demonstrate radiation sensitivity, excellent film forming properties, and significant resistance to chemicals that are used to etch the underlying substrate. In conventional resists, these imaging characteristics (resolution and radiation sensitivity) and mechanical properties (film forming characteristics and etch resistance) generally lie in opposition to one another. Resist formulations are traditionally optimized to accommodate all of these requirements. As devices dimensions continue to decrease, it is becoming increasingly difficult to optimize conventional resists to meet these demanding requirements.

1.3 Resist History

Negative tone resists were initially the primary resists used in the microelectronics industry. They were bis(arylazide)-rubber resists. These resists were two component systems that were comprised of a photoactive compound {bis(arylazide)} and a resin made of synthetic rubber. The photoactive compound provided the resist with its imaging and sensitivity requirements while the rubber provided the film forming properties and resistance to etch. A picture of the two components is shown in figure 1.3. Upon exposure to radiation, nitrogen is liberated from the azide to form a reactive intermediate that crosslinks with the rubber resin as shown in the bottom of figure 1.3.

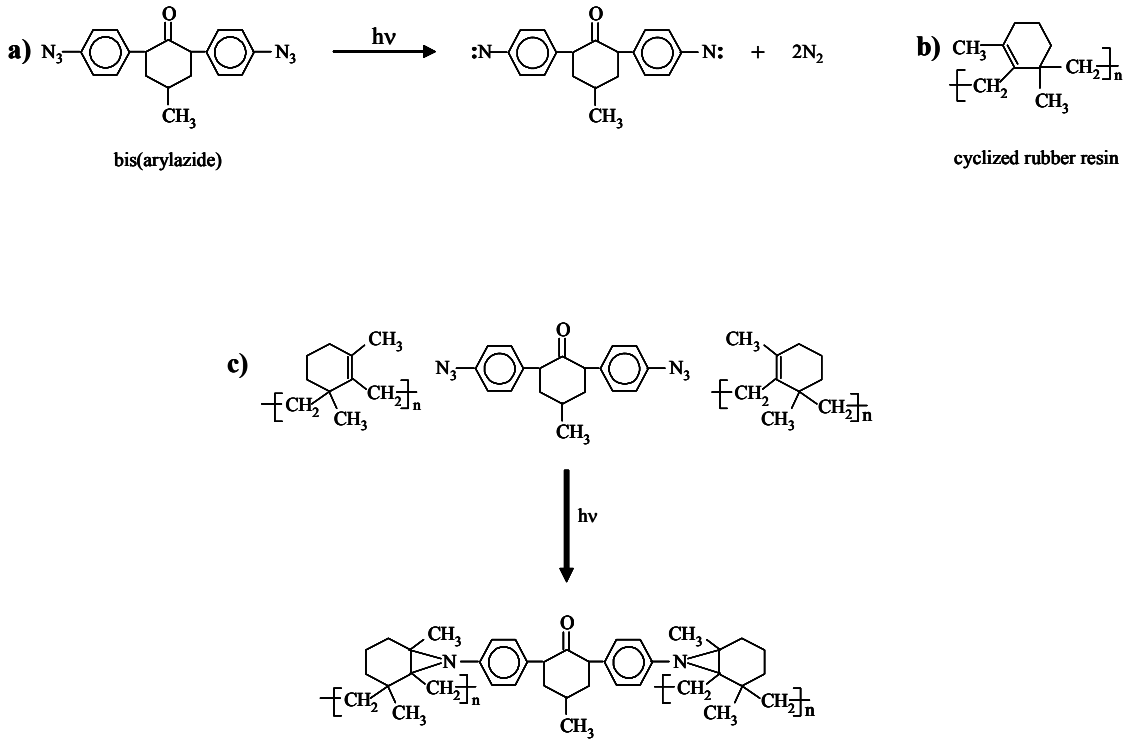

Figure 1.3: Bis(arylazide)-rubber systems. (a) bis(arylazide) sensitizer. (b) cyclized rubber resin. (c) method by which the azide reacts with the rubber**.**

These negative tone bis(arylazide) resists were replaced with positive tone diazonaphthoquinone-novolac (DNQ-novolac) resists systems. DNQ-novolac systems were able to provide higher resolution processes and better thermal stability than the previous systems. They also exhibited greater resistance to chemical etch than bis(arylazide) systems. Chemically, the resist contains a photoactive compound commonly called DNQ and a polymeric resin of novolac. The photosensitive DNQ exhibits sensitivity to ultraviolet radiation and can be used to produce high resolution patterns upon exposure to 436 nm and 365 nm radiation. This compound reacts upon exposure to light (and ambient water) to allow for an increase in solubility of the resist in developer. This developer is usually an aqueous base. The novolac resin provides the

photoresist with its excellent film forming properties and resistance to chemical etch. The structures of DNQ and novolac are given below in figure 1.4.

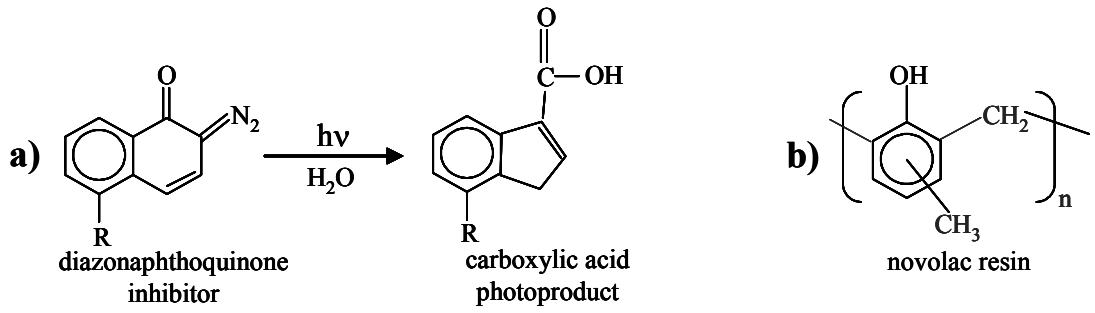

Figure 1.4: The two components of DNQ-novolac resist. This resist is comprised of (a) DNQ (its photoreaction shown) and (b) novolac (a mixture of meta and para cresol).

The ultimate resolution of DNQ-novolac systems exposed using 365 nm optical lithography tools was approximately 300 nm. In the mid-90s, it was desired to produce 250 nm critical features; therefore, processing wavelengths decreased into the deep UV (DUV: 248 nm) and it became difficult to tailor DNQ-novolac resists for this exposure technology. These difficulties were due largely to the strong absorbance of novolac resins in this spectral region. When the resin exhibits strong absorbance, light cannot penetrate through the entire thickness of the resist; therefore, a relief image cannot be created in it.

The shift was then made to using chemically amplified resists. Depending on the type of developing solvent used, chemically amplified resists can be either negative or positive resists. They are patterned in the following manner. The resist is exposed to radiation. The photoactive compound reacts to this radiation and produces a chemical catalyst. The catalyst promotes reactions in the surrounding polymer resin during a baking step. These reactions create a change in the solubility of the resin which is exploited to produce a relief image upon development. Because of the mechanism by which these resists react, chemically amplified resists exhibit sensitivities that can be up

to two orders of magnitude[11] greater than that of conventional DNQ-novolac resists. An example of a chemically amplified resist system used for creating positive toned images is shown below in figure 1.5.[12] Fluoroantimonic acid is created upon exposure to ultraviolet light. This acid catalyzes the hydrolysis of the tertiary-butoxycarbonyl protected poly(vinylphenol) resin. The tert-butyl cation, which is a product of this hydrolysis, rearranges to regenerate acid in the matrix. This regenerated acid catalyzes another chemical event. Because of this regeneration, one photochemical event can catalyze up to 1 million hydrolysis reactions in the resist.

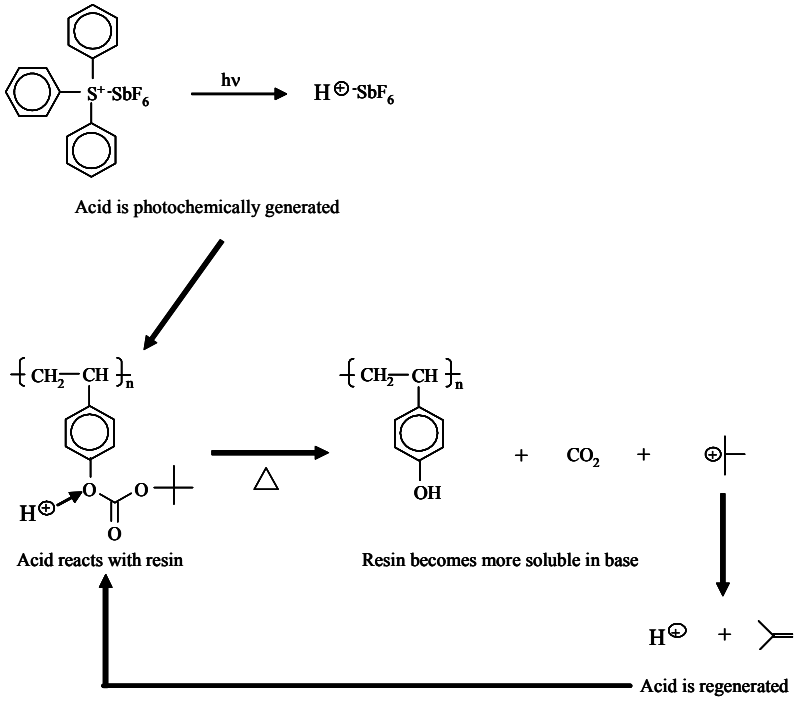

Figure 1.5: Process of creating positive toned features in chemically amplified resists.

It is expected that chemically amplified resists will not be amenable to NGL technology due to the fact that resins for these resist systems exhibit strong absorbance at wavelengths lower than 200 nm. Developing transparent polymer resins with sufficient etch resistance at wavelengths below 200 nm has proven very difficult. As mentioned in

the paragraph describing DNQ-novolac resists, strong absorbance in the resin results in difficulty creating a relief image in the resist. Additional issues for creating features in conventional resists for NGL technologies are described below.

1.4 Issues for Conventional Resists

As mentioned in the second section of this chapter, resist materials must exhibit high resolution. The resolution (R) is the minimum feature that can be printed with an exposure technology. Its equation is shown below. The most common means to achieving this high resolution is to decrease the wavelength of light used to expose the resist.

$$R = k\frac{\lambda}{NA} \qquad \textbf{Equation 1.1}$$

In the equation above, λ is the wavelength of light used to pattern the feature, NA is the numerical aperture of the optical system, and k is a process constant. For a given optical system (constant NA), as the resolution is improved by decreasing the exposure wavelength, the depth of focus is sacrificed. The equation for depth of focus is shown below.

$$D_f = \frac{\lambda}{NA^2} \qquad \textbf{Equation 1.2}$$

The depth of focus is the depth through which an image can be focused to produce a pattern within a certain tolerance. This loss of depth of focus implies the use of thinner resist materials. As one might imagine, this creates problems since the use of thinner resists is not particularly robust toward chemical etch.

In addition to resolution and depth of focus issues, traditional organic resist materials exhibit high absorption at low wavelengths. As mentioned in the previous section, this strong absorption creates problems for conventional processing. Radiation cannot penetrate the full thickness of the resist; therefore, a relief image cannot be created in the film. This absorption problem can be solved by using thinner resists or more transparent polymers. Thin resists, as mentioned previously, present etch stability problems. Finding acceptable transparent polymers is a difficult task; however, research is underway to develop them.[13-16]

These NGL technologies also exhibit shallow penetration depths; the radiation travels very short distances before its energy decays. This poses a problem for using conventional resists for NGL technology because photochemical events that occur in a small surface layer of a resist have to be exploited to pattern the entire film. No wonder there is a big question mark in the panel of the DRAM technology roadmap that represents resists used to build future devices.

1.5 Solutions

There are three means to solving these problems. The first is to use thinner conventional resists. As mentioned previously, this approach poses potential etch problems. Additionally, this approach might also exhibit potential processing problems because fundamental properties of the resist change as the material is made thinner.[17, 18] The second solution is to use more transparent materials. This approach is being actively pursued by researchers across the country.[13-16] So far, this has proven to be a formidable task. The third solution is to image at the resist surface only, and then to amplify this

surface image to create a patterned polymer film that fulfills the requirements mentioned in section two of this chapter. This is the solution that will be explored in this dissertation.

This document will discuss research performed to evaluate a novel means of creating resists for Next Generation Lithography. The next chapter will serve as a review of the ways in which various researchers have attempted to overcome the issues stated in the previous section. This chapter will also serve to introduce the novel process that will be explored in later chapters. Chapter 3 will introduce the experimental methods by which this process was evaluated as a viable means for Next Generation Lithography. The following four chapters will discuss the results obtained in evaluating this novel process for NGL. The eighth chapter will summarize the conclusions drawn and make recommendations for further study.

CHAPTER 2

METHODS OF PATTERNING POLYMERS ON SURFACES

2.1 Thin Layer Imaging

One means of mitigating the issues stated in the above chapter is to use thin layer imaging (TLI) techniques to create pattered resists. TLI contrasts to conventional resist processing in that it involves imaging through a thin layer as opposed to a thick film. This imaging layer can either be a surface layer of a single layer resist or a thin film on top of a multi-layer stack. The image created in the layer is then developed through the rest of the film using a plasma reactive ion etch (RIE) system. By using TLI, depth of focus, absorption, and penetration depth issues are resolved. One can pattern at very high resolution in a system with a small depth of focus since the image is only created in a thin layer of the resist. Since only a top portion of the resist is used for imaging, materials that are highly absorbing at the operating wavelengths can be used. Also, NGL systems that exhibit low penetration depth can also be used. An overview of some TLI schemes is presented below.

2.1.1 Bi-layer Processes

The earliest TLI process was proposed by Havas et al at IBM in 1976 using tri-layer structures to generate images.[19] Lin later developed a TLI process entitled portable, conformal mask (PCM).[20] These were the first two systems that employed TLI. Though these processes were complex, they laid the foundation for more simple

processes. The next TLI development was the implementation of bi-layer resists. A general schematic of these systems is shown in figure 2.1.

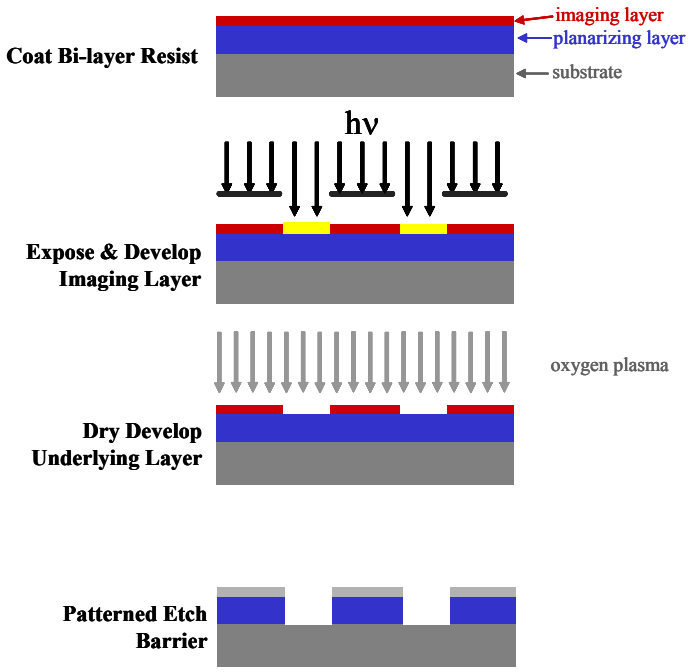

Figure 2.1: Bi-layer resist process

An imaging layer containing silicon is coated on top of a crosslinked polymeric layer, usually called the planarizing layer. The planarizing layer serves two purposes: (1) to smooth any underlying topography so that the thin imaging layer can stay within the depth of focus of the imaging tool, and (2) to provide significant etch resistance for subsequent patterning of the underlying substrate. The imaging layer is exposed and developed via a conventional means to create a thin patterned layer. The surface is then subjected to an oxygen RIE process. The patterned silicon resist is oxidized in the RIE to form a silicon dioxide layer. The bare portions of the planarizing layer are burned in the plasma, and the pattern in the imaging layer is transferred throughout the stack.

The imaging layer must exhibit high sensitivity to the process wavelength. It must also contain a sufficient amount of silicon in order to exhibit the etch resistance required for image transfer. Polysiloxane materials were initially used to satisfy these requirements; since then, however, silicon has been incorporated into materials like poly (methyl methacrylate)[21] and novolac.[22] The planarizing layer must exhibit superb etch resistance, and it is chosen for its compatibility with the imaging layer. Crosslinked novolac is most often used for this purpose. Currently, Shipley Company provides bi-layer resists for 193 nm lithography[23]; however, bi-layer processes for 193 nm lithography have not been implemented in a manufacturing environment.

2.1.2 Si-CARL Processes

Another TLI scheme that has been researched is the "Silicon Chemical Amplification of Resist Lines" or Si-CARL process. A schematic of this process is shown in figure 2.2.

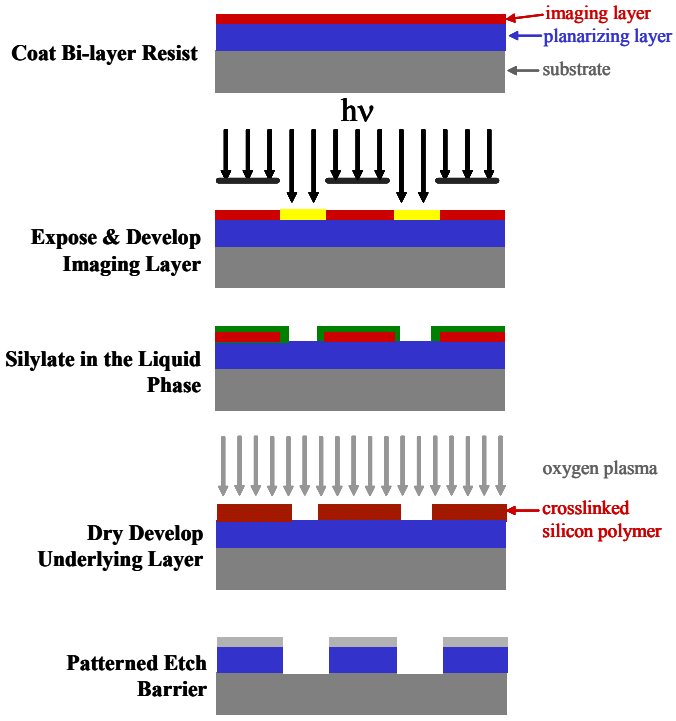

Figure 2.2: Si-CARL process

In this process, an imaging layer which does not contain silicon is coated onto a planarizing layer. It is patterned and developed via conventional lithography. Next, the resist stack is submerged into a solution of oligomeric, bifunctional aminosiloxane.[24] This aminosiloxane, or CARL reagent, reacts with anhydride groups in the imaging layer to create a cross linked, silicon rich patterned polymer. This image is then transferred to the planarizing layer via oxygen RIE.

There are a few of advantages to this seemingly complex process. The silylating agent reacts in great yield to produce a polymer with high silicon content, which improves the overall etch resistance of the resist. The depth of focus for this process is extremely large. Additionally, this technology has proven to be amenable to a variety of wavelengths, and this process has been optimized and used in the manufacture of memory chips at Siemens Corporation.

2.1.3 Top Surface Imaging via Vapor Phase Silylation

Top Surface Imaging (TSI), unlike the processes described before, uses a single resist layer. Many imaging systems have been proposed that use this technology. They are reviewed in a book by B. J. Lin.[25] These TSI processes are described by the acronyms PRIME[26], SUPER, SAHR[27], and DESIRE.[28, 29] It is this last process that we will discuss at length. A schematic of the DESIRE (**D**iffusion **E**nhanced **SI**lylated **RE**sist) process is shown in figure 2.3.

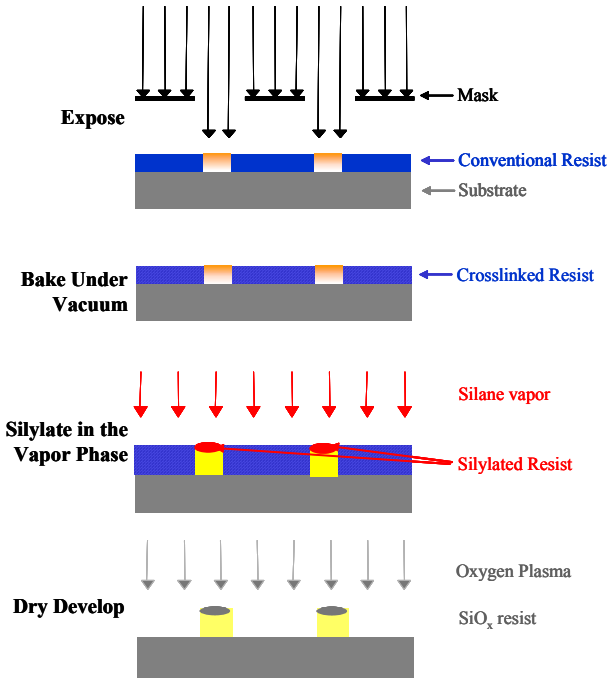

Figure 2.3: DESIRE process

A conventional DNQ-novolac resist is coated onto a wafer. This resist is exposed to patterned light in an ambient environment. The exposed DNQ decomposes and reacts with ambient water to form an indene carboxylic acid. The resist is then baked under vacuum; no water is present in the system. At this condition, the unexposed DNQ undergoes thermal decomposition to form an unstable ketene. This ketene reacts with the

novolac resin, and the unexposed portions of the film become crosslinked. This cross linking decreases the permeability of the unexposed regions to gas. The resist is then exposed to a silylating agent, which is usually an aminosilane vapor. The aminosilane permeates into the exposed regions of the resist and reacts with the phenol sites of the novolac resin as shown in figure 2.4

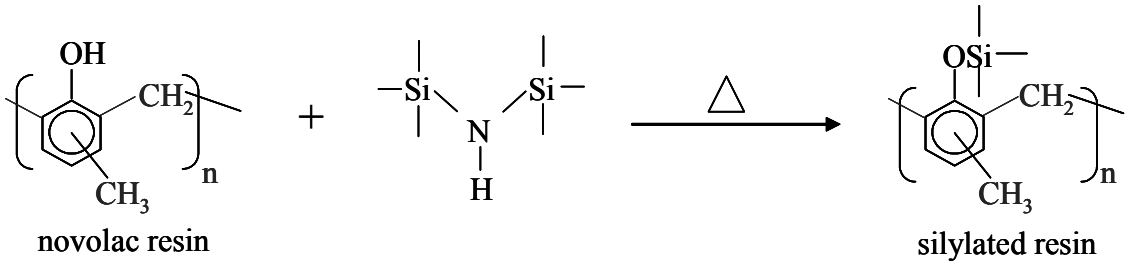

Figure 2.4: Reaction of aminosilane with novolac resin

The cross linking reaction provides a switch in permeability of silylating agent within the polymer film. This switch in solubility is exploited to produce patterned silicon regions in the film. The substrate is then placed in an oxygen RIE system. The silylated regions are converted to silicon dioxide. The unprotected crosslinked novolac burns in the plasma and the pattern is transferred through the entire resist.

Since only one film is required to be patterned, the DESIRE and other TSI processes are much simpler than other TLI processes. Since the reagent used to create the patterns is a vapor, less material is required to create patterns than in the CARL process. This TSI process, however, does have some disadvantages. Silylating agent deposits onto the surface of the entire film. During the plasma development step, silicon dioxide is created across the entire resist surface. This phenomenon is called micro masking. The plasma chemistry usually has to be altered to remove this scum from the surface of the resist, which adds complexity to the system. Another disadvantage of these diffusion

based systems is that the resist swells during the silylation step. The silylating agent adds additional mass to the polymer; to accommodate this additional mass, the polymer swells. This swelling is both vertical and lateral. During the RIE process, silicon dioxide is created in these swelled regions and pattern profiles begin to obtain the notorious "bird's beak" shape; lateral resolution is lost.

2.1.4 Digital Top Surface Imaging via Vapor Phase Silylation

To mitigate the problems associated with creating contrast via permeability as described in the previous section, a technique was developed in which reactivity dictated the location of the silylating agent. This process was first developed at IBM in 1985 and is shown in figure 2.5 below.

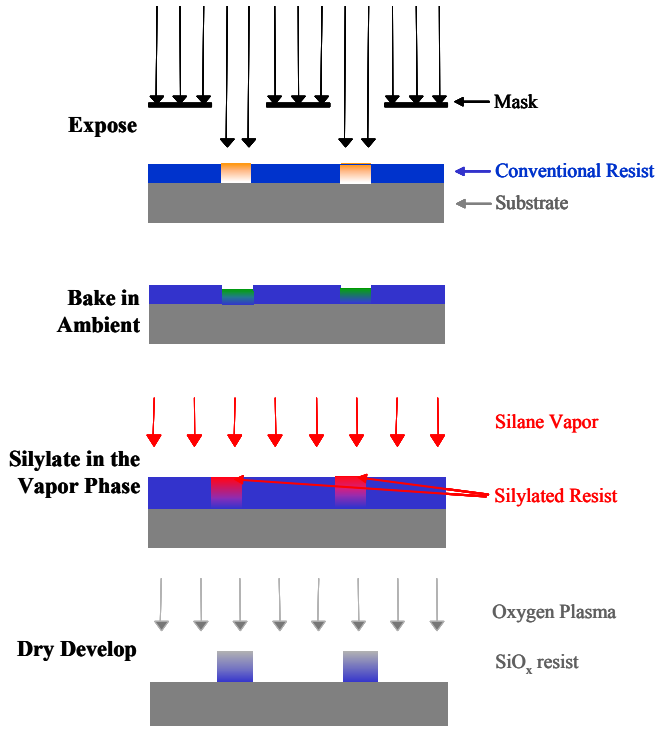

Figure 2.5: Digital TSI of a chemically amplified resist

In this system, a chemically amplified resist is exposed to a pattern. As described in the previous chapter, acid is generated in the exposed regions of the film. This acid then works to de-protect the resin at elevated temperatures. In the exposed regions of the film, tertiary-butoxycarbonyl protected styrene groups are converted to phenols. These phenols have the ability to react the silylating agent. As in the DESIRE process, the wafer is then exposed to aminosilane vapor. This vapor reacts with only the exposed regions of the film.

This is truly a digital process. Silylating reagent is able to react with only the de-protected portions of the film; therefore, silicon is only incorporated into exposed regions of the film. This process also does not exhibit swelling that processes like DESIRE demonstrate. In digital TSI, the polymer loses mass during the de-protection step. As long as the mass of the silylating agent is less than or equal to the mass of the protecting group, the material will not swell when it is silylated. This process is also a single layer process which makes it much simpler than the bi-layer processes described in the previous sections. Currently, this process is being evaluated for 193 nm lithography.[30, 31]

2.2 Absorption of Polymers on Surfaces

Another means to mitigate depth of focus, absorption, and low penetration depth issues is to absorb polymers onto surfaces. One method of doing this is by reacting polymers directly to selected regions of the surface. Polymers with difluoro hydroxyethyl and trifluoromethyl end groups have been reacted to carbon surfaces to be used as promising protectants for hard drive applications.[32] Films generated by this technique are usually range from 1 to 5 nm in length. When the surface is significantly

covered with polymer chains, the polymer concentration at the surface-solution interface becomes larger than that in the bulk. Additional chains trying to reach the surface have to diffuse against this increasing concentration gradient. Immobilization at the surface energetically becomes more unfavorable as the reaction proceeds. This is depicted in figure 2.6. Another disadvantage of using this technique is that it doesn't provide a means to directly pattern the films.

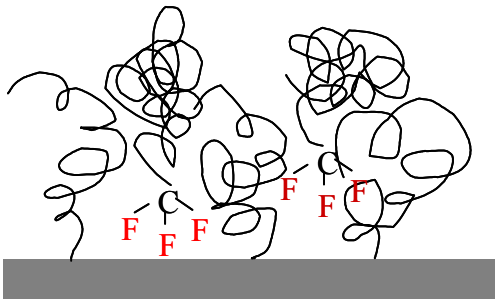

Figure 2.6: Absorption of reactive polymers on surfaces

Rühe et al also developed a means to photochemically absorb polymers on surfaces which can be used to patterned polymers absorbed onto surfaces.[33] A schematic of this process is shown in figure 2.7. A self-assembled monolayer of a benzophenone derivative is reacted to a silicon oxide surface. Polystyrene is spun coated onto the modified surface. This stack is then exposed to ultraviolet radiation. This exposure induces a reaction between the benzophenone and the polystyrene which grafts the polymer to the surface. If the exposure was a patterned one, regions of the film that were unexposed could be washed away. This process can prove to be amenable to NGL processing. The only disadvantage of this process is that it requires high exposure doses {on the order of Joules per square centimeter (J/cm^2)} to graft the polymer to the surface.

This process is currently being evaluated as a means to pattern surfaces at nanoscale resolution.

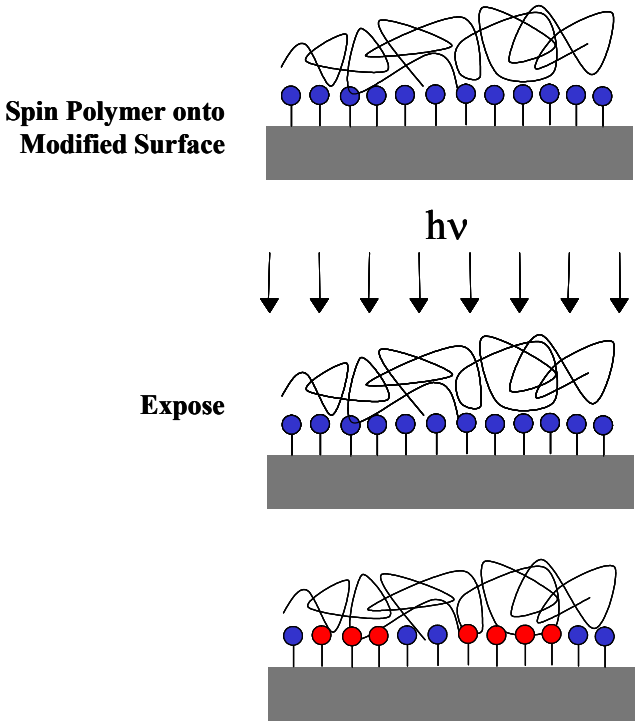

Figure 2.7: Photochemical absorption of polymers onto surfaces

2.3 Surface Initiated Polymerization

Researchers have recently investigated means of polymerizing polymers from surfaces as a means to mitigate depth of focus, absorption, and low penetration depth issues associated with NGL technologies. Researchers in Grant Willson's group at the University of Texas at Austin have been developing resists for NGL in which they expose patterns in a thin surface layer of chemically amplified resists to liberate acid in the exposed regions. They then perform gas phase cationic polymerization of silicon-containing monomers in the exposed regions. The films are then developed in oxygen plasma to create silicon dioxide in the exposed regions.[34, 35] The process is shown in

figure 2.8. The process creates robust patterned silicon dioxide masks; however, the patterned regions exhibit swelling due to the high solubility of the monomer in the resist layer. Studies are underway to design monomers with low solubility in these resist films.[36]

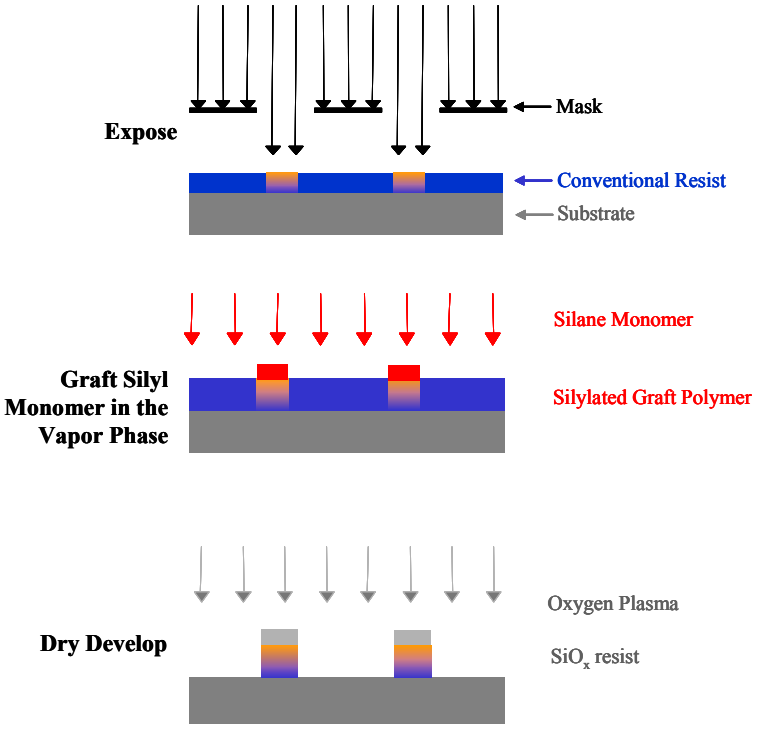

Figure 2.8: Graft polymerization lithography

Others have been developing a means to create patterned polymers from self-assembled monolayers. One means to creating polymer patterns is via free radical polymerization.[37-45] In these studies, self-assembled monolayers containing azo or peroxide free radical generators were imaged and/or heated in the presence of styrene or methyl methacrylate to produce patterned polymer films. Other researchers explored atom transfer radical polymerization of bromine or chlorine terminated monolayers the presence of either copper bromide or copper chloride produce poly(styrene), poly(methylmethacrylate), or poly(acrylamide) films up to 100 nm thick.[46-50]

Researchers at IBM have used nitroxy mediated radical polymerization to create polymer brushes of the same thickness.[51, 52] This method of patterning polymers on surfaces has often been called "grafting from" polymerization since the polymer is grafted from the self-assembled initiator bound to the surface. These methods are very promising as a means for developing new resist patterning processes. Imaging characteristics are controlled by the chemistry of the self-assembled monolayer, which is on the order of angstroms thick; therefore, no depth of focus, absorption, or penetration depth issues are associated with patterning this material. The etch properties of the final pattern are governed by the polymer grown. The chemistry of the monomer can be tailored for etch resistance. The thickness and morphology of the resist is controlled by the process conditions. Since the imaging and etch characteristics are decoupled, this process could prove to be amenable for many generations of exposure technologies. This process can be positive or negative tone as shown in figure 2.9

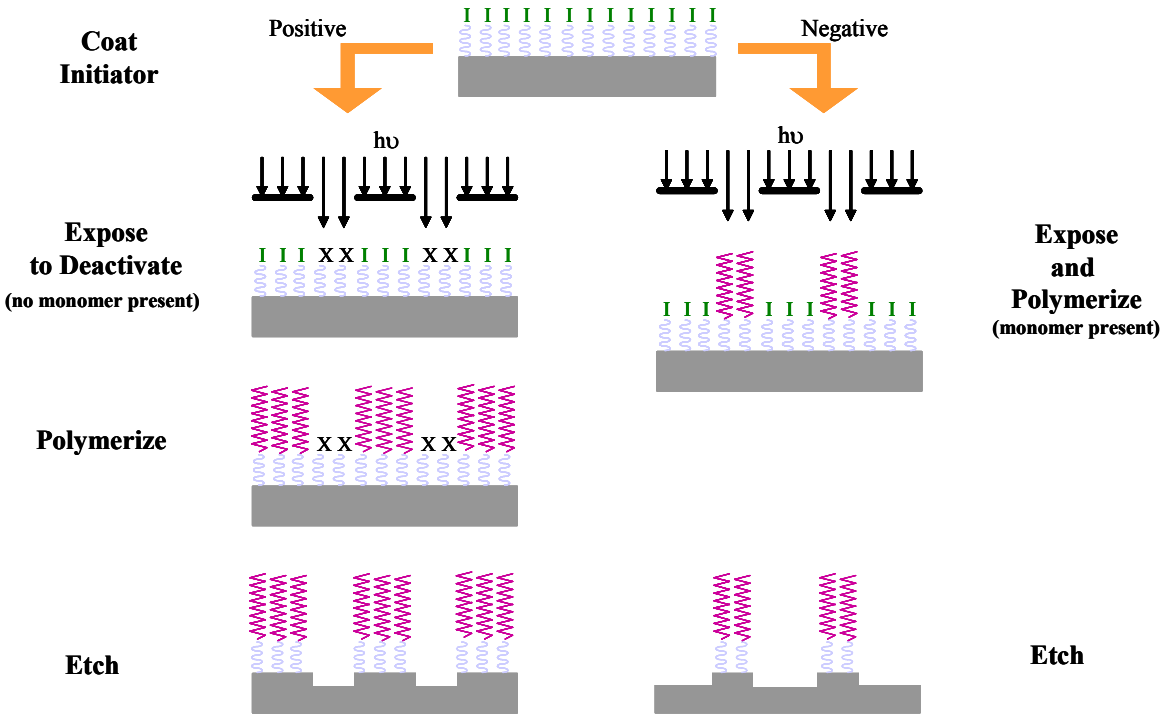

Figure 2.9: "Grafting from" polymerization to produce positive and negative toned features

In the positive tone version of this process, initiator molecules are exposed to patterned radiation in ambient to create dead sites in the film. The substrate is then heated in the presence of monomer. This process initiates polymerization of the protected sites with the monomer. The negative toned process involves exposing the initiator layer to a pattern while introducing the system to monomer.

2.4 Process Studied (SMIP)

The chemistry that we have initially investigated, entitled Surface Monolayer Initiated Polymerization (SMIP) was developed by Rühe et al and is shown in figure 2.10. It is the positive toned process of the "grafting from" polymerization shown above. (The negative tone process is not seen as amenable for NGL; it is impractical to contaminate million dollar exposure tools with vinyl monomer.) A self-assembled

initiator layer is deposited onto a silicon oxide surface which terminates in silanol groups. This initiator is exposed to patterned light in ambient. The radicals generated during exposure are quenched by atmospheric oxygen and water, and dead sites are created in the exposed regions of the film. The wafer is then placed in a hot bath with degassed styrene or methyl methacrylate. Free radicals generated during this heating step initiate polymerization of the monomer, and patterned polymeric features are grown on the surface of the wafer.

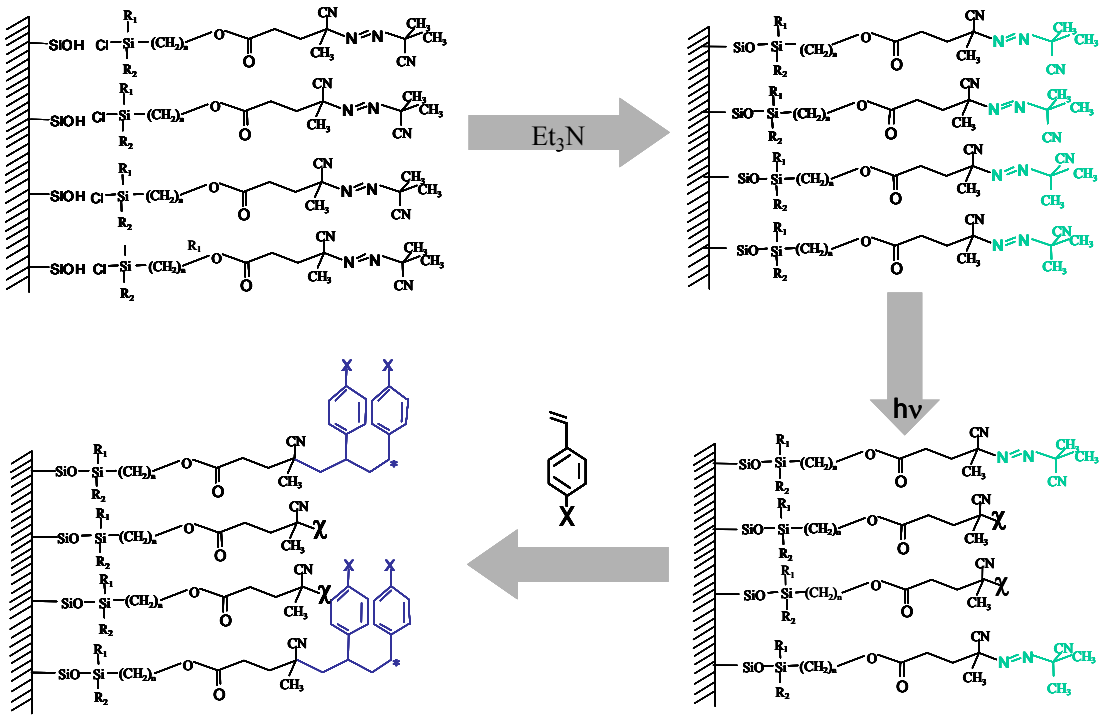

Figure 2.10: SMIP process chemistry

The initiator structure has four main sections as shown in figure 2.11 below. The circle enclosing the far left section of the compound (red circle) encloses the site for surface attachment. All initiators described covalently bind to the silanol groups that terminate silicon dioxide (SiO_2) covering a silicon wafer. The second section is the spacer (blue circle). This region can be used to modify interactions with the surface and with

adjacent molecules. It can also be used to enhance the optical properties of the initiator. The (yellow) symbol in the spacer region represents a cleavable group. After polymer is formed on the surface, it can be cleaved from the surface at this point and analyzed via conventional methods. The third section (green) is the reactive azo initiator. This compound decomposes upon exposure to both light and heat. If this compound decomposes in the presence of vinyl monomer, the monomer will polymerize via a free radical mechanism. The final section on the far right (purple) encloses the end group. This group can be free or bound to the surface. Monomers used in this study are styrene and methyl methacrylate. These compounds are known to polymerize via a free radical mechanism.[53]

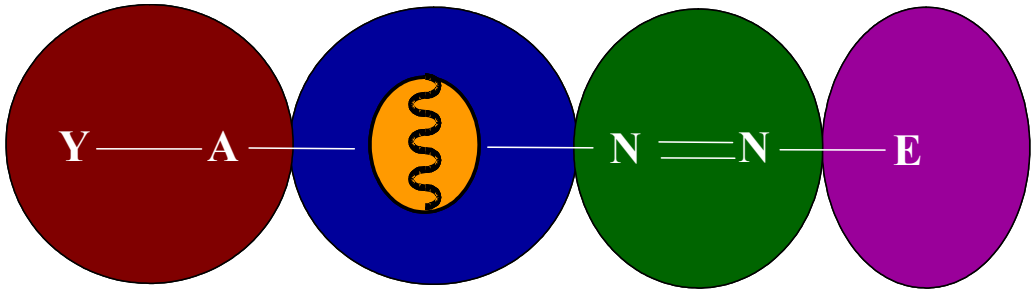

Figure 2.11: General initiator structure used for SMIP process

This process has been demonstrated by creating patterned polystyrene films on silicon native oxide surfaces.[54] In our initial studies, the total processing time was a day. It is our goal to investigate the kinetics of the process steps with the hope of optimizing each step. The kinetics of the first two process steps and methods to improve the process kinetics are presented in the next four chapters. These patterns also exhibited a significant amount of roughness. Methods of optimizing this process to obtain smooth features are presented in the subsequent chapter. An analysis of the ultimate resolution of

the process of the positive toned process and a means to optimize the resolution of this process are also given in this chapter. The final chapter of this document is a summary of the work and suggestions for further research.

CHAPTER 3

EXPERIMENTAL METHODS

3.1 Introduction

The purpose of this chapter is to introduce the experimental techniques used in this study. Three major techniques were used to analyze the chemical and physical properties of the materials used in this SMIP process and to evaluate the feasibility of this SMIP process. To analyze the rates of deposition of initiator molecules on SiO_2 surfaces, a quartz crystal microbalance with dissipation monitoring (QCM-D) was used. X-ray photoelectron spectroscopy (XPS) was used to analyze the rates of decomposition of these monolayers on flat surfaces. Atomic Force Microscopy (AFM) has been used to analyze the roughness of the surfaces used for this SMIP process, to view patterns grown in the monolayer, and to analyze the roughness of the blanket films and patterned polymers grown via SMIP. An overview of the basic physics of these techniques is given in the subsequent sections.

3.2 Sample Preparation

Polymerization experiments were performed on 330 – 432 micrometer (μm) thick silicon wafers that were p-type doped to achieve a sheet resistance ranging from 1 to 20 Ohm-centimeter. Sample preparation for this process was very involved. The sample preparation and process conditions for each of the steps are given below.

3.2.1 Surface Preparation for Monolayer Deposition

Various methods for cleaning substrates for deposition experiments were used. After cleaning samples via these various methods, the chemical composition and surface roughness of the substrates were evaluated to determine the best method for preparing the surface for monolayer deposition.

3.2.1.1 Plasma Cleaning

The plasma clean consists of placing surfaces in a Harrick Scientific plasma chamber. Air is ionized in the plasma chamber. The purpose of this process is to physically remove any contaminants from the surface of the substrate. This plasma is predominantly nitrogen; therefore, it might have passivate the silicon dioxide surface and prevented molecules from reacting to it.[55]

3.2.1.2 RCA Cleaning

The RCA clean is an extensive cleaning technique in which a substrate is subjected to three liquid baths that remove specific contaminants from it.[56] The first bath is called the SC-1 bath and consists of water, hydrogen peroxide, and ammonia mixed in a volume ratio of 5: 1: 1 (water: peroxide: ammonia). It is heated to 60˚C, and the substrate sat in this solution for 10 minutes. The purpose of this bath is to remove organic contaminants and trace metals from the surface. The second bath was the hydrofluoric acid (HF) bath. This bath is a 50:1 volume mixture of water and HF. (There are 50 parts water) The wafer sits in this bath for 15 seconds at room temperature. The purpose of this bath is to remove the native oxide from the silicon surface. The third bath is the called the SC-2 bath. It consists of water, hydrogen peroxide, and hydrochloric acid (HCl) mixed in a 5: 1: 1 volume ratio and heated to 60˚C. The substrate sits in this bath

for 10 minutes. The purpose of this bath is to remove alkali ions and residual metals from the silicon surface. After each of these process steps, the wafer is rinsed with de-ionized (DI) water for 10 minutes. This process not only thoroughly cleans the silicon wafer surface; it creates a fresh oxide on which material can be deposited.

3.2.1.3 Acid Treatment

This procedure was adopted from an XPS study on silicon.[57] The purpose of this step is to increase the concentration of hydroxyl groups available on the surface of the native oxide of the wafer. The wafer is placed in a 1 molar nitric acid (1M HNO_3) solution for 2 hours, removed from the solution, and dried in a nitrogen stream.

Various combinations of these procedures have been used to analyze the effect of the surface treatment on the rate of deposition and the overall concentration of monolayers deposited onto silicon oxide surfaces.

3.2.2 Material Processing for Polymerization Experiments

In order to create patterned polymer surfaces, materials have to be processed in a specific manner. Below is an outline of the procedures used to create polymers grafted to silicon surfaces via the SMIP process.

3.2.2.1 Monomer Preparation

Styrene and methyl methacrylate monomers have been polymerized in these experiments. Styrene monomer was chromatographically purified over aluminum oxide, distilled in vacuum from copper (II) chloride, and stored under argon at 0 degrees Celsius (ºC). Methyl methacrylate monomer was purified over a copolymer of styrene and divinylbenzene. It was purified at the point of use.

3.2.2.2 Degassing the System

Purified monomer was placed in a test tube with the substrates. The test tube was then connected to a shlenk line. Three freeze-pump-thaw cycles were performed on the monomer/substrate mixture. The ultimate pressure of the pump cycle was 10^{-2} torr {10 millitorr (mTorr)}. The substrate was then placed in either a hot water bath or an oil bath and allowed to polymerize for the desired time.

3.2.2.3 Cleaning of Substrates after Polymerization

After polymerization, the substrates were placed in a sohxlet apparatus for at least 6 hours. Poly(styrene) films were extracted in toluene in the sohxlet apparatus. After the sohxlet extraction, the films were washed in toluene, acetone, methanol, isopropanol, and water. Poly(methyl methacrylate) (PMMA) films were extracted in methanol. After the sohxlet procedure, the PMMA films were rinsed in methanol, isopropanol, and water.

3.3 Chemical Characterization via XPS

X-ray photoelectron spectroscopy (XPS), also known as electron spectroscopy for chemical analysis (ESCA), is a semi-quantitative, surface-sensitive technique for analyzing the chemical composition of surfaces. In XPS, monochromatic x-rays impinge upon a surface and photoelectrons are emitted from the sample. By analyzing the energy distribution of the photoelectrons, the chemical composition and bonding characteristics of the sample can be determined. The information depth for XPS is limited to about the top 50 Angstroms (Å) of the sample.[58] This depth is set by the distance the photoelectrons can travel in a solid material without undergoing inelastic collisions; therefore, XPS is a very surface-sensitive technique.

XPS is based on the "photoelectric effect". When an x-ray of known energy impinges on a sample, photoelectrons from the inner shell electrons of the sample are emitted. The kinetic energy of these photoelectrons is dependent on the binding energy (BE) of the electron and the x-ray photon energy.[59] A schematic illustrating this relationship is shown in Figure 3.1.

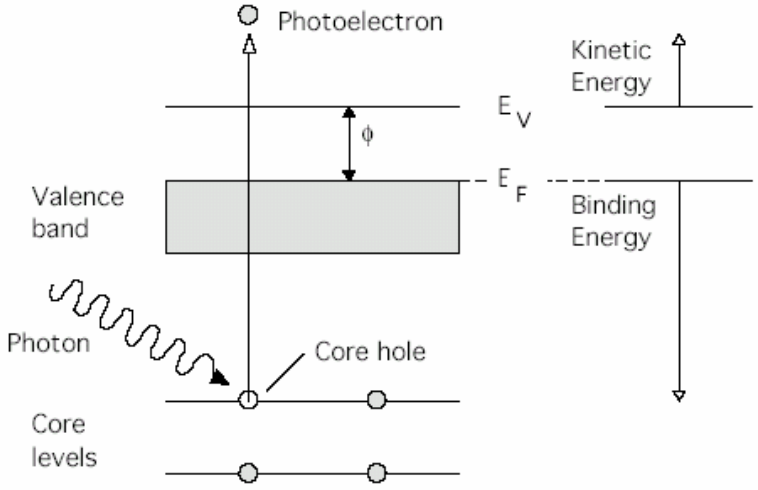

Figure 3.1: Schematic of the photoelectron effect in XPS

In figure 3.1, E_V and E_F are the vacuum and the Fermi energy levels respectively. The symbol ϕ represents the work function of the spectrometer ($|E_F - E_V|$) and is constant for a given spectrometer. Each element has a unique set of core energy levels, which correspond to specific binding energies. These binding energies will shift depending on the chemical environment (bonding structure) in which they reside. As a result, the kinetic energy distribution of the ejected photoelectrons can be used to identify the composition and bonding states of the sample. The binding energy may be calculated from the measured kinetic energy of the photoelectron by the following relationship.

$$BE = h\upsilon - KE - \phi$$ **Equation 3.1**

In equation 3.1, *BE* is the binding energy of the electron in its core state, $h\nu$ is the kinetic energy of the incident x-ray (1486.6 eV), *KE* is the kinetic energy of the photoelectron, and ϕ is the work function of the spectrometer.

The surface hydroxyl density of silicon wafers and the rates of decomposition of initiator layers were determined using a Physical Electronics (PHI) 1600 XPS system. Monochromatic Aluminum K_α x-rays were generated using a water-cooled anode operating at 350 Watts. Data was collected at a chamber pressure below 5 x 10^{-9} Torr. Sample alignment, prior to data acquisition was performed by maximizing the photoelectron intensity corresponding to the primary carbon 1s peak located at a binding energy of 285eV. Sample charging did not occur during sample analysis; therefore, data was analyzed as received. Sometimes data were collected at different take off angles on the same sample in order to maximize the intensity of the elements of the surface species. Relative compositions of the various species in the deposited films were determined by curve fitting each spectral region, assuming all peaks to be perfectly Gaussian, with a constant full width half maximum (FWHM).

3.4 Physical Characterization

3.4.1 QCM-D

Quartz crystal microbalance with dissipation monitoring (QCM-D) has been used to measure the rates of deposition of initiator molecules onto surfaces and to monitor the method by which the initiator deposits onto the surface. Quartz crystal microbalance (QCM) techniques exploit the piezoelectric properties of quartz. Piezoelectric (meaning "pressure electric") materials oscillate in an applied electric field. The frequency of oscillation of the crystal changes when mass is added or removed from the surface of the crystal. This technique is sensitive to mass changes on the order of nanograms per square centimeter (ng/cm^2).[60] In this QCM-D technique, frequency shifts are monitored not only at the fundamental frequency of five megahertz (5 MHz); shifts are monitored at the 3^{rd}, 5^{th}, and 7^{th} overtones of this fundamental frequency (15 MHz, 25 MHz, and 35 MHz, respectively). In addition to monitoring the resonant frequency of the crystal, QCM-D measures the dissipation factor exhibited by the quartz crystal. This is done by monitoring the decay in the frequency of the crystal after the oscillator circuit is turned off. Depending on the viscoelastic properties of the material on the crystal surface, the frequency will decay slowly or rapidly. Rigid, solid-like materials will exhibit slow frequency decay. Soft, viscoelastic materials will exhibit fast frequency decay.[61] These phenomena are represented in figure 3.2.

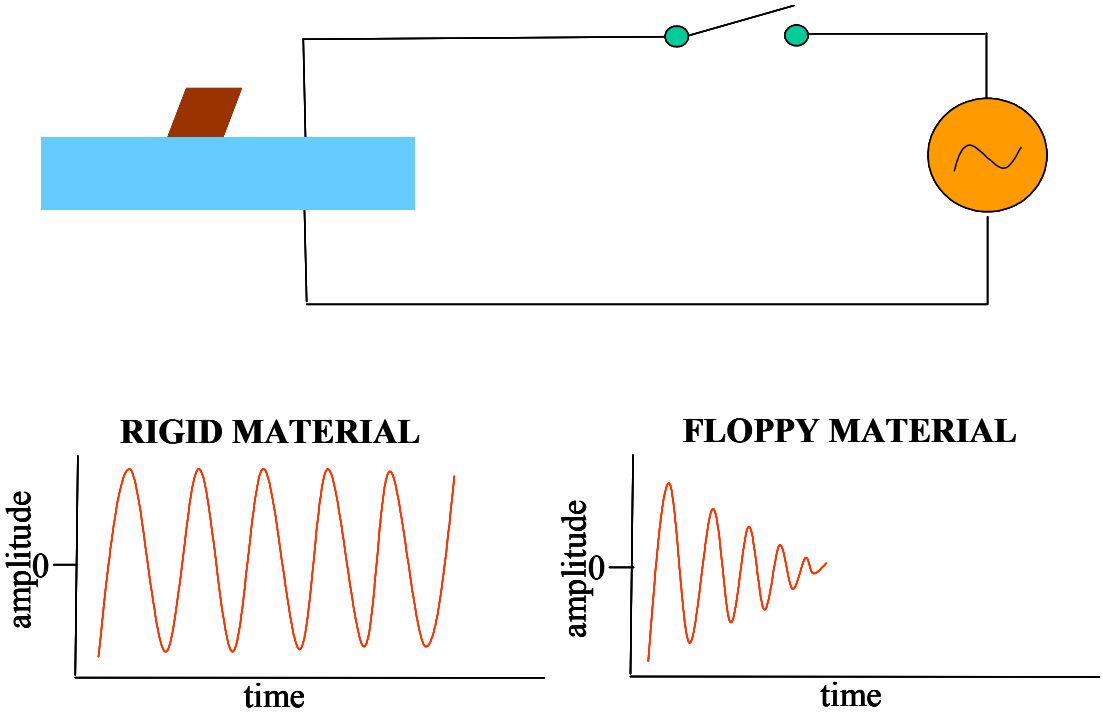

Figure 3.2: Schematic of QCM-D technique

Dissipation factors of the fundamental frequency along with the 3rd, 5th, and 7th harmonics are measured using this QCM-D technique.

Quartz crystals are usually coated with metal electrodes and placed in a cell holder to be connected to an oscillatory circuit. An AC voltage is applied across its electrodes and the crystal oscillates in thickness shear mode. In this mode, a shear wave is created through the thickness of the film. At the resonant frequency, the node of this wave is located in the center of the crystal. When a rigid mass is added or removed from the surface of the crystal, it is treated as an equivalent amount of quartz. The node of the shear wave created in the crystal accommodates this change in mass. A schematic of this phenomenon for mass being added to the quartz surface is shown in figure 3.3.

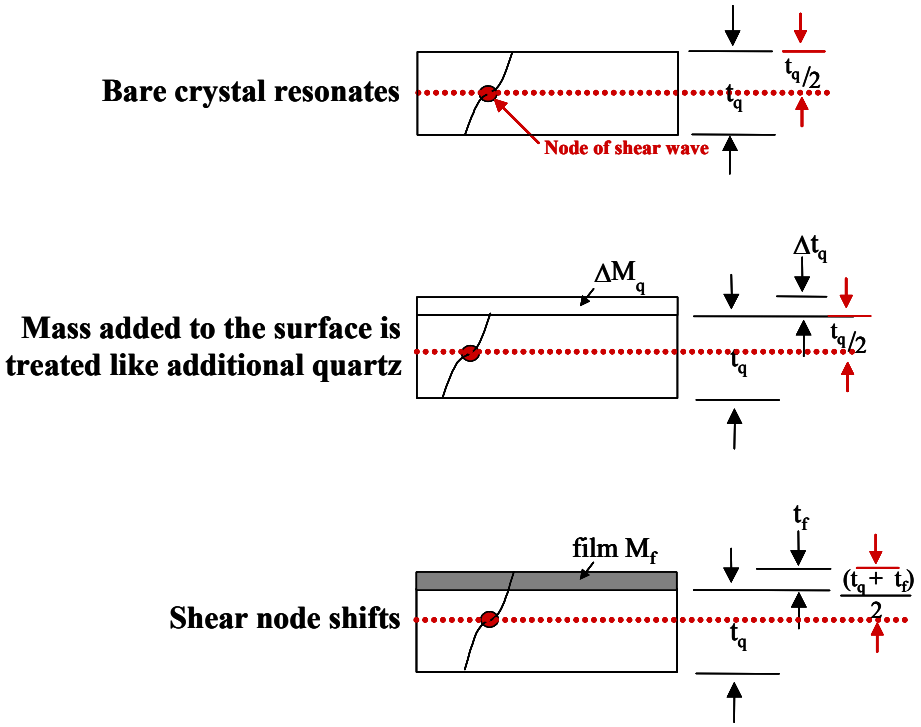

Figure 3.3: Schematic of the process of monitoring mass addition to QCM surfaces.

The mass density (in units of ng/cm^2) of the rigid film being added to the surface can be calculated via the Sauerbrey equation which is shown below.

$$\Delta m_f = \frac{-C_f \bullet \Delta f}{n} \qquad \textbf{Equation 3.2}$$

In this equation, Δf is the frequency shift of the crystal, n is the overtone number, and C_f is the crystal constant. For the crystals used in this study, the constant was 17.7 ng Hz^{-1} cm^{-2}. In the case of some of these small initiator layers absorbing onto SiO_2 surfaces, the absorbed film is not rigid and the Sauerbrey relation does not hold. The material is viscoelastic and the mass added will not directly couple into changes in frequency of the crystal. The dissipation of the crystal, therefore, needs to be measured to account for the change in mass as well as the viscoelastic properties of the material added. The

dissipation (D) is defined as the energy lost during one oscillation cycle with respect to the total energy stored in the oscillator. It is written as follows.

$$D = \frac{E_{lost}}{2\pi E_{stored}}$$ **Equation 3.3**

This dissipation is measured by recording the reaction of a freely oscillating crystal after the oscillator circuit has been turned off. By monitoring both the resonant frequency and dissipation at multiple frequencies, properties of the absorbing films can be characterized in detail.

AT-cut quartz crystals with gold electrodes and a thin film of SiO_2 deposited onto the top face were purchased from Q-sense Corporation. The fundamental frequency of these crystals was 5MHz. These crystals were used in a QAFC 302 axial flow cell and connected to an oscillator circuit.[62] Both of these components were also purchased from Q-sense Corporation. Resonant frequency and dissipation values were monitored at the fundamental frequency of 5 MHz and 3rd, 5th, and 7th overtones of 15 MHz, 25MHz, and 35 MHz. This tool was not only used to monitor the rate at which initiator deposited onto SiO_2 surfaces; it aided in gaining insight into the process by which initiator deposited onto SiO_2 covered surfaces.

3.4.2 Atomic Force Microscopy

Atomic Force Microscopy (AFM) was used to observe the formation of patterns in initiator monolayers and polymer layers. It was also used to probe the formation of blanket films onto silicon oxide surfaces. AFM is a technique that has been used for the past 20 years to obtain information about the microstructure of surfaces. The mode of operation is very simple. An atomically sharp tip is scanned across the surface to be analyzed. This tip is attached to the backside of a reflective cantilever, and it is controlled

by feedback mechanisms that enable the scanner to maintain constant force above the sample surface. A laser is focused on the cantilever and deflected into a position sensitive detector. Sensitivity of less than an Angstrom is achieved via this method.[63] A schematic of the general set up is shown in figure 3.4.

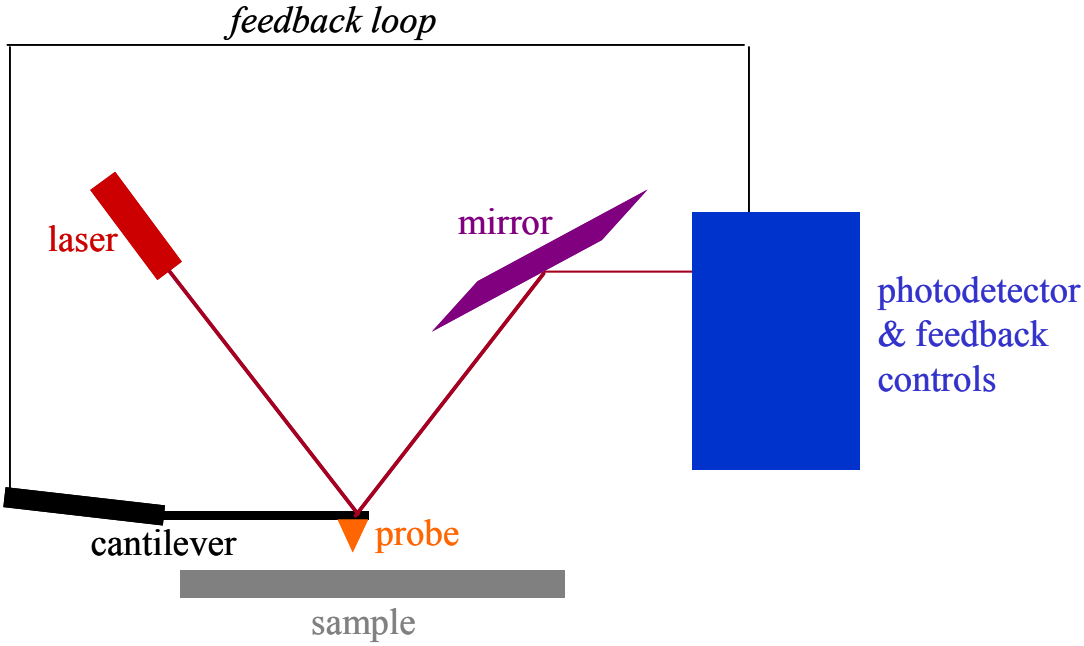

Figure 3.4: Schematic of the components of an AFM

3.4.2.1 Contact Mode

Contact mode is the most common mode used in AFM. In this mode, silicon nitride probes and cantilevers are used. A Si_3N_4 tip scans the sample in close contact with the surface. The force on the tip is repulsive, and it is set by pushing the cantilever against the sample surface with a piezoelectric positioning element. The deflection of the cantilever is sensed and compared in a DC feedback amplifier to some desired value of deflection. If the measured deflection is different from the desired value, the feedback amplifier applies a voltage to the positioning element to raise or lower the cantilever to

restore the desired deflection. The voltage applied to the positioning element is a measure of the height of the features on the sample surface, and it is displayed as a function of the lateral position of the sample. In this study, the AFM was operated in contact mode to collect images of patterns in the initiator layers.

3.4.2.2 Lateral Force Mode

The AFM was operated in later force mode (LFM) in conjunction with contact mode imaging to obtain pictures of patterns grown in initiator monolayers. The theory behind this feature is very simple; cantilevers scanning laterally (perpendicular to their length) torque as they encounter high friction sites. Low friction sites torque the cantilever less.[64] After obtaining a good topographical scan of the initiator layer on the surface in contact mode, the scan angle of the system was set to 90˚ and the friction on the cantilever tip was monitored. This friction measurement amplified patterns that were created in the monolayer with ultraviolet and electron beam radiation.

3.4.2.3 Tapping Mode

The tapping mode technique allows high resolution topographic imaging of sample surfaces that are easily damaged, loosely hold to their substrate, or are difficult to image by other AFM techniques. In this mode, silicon cantilever probes are used. They are alternately placed in contact with the surface to provide high resolution imaging and then lifted off the surface such as not to scrape it. The cantilever oscillates at its resonant frequency using a piezoelectric crystal. This crystal causes the cantilever to oscillate with a high amplitude (on the order of 10 nm) when the tip is not in contact with the surface. The oscillating tip is then moved toward the surface until it begins to lightly touch the surface. During scanning, the vertically oscillating tip alternately contacts the surface and

lifts off at frequencies ranging from 50 to 500 kilohertz (kHz). As the oscillating cantilever begins to intermittently contact the surface, the amplitude of cantilever oscillation is reduced due to energy loss caused by the tip contacting the surface. The reduction in oscillation amplitude is used to identify and measure surface features. In addition to the amplitude of oscillation diminishing upon contact with the surface, the phase of oscillation also diminishes. This feature can be exploited to distinguish the hardness or softness of material deposited on the surface. Tapping mode AFM was used to analyze the morphology of blanket and patterned polymer films grown on silicon surfaces.

CHAPTER 4

DETERMINATION OF SURFACE REACTIVITY

4.1 Introduction

The first step in this SMIP process is to deposit the initiator molecules onto the substrate. In order to maximize the number of initiator molecules that assemble onto the oxide, it is desired to create a surface in which the number of hydroxyl groups terminating the SiO_2 surface is maximized. This chapter discusses means to quantify the number of hydroxyl groups terminating the SiO_2 surface. Two means of quantifying the number of hydroxyl groups on the surface are presented. One of these methods proved amenable for giving semi-quantitative information as to the number of hydroxyl groups on the surface, and the relative number of hydroxyl groups terminating the SiO_2 surface using this method is presented as a function of the surface treatment. The roughness of the surface as a function of surface treatment is also presented. The numbers from the previous analyses were used to determine the surface treatment most appropriate for this SMIP process.

4.2 Background

One goal of this section of the dissertation is to determine the number of hydroxyl sites emanating from a planar oxide surface. Most of the reports that discuss quantifying the number of hydroxyl sites terminating silicon dioxide surfaces are found in the heterogeneous catalysis literature. These studies report a means to quantify hydroxyl

content on high surface area silica. It is hoped that the procedures used in these reports can be modified to account for the hydroxyl content on planar oxide surfaces.

There is one general procedure used to determine the number of hydroxyl groups terminating from high surface area silica. It involves using a capping agent to react with the silica. This capping agent is usually comprised of a compound that can be easily identified via either elemental analysis or Nuclear Magnetic Resonance Spectroscopy (NMR); therefore, one of these simple procedures can be used to determine the amount of capping agent that has reacted to the surface. The elemental analysis or NMR data can then be used to calculate the number of hydroxyl groups emanating from the silica. One of the most common capping agents used in these procedures is hexamethyldisilazane (HMDS).[65-68] In this reaction, the HMDS reacts with the silanol and terminates the surface with trimethylsilyl groups as shown the figure 4.1. Subsequent NMR then can be used to determine the amount of organic loading on the surface which can then be correlated to the number of hydroxyl groups emanating from the surface. In modifying this procedure to account for a flat surface, one can use an alternate technique to NMR to determine the amount of capping agent on the surface. The simplest technique to analyze chemical surface content is XPS. Unfortunately this technique cannot be used in this experiment. The capping agent contains silicon and carbon. Silicon is already in the sample, and carbon is a common surface contaminant. It would therefore not be easy to distinguish between capping agent, the silicon oxide surface, and surface contaminants.

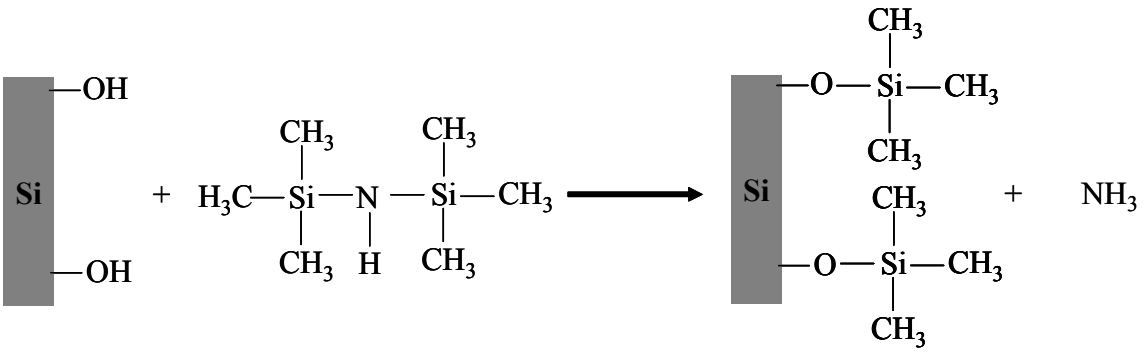

Figure 4.1: Reaction of HMDS with hydroxyl groups terminating a silicon oxide surface

Another method described by Susannah Scott and co-workers utilizes vanadium compounds to determine the number of hydroxyl groups terminating silica surfaces. In this report, they use vanadium oxytrichloride to react with the surface.[69] The reaction proceeds in a manner shown in figure 4.2. The authors argue that this vanadium compound only reacts with one hydroxyl site. They then use NMR to determine the number vanadium compounds attached to the surface. XPS can be used to determine the loading of vanadium on a planar silicon oxide surface. The vanadium $2p_{3/2}$ photoelectron emission line for $VOCl_2$ (the product of the reaction between $VOCl_3$ and the surface) occurs between 515.5 and 517.5 eV. These lines are close to the oxygen 1s photoelectron emission line which occurs at 540 eV; however, because of the strong sensitivity the XPS has to the vanadium emission (The sensitivity factor for vanadium $2p_{3/2}$ emission is 1.456. The sensitivity factor for oxygen 1s emission is 0.733), it is very easy to detect vanadium on the oxide surface via XPS.

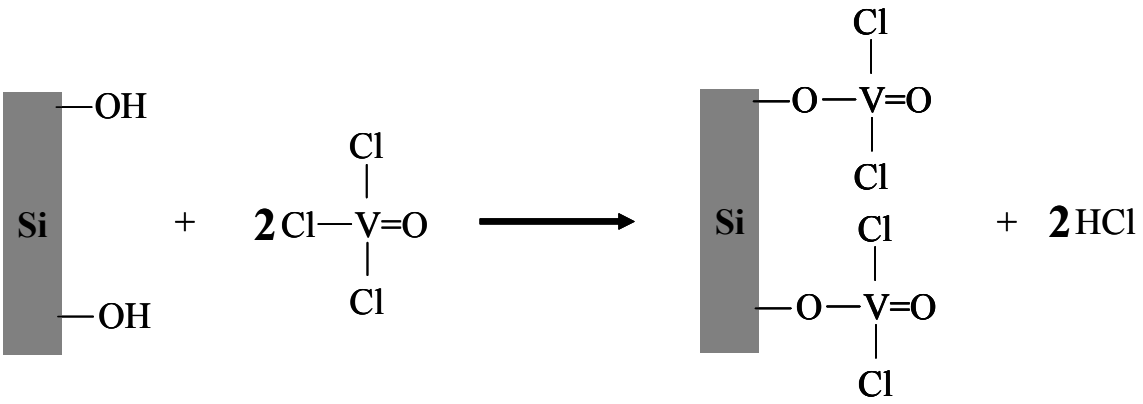

Figure 4.2: Reaction of $VOCl_3$ with hydroxyl groups terminating a silicon oxide surface

Another experiment was conducted to determine the number of hydroxyl groups emanating from the surface, and it was similar to the experiment described above. Instead of using a capping agent in a surface reaction, a self-assembled monolayer (SAM) that contains a tag which is sensitive to surface analysis was reacted to the surface. The oxide surface was reacted with a 5mM (in toluene) solution of a per-fluorinated derivative of octadecyldimethylchlorosilane called (heptadecafluoro-1,1,2,2-tetrahydrodecyl)dimethylchlorosilane. The fluorine content was measured in the XPS.

The second goal of this experiment is to determine the effect the surface treatment has on the roughness of the surface. The roughness of the surface plays a role in the amount of material that can deposit onto the surface. As the roughness of the surface increases, the specific area of the surface increases. This increase in surface area affects the amount of initiator that deposits onto the surface. AFM was used to determine the roughness of silicon chips after being exposed to specific surface treatments. The experimental procedure and results of these experiments are given below.

4.3 Materials and Experimental Procedure

4.3.1 Materials

$VOCl_3$ was stored in a sealed glass bulb and degassed by performing three freeze-pump-thaw cycles before use. Toluene (HPLC grade), was used as received. (Heptadecafluoro-1,1,2,2-tetrahydrodecyl)dimethylchlorosilane was purchased from Gelest Corporation without further purification. 5mM solutions of this material in toluene were mixed and used within 12 hours of performing experiments. All of the studies were performed on 1" x 1" p-type doped silicon wafers. The wafers were cleaned via one of the five following methods: RCA clean, plasma treatment, acid treatment, plasma treatment followed by an acid treatment, and no treatment. After each wafer was exposed to the appropriate surface treatment, one of the following reactions was performed.

4.3.2 Experimental Procedure: Vanadium Reaction

The substrates were placed in a clean glass reaction chamber shown in figure 4.3. This is basically a distillation apparatus. Vanadium oxytrichloride ($VOCl_3$), which was a clear yellow color, was connected to the apparatus where to the distillation flask is shown in figure 4.3. The flask that contained the $VOCl_3$ was separated from the rest of the distillation apparatus by a high vacuum Teflon valve; the $VOCl_3$ was never exposed to the atmosphere after it was purified. After connecting the flask to the distillation apparatus, the $VOCl_3$ was placed in a sand bath which was heated to 40˚C. The wafer chips were placed in the collection flask. Vacuum was pulled on the entire system through a port near the collection flask, and the $VOCl_3$ was allowed to travel to the other side of the column due to the temperature and pressure gradients established. After one hour of reaction time, the $VOCl_3$ was removed from the sand bath. The valve that

separated the $VOCl_3$ from the rest of the apparatus was closed. The vacuum remained on for another 1.5 hours. This procedure was performed to remove any physisorbed material from the chamber. After this period, the vacuum was turned off, the substrates were removed from the collection flask, and they were placed in the XPS chamber for analysis.

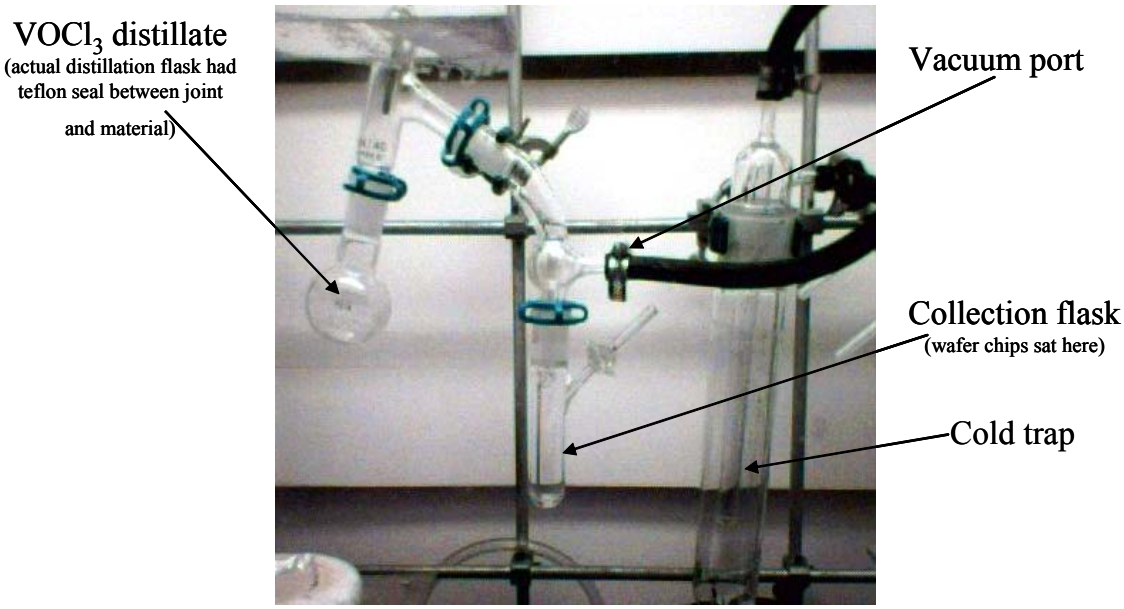

Figure 4.3: Apparatus used for $VOCl_3$ reaction

4.3.3 Experimental Procedure: Fluorinated SAM Reaction

Wafer chips were exposed to a 5mM (in toluene) solution of (heptadecafluoro-1,1,2,2-tetrahydrodecyl)dimethylchlorosilane for 14 hours to ensure maximum surface coverage. They were then removed from solution, rinsed with toluene, acetone, methanol, isopropanol, and finally water. Finally, they were dried in a nitrogen stream and placed in an XPS chamber for analysis of surface chemical composition. All XPS analysis was performed at a take off angle of 45˚. The area of the fluorine 1s photoelectron emission spectrum for each measurement was normalized to its respective oxygen spectrum. (Oxygen in the sample came from the oxide layer and any oxygen that adsorbed onto the

surface from the ambient. Since the entire set of wafer chips were exposed to ambient conditions for a short and equal amount of time, the airborne contaminants did not adversely affect the analysis.)

4.4 Results and Discussion

4.4.1 Vanadium Experiments

After performing the vanadium reaction, the vessel was completely covered with a yellow/red vanadium oxychloride film as shown in figure 4.4 below. (It is unknown as to how many chlorine atoms emanated from the vanadium after the reaction.) The silicon wafers were also covered with a film that produced a color ranging from blue to red on the surface. Since the film is visible, it must have an optical thickness of at least 100 nm. This optical thickness is the product of the true film thickness and its refractive index. If this film is truly a monolayer, then its refractive index must be significantly high. From visible inspection, it is easy to assume that a monolayer did not form on the surface.

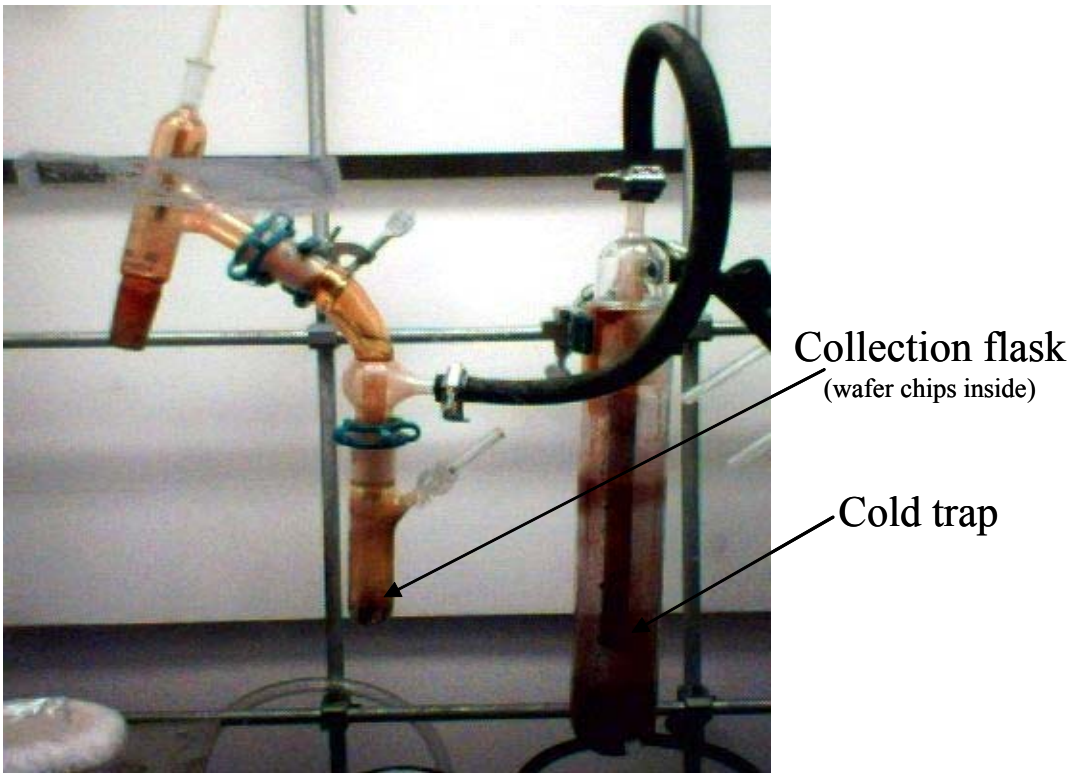

Figure 4.4: $VOCl_3$ apparatus after completion of surface reaction

To quantify this assumption, one can analyze the XPS data. A survey spectrum collected at a take off angle of 45˚of a sample removed from the vanadium reaction flask is shown in figure 4.5 below. This spectrum shows XPS photoemission lines emanating from oxygen (540 eV), carbon (283 eV), and vanadium (627 eV, 515 eV, 66 eV, and 37 eV). No chlorine or silicon emission lines are shown. Since no chlorine is present in the system, it is safe to assume that the material hydrolyzed in ambient. At a 45˚ take off angle, photoelectrons from the top 50Å of the film are emitted into the detector. Since there was no silicon emission, it is safe to assume that this element is not in the top 50Å of the film. Two conclusions can be drawn from this survey spectrum. The vanadium compound hydrolyzed, and the layer of vanadium was thicker than 50Å.

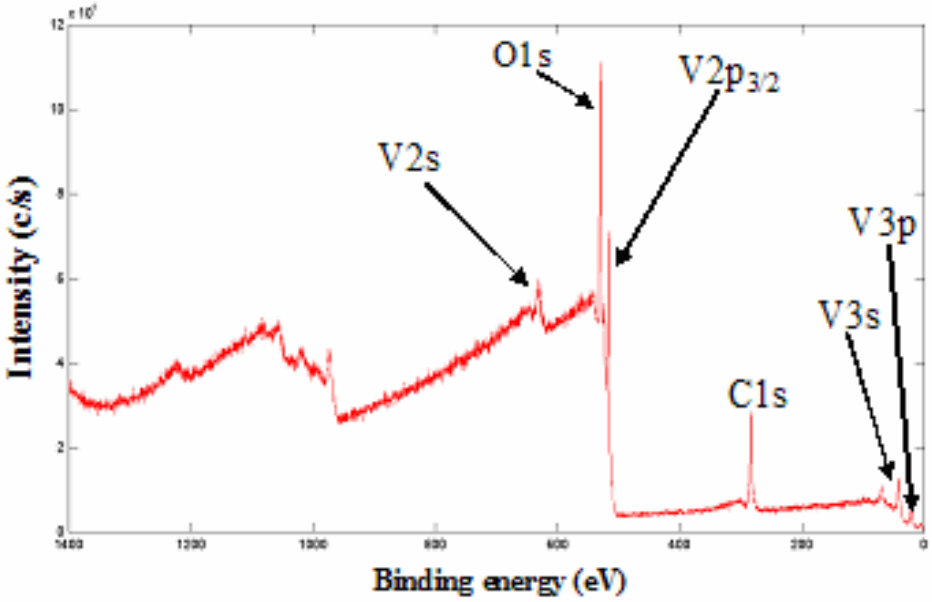

Figure 4.5: Survey spectrum of wafer chip reacted with $VOCl_3$

After scanning this sample, it was washed with acetone, then methanol, isopropanol, and finally water. At the water washing step, the color disappeared. The sample was dried in a nitrogen stream and placed back into the XPS chamber. Another survey scan at a take off angle of 45˚ was taken. This scan is shown in figure 4.6 below. There is no vanadium present on the surface. Silicon is present in this scan. Magnification of the vanadium $2p_{3/2}$ emission from this sample before and after washing is shown in figure 4.7. There are no peaks in this region after the sample was washed. Water washed the vanadium off of the sample. Since a monolayer was not formed on the surface with this vanadium compound and this compound easily washed off with water, it was not used to determine the number of hydroxyl groups emanating from the native oxide surface of the wafer.

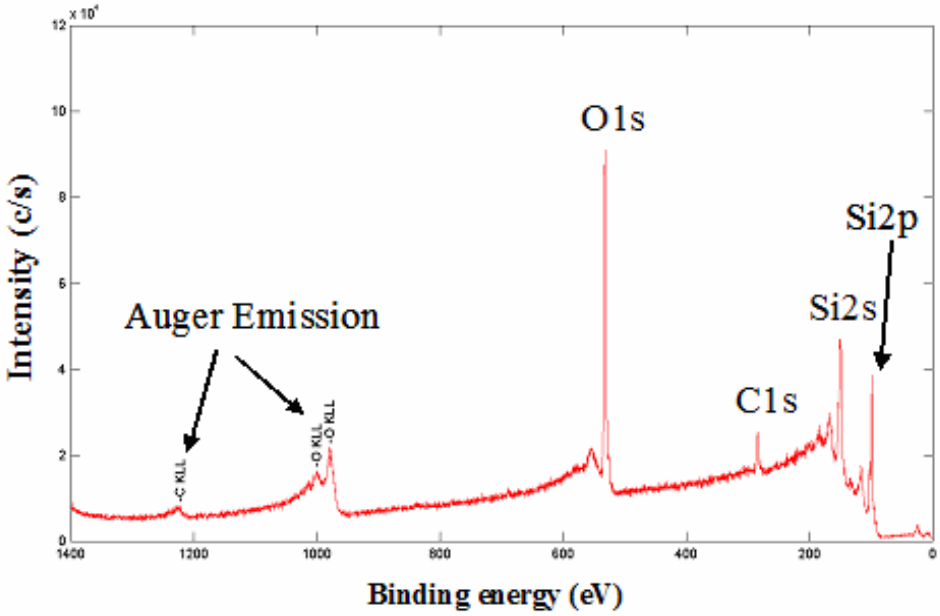

Figure 4.6: Survey spectrum of surface that was washed after the vanadium reaction

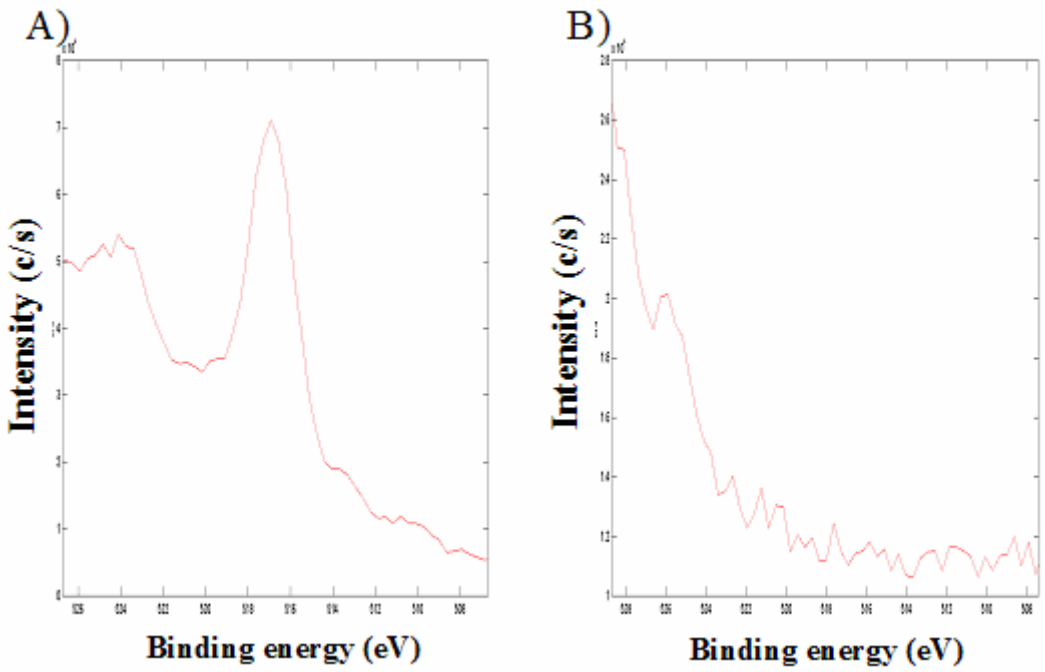

Figure 4.7: Vanadium $2p_{3/2}$ region of x-ray photoelectron spectrum a)after reaction with $VOCl_3$ and b) after washing $VOCl_3$ covered surface with water

4.4.2 Fluorinated SAM Experiments

The results of the fluorinated SAM experiment is shown in figure 4.8.

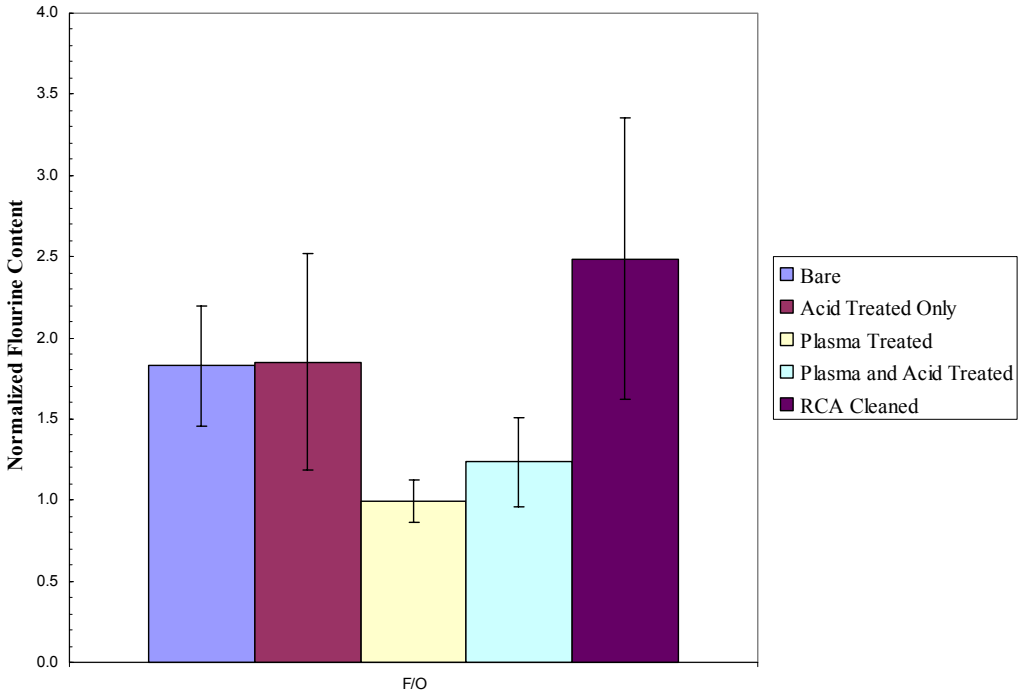

Figure 4.8: Chemical reactivity of silicon surfaces subjected to different surface treatments

As can be seen by the graph above, the RCA clean produced the most reactive surface. The acid treatment came in close second. The RCA clean involves removing the native oxide (HF washing step) and growing a fresh oxide in the subsequent processing steps. It is believed that this procedure is the most crucial in dictating the reactivity of the surface. If it is not the desire to etch this oxide layer (as will be the case in the next chapter), the acid treatment would be the most optimal procedure for maximizing the number of hydroxyl groups on the native oxide surface.

4.4.3 Roughness Experiments

The results of the roughness experiments are shown in figure 4.9. The chemical treatment that provided the smoothest surface was the acid treatment.

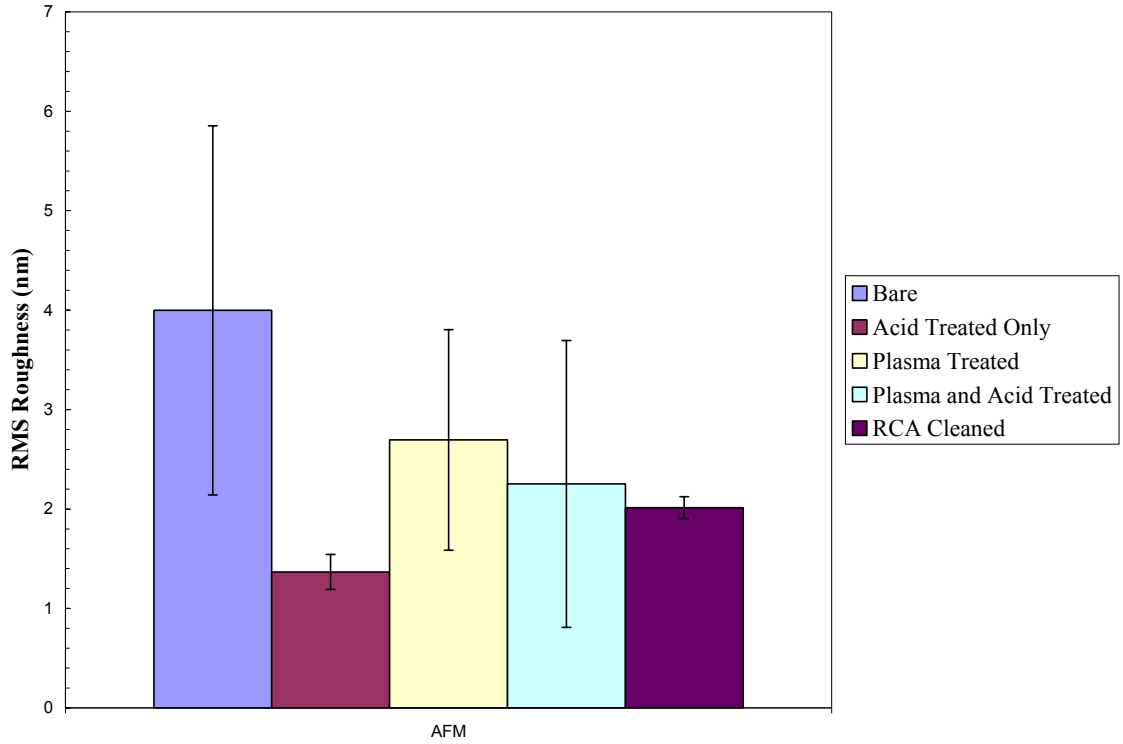

Figure 4.9: Roughness of silicon wafers after surface treatment

4.5 Conclusions

The goal of this chapter is to determine the effect the surface treatment had on both the chemical and physical properties of the native oxide used in this SMIP process. A technique used in the heterogeneous catalysis literature utilizing a vanadium chemistry to determine the chemical availability of hydroxyl groups on high surface area silica surfaces was not deemed adequate to determine the number of hydroxyl groups terminating native oxide surfaces on flat wafers. From analyzing the amount of fluorinated material that reacted with the surface, it was deemed that the RCA clean

provided the surface with the most reactive surface for the deposition process. The acid treatment provided the second most reactive surface for deposition. The acid treatment provided the smoothest surface for deposition. The RCA clean came in second in terms of smoothness. In order to create the smoothest, most reactive surfaces, either the RCA clean or the acid treatment can be employed.

CHAPTER 5

CHLOROSILANE DEPOSITION

5.1 Introduction

The first step in this SMIP process is to deposit the initiator molecules onto the substrate. Specifically, the chlorosilane end groups of the initiator react with the hydroxyl groups terminating the SiO_2 surface, and the initiator self-assembles onto the oxide. Chlorosilane terminated molecules have been extensively studied over the past 20 years to create self assembled monolayers (SAMs) that modify glass surfaces[70]; however, there is debate about the rates and structure of the monolayers that are deposited. The information presented in this chapter serves as a means to clarify some of the issues present in the literature. This chapter discusses the rates of deposition of octadecyltrichlorosilane (OTS), octadecylmethyldichlorosilane (ODS) and octadecyldimethylchlorosilane (OMS) molecules to SiO_2 surfaces by means of the QCM-D technique. Specific features of the absorption of these molecules are also discussed. Optimization of the initiator structure based on the model data is presented. Finally, the rate of deposition of the initiator molecule is predicted from the model silane data.

5.2 Materials Studied

Due to the lack of abundant availability of initiator, model silanes of OTS, ODS, and OMS were used in this study to mimic the deposition of the initiator on quartz surfaces. The structure of the initiator and the model silanes are shown in figure 5.1.

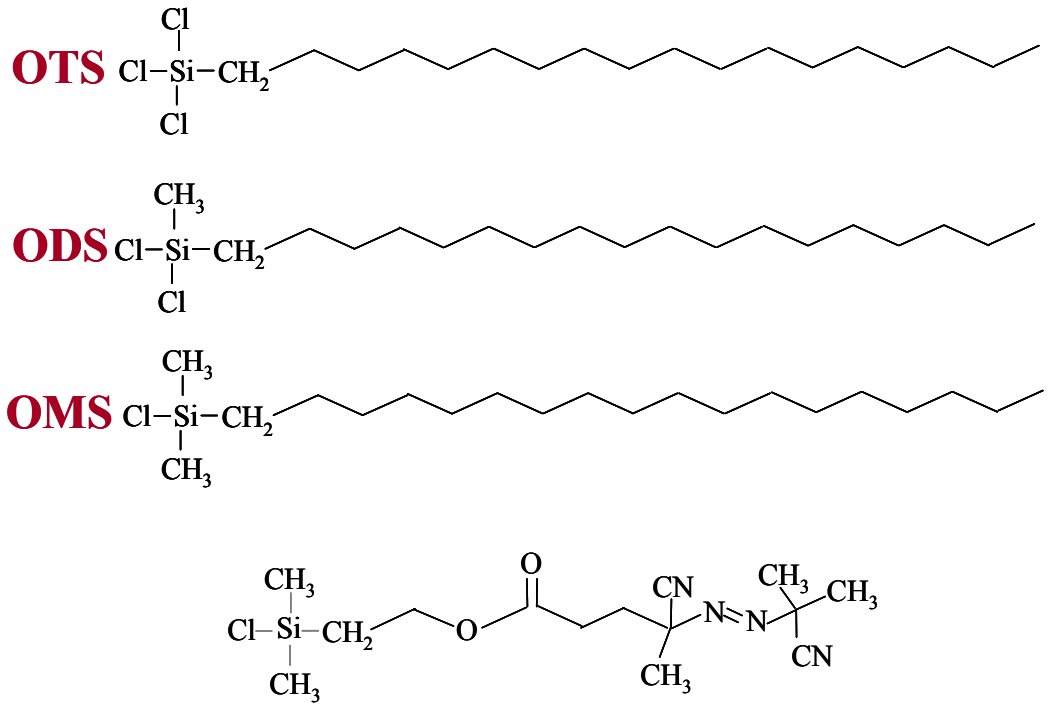

Figure 5.1: Structure of compounds investigated in this study. (OTS) n-octadecyltrichlorosilane, (ODS) n-octadecylmethyldichlorosilane, (OMS) n-octadecyldimethylchlorosilane: the model compounds used for QCM-D experiments; the initiator investigated in this study

5.3 Review of Previous Literature

There are conflicting reports concerning the structure and rates of deposition of silane compounds on surfaces. Most of the studies in the literature have investigated the rates of absorption of OTS onto SiO_2 surfaces, be they silica beads[40, 71] or powders, glass or fused silica[72-74], or thermally grown or native oxide on silicon wafers.[73, 75-77] The investigations regarding the rates of deposition and structure of the SAMs created from these materials can be summarized in the following manner. There is debate as to how OTS deposits onto SiO_2 surfaces. Some argue that the deposition follows a first order Langmuirian kinetic law[73, 76] which is represented in equation 5.1. In the following equations, Γ is the graft density (number of molecules reacting with the surface per unit

area) of the reacting molecule, k is the rate constant of deposition, and C_0 is the bulk concentration of absorbing molecules in solution. A Langmuirian kinetic law assumes that the surface reaction rate is dictated solely by the chemical reaction between the molecules and the surface. The rate constant that defines the deposition reaction of the silane on the surface remains constant throughout the deposition; therefore, the amount of material on the surface should plateau after a significant conversion is reached (as shown in the example in figure 5.2

$$\frac{d\Gamma}{dt} = -kC_0\left[1 - \frac{\Gamma}{\Gamma_{max}}\right] \qquad \textbf{Equation 5.1}$$

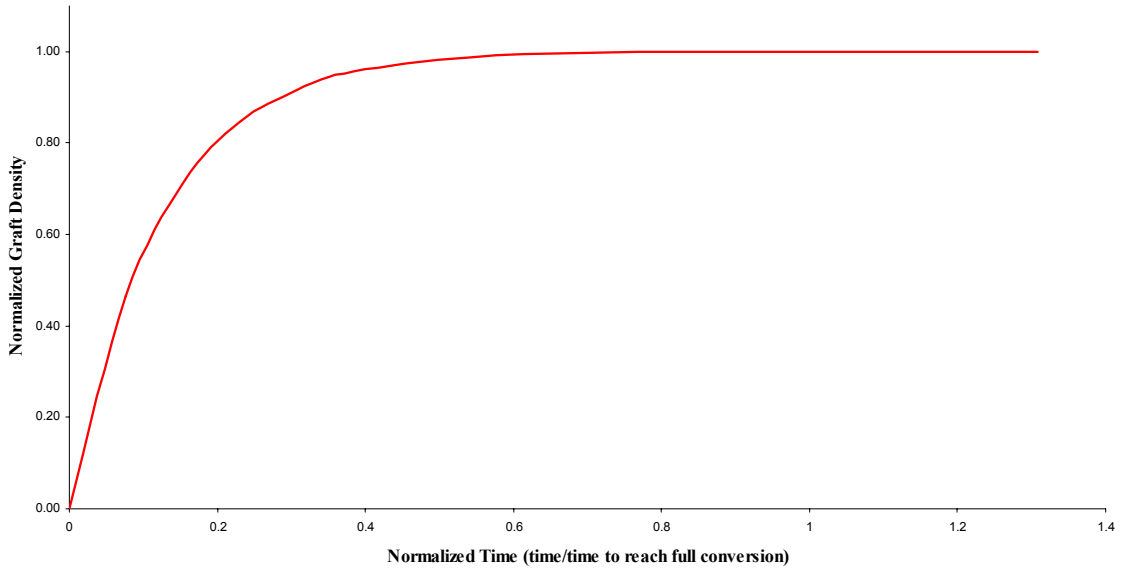

Figure 5.2: Example of Langmuir kinetics

Other researchers have found that the surface concentration never reached a plateau, even after significant time periods. These researchers have proposed alternate models to their data. Helmy et al[78] modeled the deposition of OTS (and other molecules that undergo self-assembly upon reacting with oxides), with a two term Langmuirian model (shown in equation 5.2 below). Their rational for this model is given as follows.

The initial fast reaction rate occurs when the reaction sites are not occupied. As the absorbing molecules reach ~70% coverage, the growth is described by the slow exponent (second term). They mention that the slowing of this process can be caused by slow diffusion of new molecules that must pass through a layer of molecules that are already grafted or by blocking of reactive sites by solvent molecules or other depositing molecules.

$$\frac{\Gamma}{\Gamma_0} = 1 - \alpha e^{-k_1 Ct} - \beta e^{-k_2 Ct} \text{ where } \alpha + \beta = 1 \qquad \textbf{Equation 5.2}$$

Krishnan et al[75] proposed a mechanism in which the molecules react via a Langmuirian mechanism; however, the activation energy of deposition increases as the reaction proceeds (as shown in equation 5.3 below). This increase in activation energy is due to the fact that as the surface becomes occupied, it becomes more difficult for the reacting material to find reactive sites. This mechanism is the most physically feasible of all those presented. After integrating this expression, an equation is established in which the surface density of material continually increases after long reaction times. Krishnan et al probed the deposition of OTS onto the native oxide on silicon surfaces using attenuated total reflection infrared spectroscopy (ATR-IR) and were able to fit their experimental data to this model with extremely low error. In the following equation, E_A^0 is the initial activation energy of the reaction, k_a is the rate constants associated with depositing the molecule to the surface, and k_2 is the rate constant associated with the change in activation energy as the reaction proceeds.

$$\frac{d\Gamma}{dt} = k_a C_b \exp\left[-\frac{E_A^0 + k_2\Gamma}{RT}\right] = k_a' C_b \exp\left[-k_2'\Gamma\right] \qquad \textbf{Equation 5.3}$$

Reports of the rates of deposition of ODS on SiO_2 surfaces are not present in the literature, and only a few researchers have reported the rates of absorption of OMS onto SiO_2 surfaces. Helmy et al investigated the rates of deposition and OTS and OMS on titanium oxide surfaces. They found that the rate of absorption of OMS molecules was significantly lower than those of the OTS molecules. Their data also supports that of Angst et al[79] who also reported that the monolayers of OMS were not as ordered as those of OTS. They argue that the three chlorines on the OTS enable the molecules to cross-link with each other as well as react with the surface. This cross-linking facilitates the formation of a well ordered monolayer. They also argue that the methyl groups that branch off of the silicon atom in the OMS molecule prevent the OMS molecule from forming a dense ordered monolayer on the surface. The data and analysis presented in this document serve to add to this growing body of knowledge.

5.4 Experimental Conditions

Toluene (HPLC grade), was used as received. OMS, ODS, and OTS were purchased from Gelest Corporation without further purification. 5mM solutions of these materials in toluene were mixed and used within 3 days of performing experiments. In QCM-D experiments, toluene washed over the quartz crystal at least five times prior to monolayer deposition. This ensured that the frequency shift associated with the monolayer deposition was solely due to the monolayer (not the solvent). All of the deposition experiments were performed in static mode. The solutions sat in a volume of 100 microliters (μL) above the quartz crystal until the experiment was complete. Given this volume and concentration, approximately 10^{17} molecules of OTS, ODS, or OMS were in the chamber at any given time. If one assumes that the separation between a

silicon atom and an oxygen atom in SiO_2 is 3.58 Å and measures the area of the Q-sense crystals (which is 0.5 cm^2), one can calculate the number of silicon atoms on a surface. If a further assumption is made that each surface atom (silicon and oxygen) terminates in a hydroxyl group on the surface (This is the maximum possible number of hydroxyl groups that could be on the surface.), one counts a concentration of 10^{15} hydroxyl sites on the QCM crystals. The concentration of OTS, ODS, or OMS in solution is at least two orders of magnitude greater than the number of reactive sites on the crystal. There is no way that there can be a concentration gradient of absorbing molecules in the flow cell; therefore, no transport phenomena should have occurred during these experiments.

5.5 Results and Discussion

5.5.1 QCM-D Analysis of Model Silane Deposition

5.5.1.1 Validity of Sauerbrey Relationship

As mentioned in Chapter 3, the Sauerbrey relationship is a simple formula used to calculate the specific mass added to the surface of a quartz crystal. This relationship assumes that the mass added to the quartz crystal can be treated as an equivalent amount of quartz. This assumption is valid if the frequency shift is less than 5% of the fundamental frequency of the crystal and if the material added to the surface is rigid. There are two means to use the QCM data to see if the material deposits in a rigid manner. The first is to normalize the deposition data. If a plot of the frequency shift of all of the overtones divided by its overtone number results in lines that essentially lie on top of each other, the material can be assumed to be rigid.[80] If the plots do not directly lie on top of each other, another test can be used. This heuristic is called the D/f analysis. If the

change in dissipation is at most five times less than the magnitude of the frequency shift of the crystal, the material can be assumed to be rigid.[81] This phenomenon can be tested by plotting the shift in dissipation against the (negative) frequency shift of the crystal. If the overall slope of this line (the absolute magnitude in dissipation shift divided by the absolute magnitude in frequency shift) is less than or equal to 0.2, the material is considered rigid and can be approximated by the Saubery relationship.

5.5.1.2 D/f Plots

In addition to validating the Sauerbrey relationship, the D/f plots also give information as to the structure of the molecules that deposit onto surfaces. OTS and ODS molecules investigated in this study have the potential of forming networks on crystal surfaces. Analyzing the D/f plots will help one elucidate whether or not these materials form networks. If a material is rigid and obeys the Sauerbrey relationship, the D/f plot will look like the example shown in figure 5.3a. Since the material deposits onto the surface in a rigid manner, the dissipation factor will be basically unaffected. The D/f plot will proceed along a shallow slope. (The change in frequency does not produce a significant change in dissipation factor.) The layer then becomes saturated with absorbing molecules. The dissipation factor will essentially remain constant as a few more molecules add to the surface (the frequency continues to decrease) and the slope of the D/f line will approach zero. Once the layer is fully saturated with molecules, D and f will remain essentially constant and a cluster of points will appear at the right of the graph. The absolute change in dissipation divided by the absolute change in frequency is less

than 0.2.

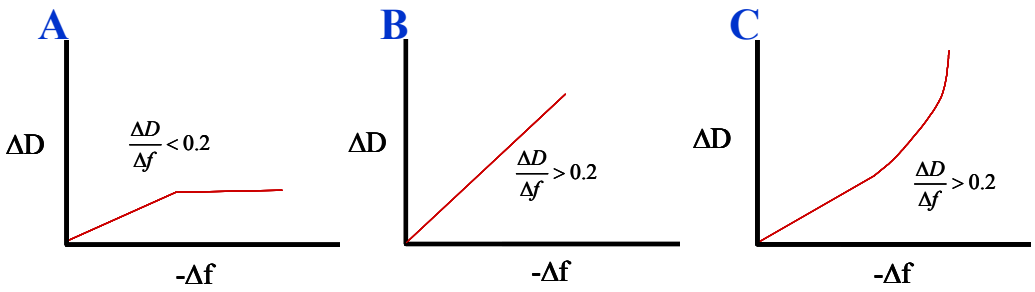

Figure 5.3: Example D/f plots of different types of material depositing onto QCM surfaces. (a) a rigid material depositing on the surface, (b) a floppy material depositing on the surface, and (c) a material depositing and forming networks on a surface

A D/f plot of a viscoelastic material depositing onto a surface looks similar to that shown in figure 5.3b. Since the material deposits onto the surface in a floppy manner, the dissipation factor increases at a rate comparable to the shift in frequency; the slope of the D/f line is greater than 0.2. At the end of the deposition process, the dissipation and frequency will remain constant, and a cluster of points will appear at the top right corner of the graph. Figure 5.3c is an example of the D/f plot that results from a material that has more than one reactive group and is able to form networks on the quartz surface. ODS and OTS are examples materials that have the potential to form networks. Initially, the molecule deposits onto the surface in either a floppy or rigid manner. The frequency and dissipation factors shift according to the phenomenon shown in the initial stages of figure 5.3a or 5.3b. After the surface becomes saturated, the material begins to form a network on the surface. The network material is not as rigid as the initial layer formed, and the dissipation begins to increase at a rate greater than the frequency shift associated with the extra mass added to the surface. The slope of the curve increases significantly.

By analyzing the frequency shift and the D/f plots of these model silanes, one can gain insight into the rate of deposition and the structure of model silanes onto silicon oxide surfaces.[82] This information can be used to predict the rate of deposition and structure of these SMIP initiator layers on surfaces.

5.5.1.3 Deposition of Octadecyltrichlorosilane on Quartz Surfaces

The QCM-D was initially used to model the deposition of OTS on surfaces in order to compare the QCM-D data to the abundant amount of data in the literature. The frequency shift associated with depositing OTS onto an untreated quartz crystal is shown in figure 5.4 below. The normalized frequency shifts do not lie on each other; the Sauerbrey relationship is an invalid means to approximate the data. It also appears that it takes a long time for this material to absorb onto quartz surface. The shift in frequency remains constant only after 100 minutes of absorption.

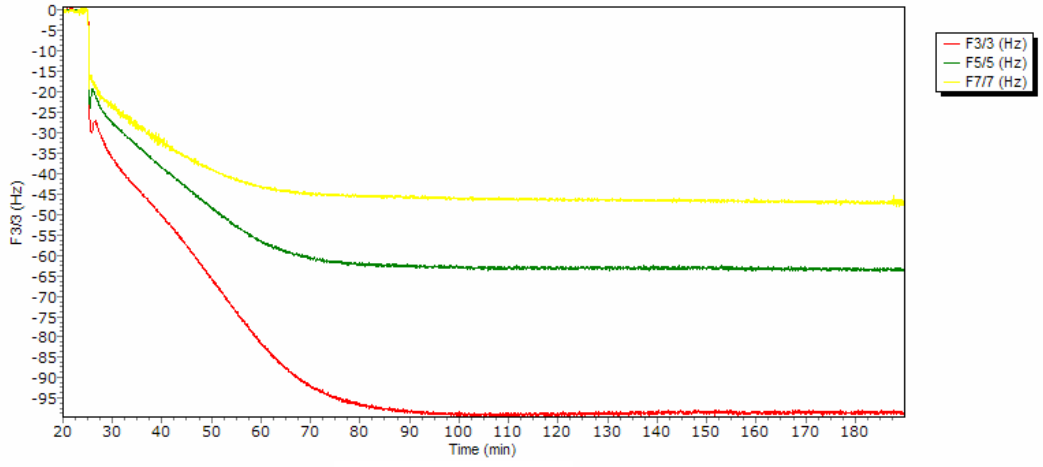

Figure 5.4: Frequency shift associated with deposition of 5mM OTS in toluene onto a new quartz crystal.

Analysis of the D/f plots gives some insight as to how this material deposits onto the surface of the quartz crystal. The D/f plot associated with the third harmonic of this process is shown below. This plot mimics the general shape shown in figure 5.3c. There is clear evidence that this material forms a network on the surface of the quartz crystal.

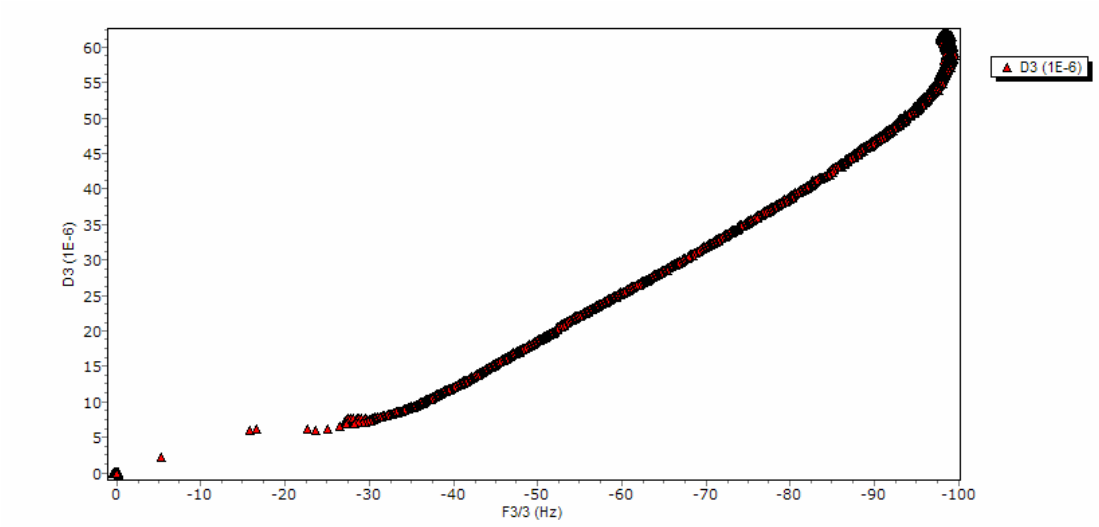

Figure 5.5: D/f Plot associated with the absorption of OTS onto a quartz crystal

After the OTS layers absorb to form a layer on the surface of the crystal that corresponds to a 20 Hz mass uptake, the layer starts to form networks on the surface. The A frequency shift of 20 Hz occurred almost immediately after introduction of the OTS molecules; therefore, the rate of deposition of these materials is very fast. The overall slope of the D/f plot associated with OTS absorption is 0.6, which is considered by the QCM-D heuristic to be a viscoelastic layer. Other researchers analyzed the rigidity of the layer via IR; the vibrations associated with the methylene stretches exhibit a higher frequency in the amorphous state than in the rigid state. After about an hour, the vibrations associated with methylene stretching exhibit a negative frequency shift of about 20 cm^{-1}, which indicates that the layer is rigid on the surface. This experiment can

be performed on the OTS layers QCM analysis to see if the 0.6 D/f slope corresponds to a rigid layer in the IR.

5.5.1.4 Deposition of Octadecylmethyldichlorosilane on Quartz Surfaces

The deposition of dichlorosilanes is a little more complex than that of OTS. Depending on the surface treatment, the frequency shift and the D/f plots associated with the deposition of the dichlorosilanes exhibits different behavior. In figure 5.6 below is a plot of the deposition of ODS onto a previously used crystal that was treated with acid before deposition. In the initial stages of the deposition, the normalized frequency shifts tend to lie on top of each other. As the deposition proceeds to higher conversion, the normalized frequency shifts deviate from each other, and the material appears to deposit on the surface in a viscoelastic manner.

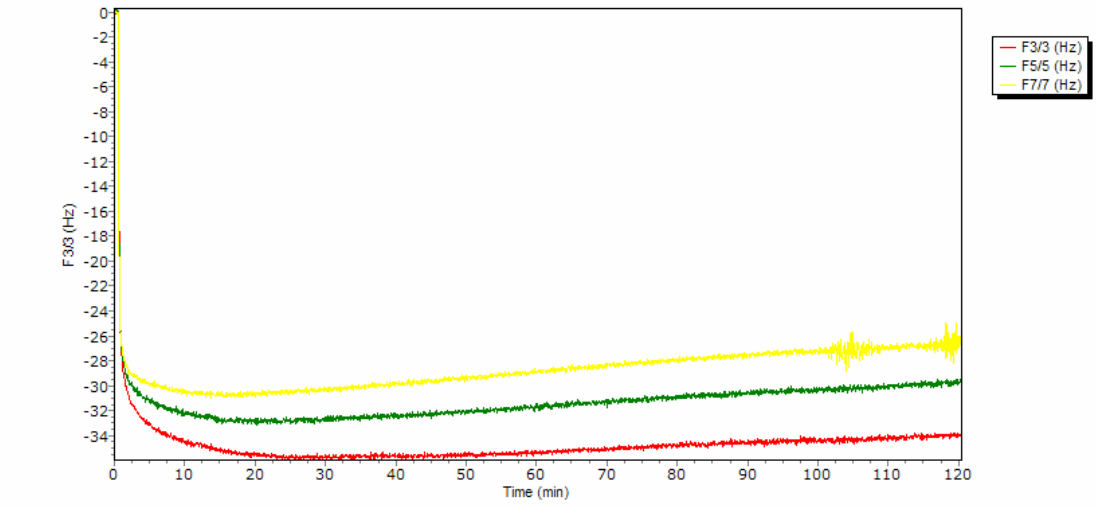

Figure 5.6: Frequency shift associated with the deposition of ODS onto an old quartz crystal that was treated with acid only.

The D/f plot of this deposition is shown in figure 5.7. The ODS molecules appear to deposit via a rigid mechanism. (The slope of the D/f plot is around 0.10) After the

material deposits enough mass to create a 20 Hz shift in the fundamental frequency of the crystal, the ODS molecules appear to form a network on the surface as exhibited by the increase in slope of the D/f plot after 20 Hz of deposition.

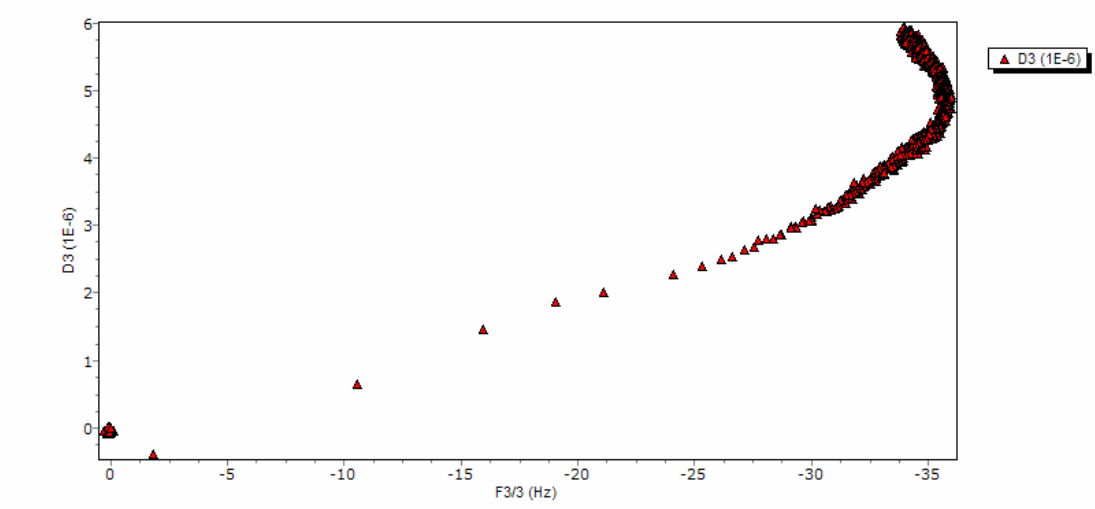

Figure 5.7: D/f plot associated with the deposition of ODS on a previously used QCM crystal treated with acid only.

The deposition of ODS on a more precisely treated crystal proceeds in a different manner. The frequency shift associated with the deposition of ODS on a new crystal that has been plasma treated and then acid treated is shown in figure 5.8. The normalized frequency shifts of the overtones lie on essentially the same line for the duration of the experiment, which indicates that the ODS molecules are depositing in a rigid manner. The ultimate frequency shift associated with the deposition of these molecules is about 24 Hz, which corresponds to a molecular uptake of about 7 x 10^{14} molecules/cm^2 or 10 μmol/m^2. This level of uptake is comparable to levels reported of trichlorosilanes depositing onto silicon oxide surfaces.[71]

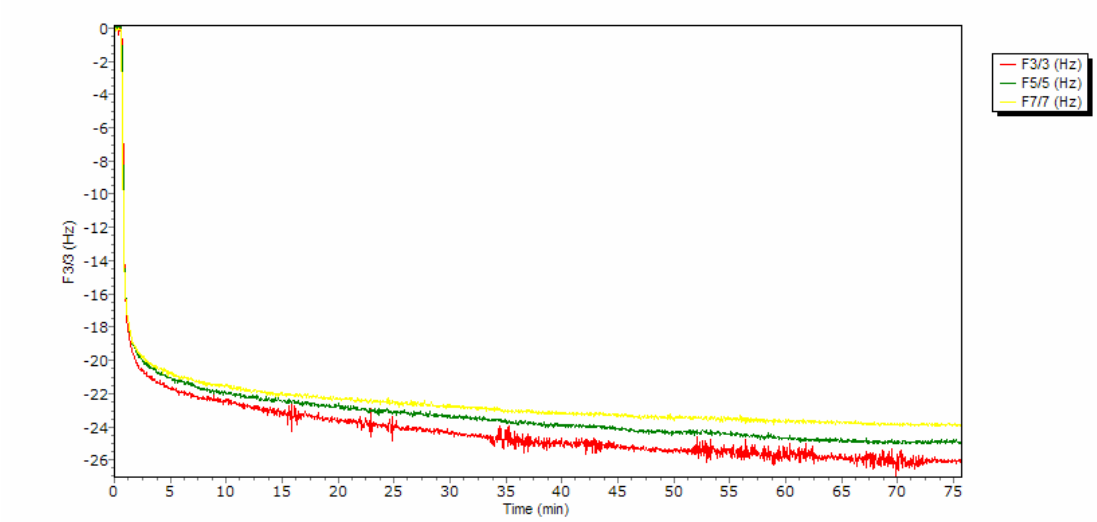

Figure 5.8: Frequency shift associated with the deposition of OMS onto a new crystal that was plasma and acid treated

The D/f plot of this absorption process supports the claim that the material deposits in a rigid manner. In figure 5.9 is the D/f plot of associated with this deposition process. The plot mimics the example plot shown in figure 5.3a; the deposition of the material can be modeled by the Sauerbrey relationship. (The slope of the D/f plot is 0.15)

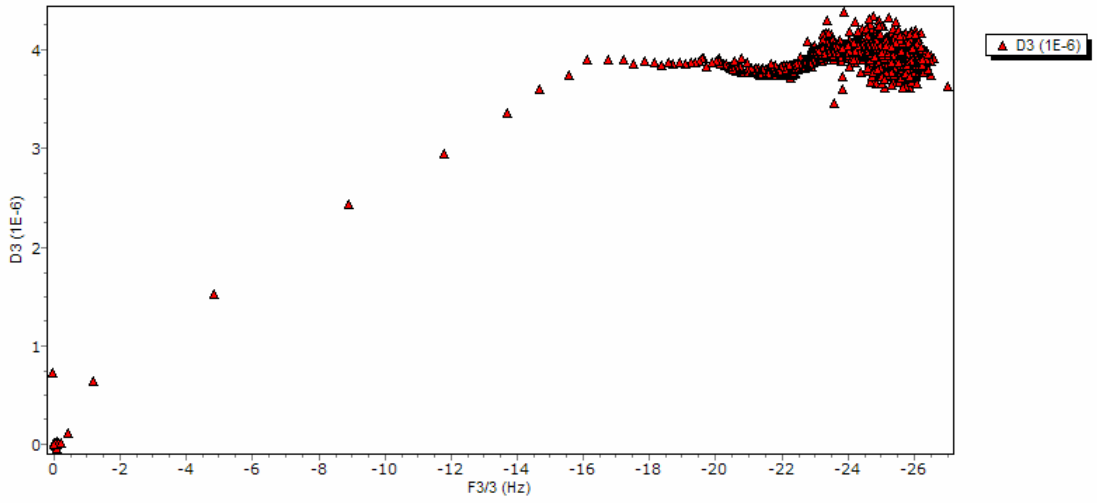

Figure 5.9: D/f plot associated with the deposition of ODS onto a new crystal that has been plasma and acid treated

Since the mass uptake is directly proportional to the frequency shift of the crystal (Sauerbrey relationship), the frequency shift can be directly modeled to ascertain the rates at which ODS molecules deposit onto surfaces. In figure 5.10 is shown the mass uptake associated with this deposition modeled by both the Simple Langmuir equation (equation 5.1) and the Langmuir equation modified to account for an increase in the activation energy as the reaction proceeds (equation 5.3). (This fitting was performed using the Solver tool in Microsoft Excel.) As seen in this graph, the fit is somewhat off at the initial stages of deposition for both models. A better equation is needed to model the entire process of deposition of the ODS molecules. The D/f plot does give information about the time associated with processing this material. The slope of the D/f plot becomes flat after 16 Hz of material has been placed on the surface. A 16 Hz uptake takes place within 5 minutes of depositing the ODS onto the surface. After 20 minutes, the layer is essentially saturated. Therefore, ODS can be processed to form a monolayer on silicon oxide surfaces in less than half an hour.

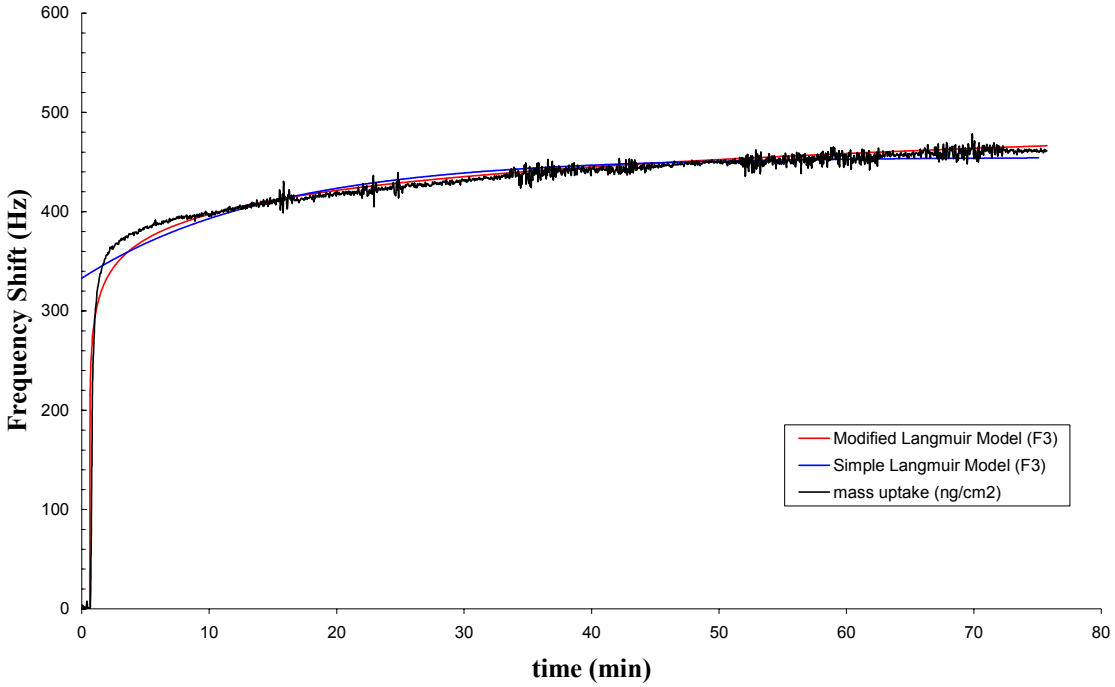

Figure 5.10: Models used to approximate the deposition of ODS on quartz crystal surfaces that have been treated with plasma and acid

5.5.1.5 Deposition of Octadecylmonochlorosilane on Quartz Surfaces

The frequency shift associated with the deposition of octadecyldimethylchlorosilane onto quartz crystal surfaces is shown in the figure 5.11. This molecule deposits in a manner in which the monolayer is more floppy than the monolayer of ODS, yet the layer does exhibit some order. The frequency shifts of the overtones associated with the absorption of OMS onto an acid treated quartz crystal surface are shown below. The normalized frequency shifts overlap with an error of about 6Hz.

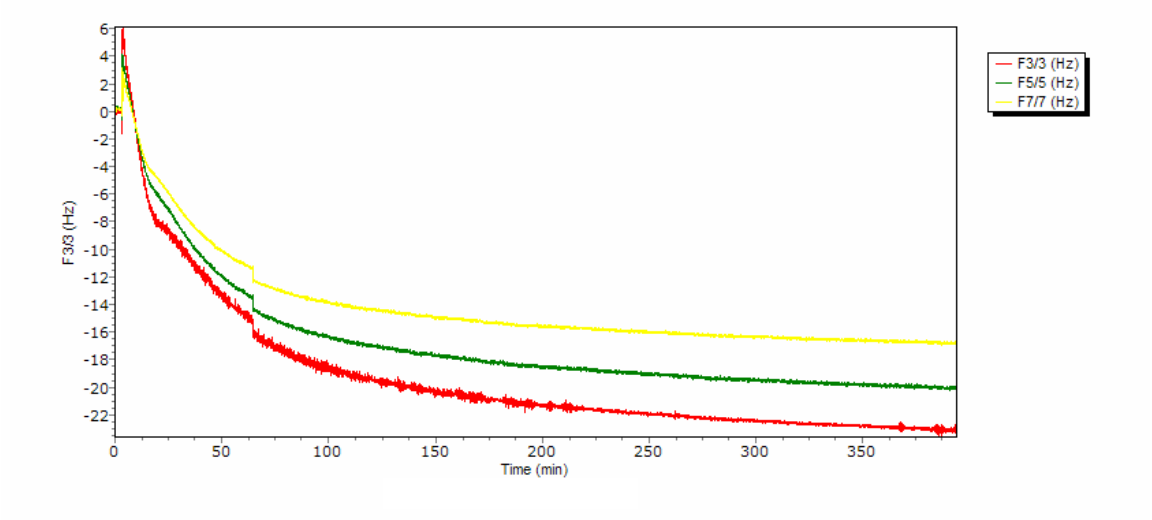

Figure 5.11: Frequency shift associated with the absorption of OMS onto an acid treated quartz crystal surface

The D/f plot of the deposition of this molecule is shown in figure 5.12. The overall slope of the D/f plot is about 0.6; therefore, it is questionable if this process can be modeled via Langmuir reaction kinetics. An attempt was made to model this data with both the simple and modified Langmuir models. The error could not be minimized when modeling the data via the modified Langmuir model (as shown in Figure 5.13). As shown by the figure 5.11 above, it takes approximately 6 hours for the frequency to decrease by 20 Hz. It takes the dichlorosilane minutes to decrease by the same amount. The rate constant for absorption is obviously an order or magnitude smaller for the absorption of monochlorosilanes than for dichlorosilanes. If it takes half an hour for the ODS to form a saturated layer, then it takes about 1.5 hours for the OMS to saturate the surface.

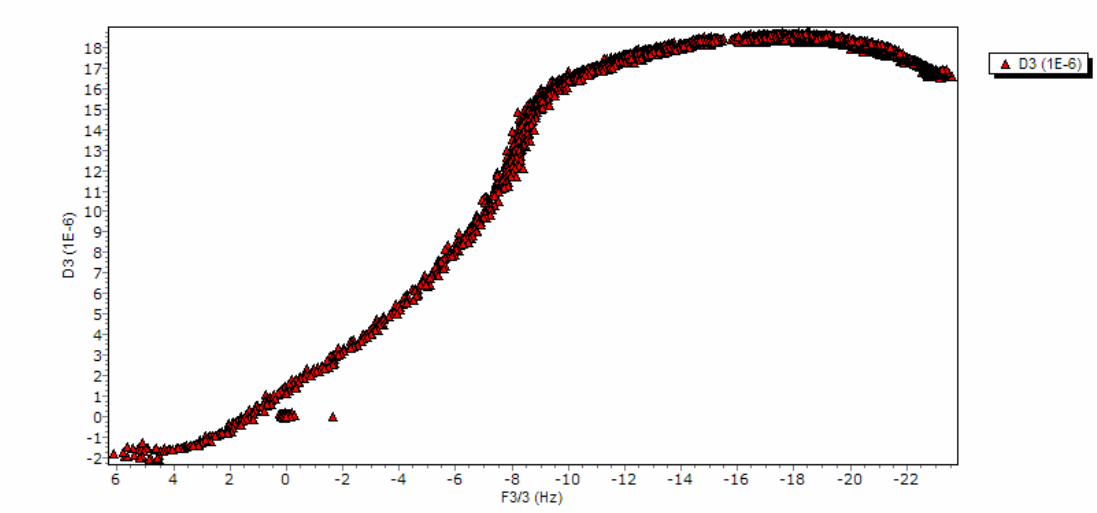

Figure 5.12: D/f plot associated with the absorption of OMS onto an acid treated surface

The rate of deposition of the OTS molecules is faster than that of the ODS molecules which is faster than that of the OMS molecules. The OTS molecules, however, quickly form networks on the quartz surface, and the deposition of these molecules cannot be controlled. ODS molecules, however, can be made to deposit in an ordered monolayer on a silicon oxide surface if that surface is treated in a way that the number of surface reactive sites is enhanced. OMS deposits to form a layer that is not as rigid as ODS. OMS also deposits onto quartz surfaces at a rate that is significantly slower than that of ODS.

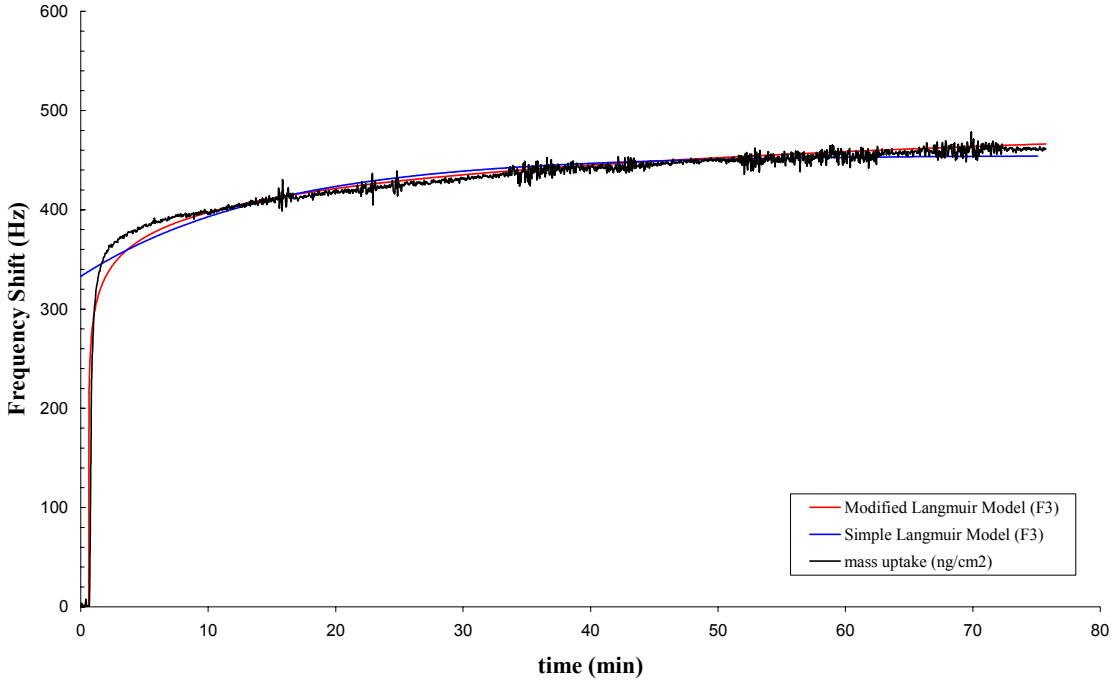

Figure 5.13: Modeling of OMS absorption onto acid treated surface

5.5.2 Prediction of Initiator Deposition

The end group of the initiator is a monochlorosilane; therefore, it should deposit at essentially the same rate as that of OMS. It should, therefore, take hours for initiator molecules to form a monolayer on SiO_2 surfaces. The initiator is shorter and that of OMS and therefore has the potential to form a more rigid layer[83]; however, the initiator also contains carbonyl and azo groups which may adversely affect its ability to pack well on the surface. Further analysis of the impact of the structure of this particular initiator on its packing is needed.

	Simple Langmuir Model	Modified Langmuir Model	
	k	k_a'	k_2
ODS	6.17×10^3	8.07×10^4	4.19×10^1
OMS	1.95×10^3	1×10^{-2}	6.7×10^3

Table 5.1: Summary of rate constants obtained from modeling QCM deposition data

5.6 Proposed Optimal Initiator Structure

A time scale on the order of hours for absorbing the SMIP initiator is unacceptable for processing samples for this NGL process. The chemistry of the initiator needs to be tailored for faster deposition. A simple way to alter the structure of this initiator to increase the rate of absorption of the initiator is to change the chemistry of its anchor group. This can be done by synthesizing an initiator with a dichlorosilane end group. The synthesis of this dichlorosilane initiator has been reported by Prucker et al[39] and alters only one step in the monochlorosilane initiator synthesis. The structure of this dichlorosilane initiator is shown below in figure 5.14.

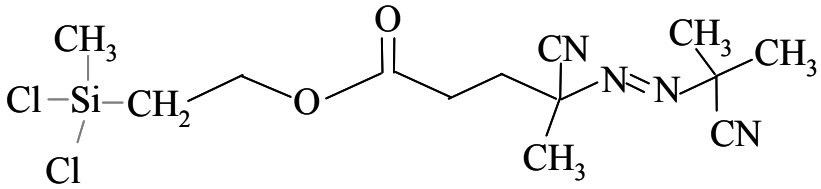

Figure 5.14: Initiator structure optimized for surface deposition

5.7 Conclusion

The rates of deposition and structure of chlorosilane molecules onto quartz crystal surfaces has been investigated to predict the rates of absorption of SMIP initiators on

silicon oxide surfaces. The rates of deposition depend on both the method by which the surfaces have been treated and the anchoring group of the depositing molecule. Trichlorosilanes deposit onto surfaces quickly; however, the structure of the monolayer deposited cannot easily be controlled. Dichlorosilane molecules can be tailored to form ordered monolayers onto quartz surfaces with relatively high rates of deposition. Monochlorosilanes form floppy layers onto quartz surfaces with rates of deposition that are an order of magnitude lower than that of dichlorosilanes. SMIP initiator layers used in these studies are monochlorosilanes; therefore, it is predicted that they deposit on quartz surfaces at relatively low rates. In order to optimize the rate of deposition of the initiator layers onto the surfaces, its chemistry can be modified to contain a dichlorosilane end group. This dichlorosilane can decrease the time of deposition significantly. It is uncertain as to whether or not this layer will form a well ordered monolayer on the surface. The impact of the structure of the initiator on its packing density and rigidity needs to be explored.

CHAPTER 6

PHOTOCHEMICAL DECOMPOSITION OF INITIATORS

6.1 Introduction

The second step of the processes involved in creating patterned polymer films via this SMIP process is to photochemically decompose the initiator layer to create a pattern in it. After the photochemical decomposition, the remaining initiator sites are thermally decomposed in the presence of monomer to form patterned polymer films. This chapter discusses the deep ultraviolet (DUV: 248 nm) photochemical decomposition of the initiators used for this process. The photochemical sensitivity of these compounds are compared to other SAMs being evaluated as ultra-thin etch masks. A means for optimizing the rate of photochemical decomposition of the initiator ends this chapter.

6.2 Materials Studied

The general structure of the initiators was mentioned in Chapter 2 and is briefly reviewed in figure 6.1. The initiator has four basic sections: the anchoring group, the spacer, the free radical generator (azo group), and the end group. Two initiators were analyzed in this study. Both of these initiators have chlorosilane anchoring groups for attaching the initiator to hydroxyl terminated SiO_2 surfaces. Both initiators also have ester groups in the spacer unit. These ester groups serve as the cleavable unit in the initiators. The difference between the two materials lies in the end group. Initiator A has a chlorosilane end group which allows the molecule to be doubly attached to surface. Initiator B has a methyl terminated end group.

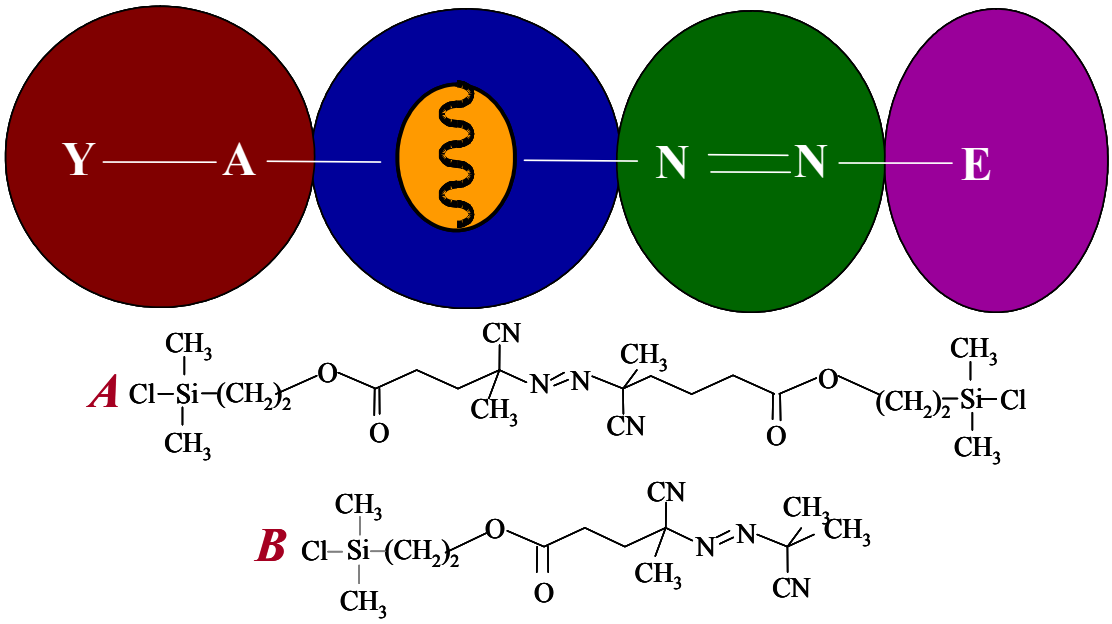

Figure 6.1: General initiator structure and specific initiators used in this study

6.3 Data Calibration

The rates of decomposition of these initiators were monitored via XPS. X-rays that impinge upon the sample from the XPS also decompose the initiator; therefore, before analyzing the decomposition of these initiators, a calibration curve was established to determine the extent to which the x-rays decomposed the monolayer. A silicon sample coated with the initiator was placed in the XPS and data scans were collected at various time intervals while the x-ray exposed the surface.

6.3.1 Determining the Location of the Azo Peak

The first task in evaluating this data was to determine the location of the azo (N=N) peak. There are two types of nitrogen in the system: The first stems from the nitrogen triply bound to carbon in the cyano (C≡N) group in the initiator molecule. The

second stems from the azo group. A scan of the nitrogen region of the initiator A is shown in figure 6.2. The largest peak in the spectrum centered at 400.22 eV is assigned to the nitrogen in the cyano group. This assignment was made based on literature values;[84, 85] therefore, the second peak at 401.65 eV was assigned to the azo nitrogen. In these initial scans, the full width half maximum of both peaks was equal and assigned to 1.15 eV. For all subsequent fitting, the full width half maximum of both of the peaks was equal.

The area under the azo (N=N) peak in the XPS spectrum was normalized to the area of the SiO peak (at 103.3 eV). The electrons reaching the detector were emitted from the top 50Å of the film which consisted of ~20 Å of the initiator layer, the ~20 Å of native silicon dioxide, and about 10Å of the underlying silicon substrate. The thickness of the monolayer decreased as it decomposed, and a greater contribution of the electrons reaching the detector were emitted from the silicon substrate. In the stack that was analyzed, a constant number of electrons were emitted from the silicon oxide layer. In the silicon spectrum, the SiO peak, which identifies the presence of the native oxide, was used as a constant of normalization.

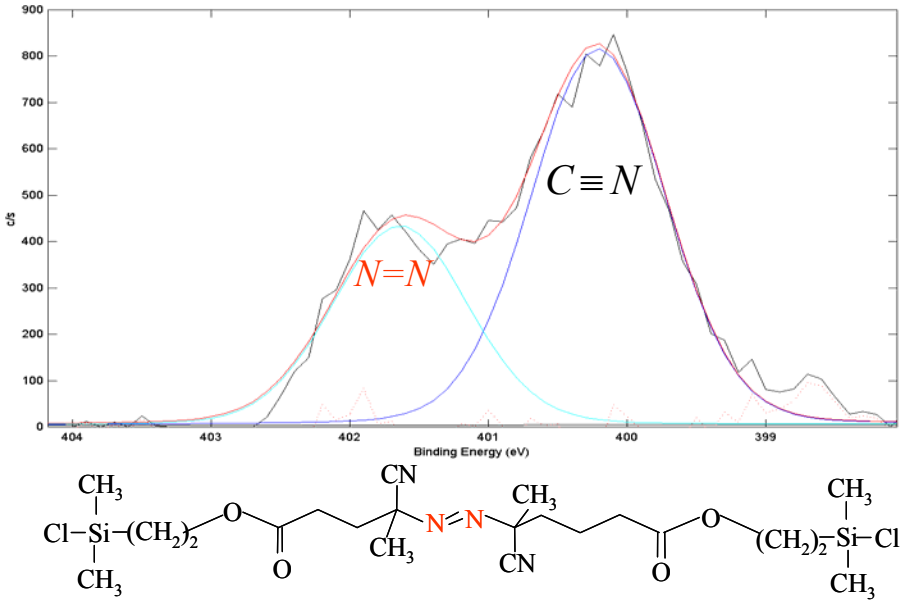

Figure 6.2: Nitrogen spectrum of initiator A unexposed. This serves as an example of the shape and fit of the nitrogen spectrum before the initiator has undergone DUV exposure.

After identifying the azo peak and the peak to which it should be normalized, a calibration curve for the decomposition of the initiator upon exposure to x-rays was generated. A plot of the natural logarithm of the azo peak area versus exposure time to the x-rays from the XPS system is shown in figure 6.3. This plot exhibits a linear relationship; therefore, the decomposition of the monolayer in the XPS is a first order process. This calibration plot was used to adjust all XPS measurements of the azo peak area to account for the varying lengths of time that samples were exposed to the x-ray beam during XPS analysis. Most of the XPS spectra were acquired in less than 2 minutes; therefore, only small amounts of initiator decomposed as a result of data collection.

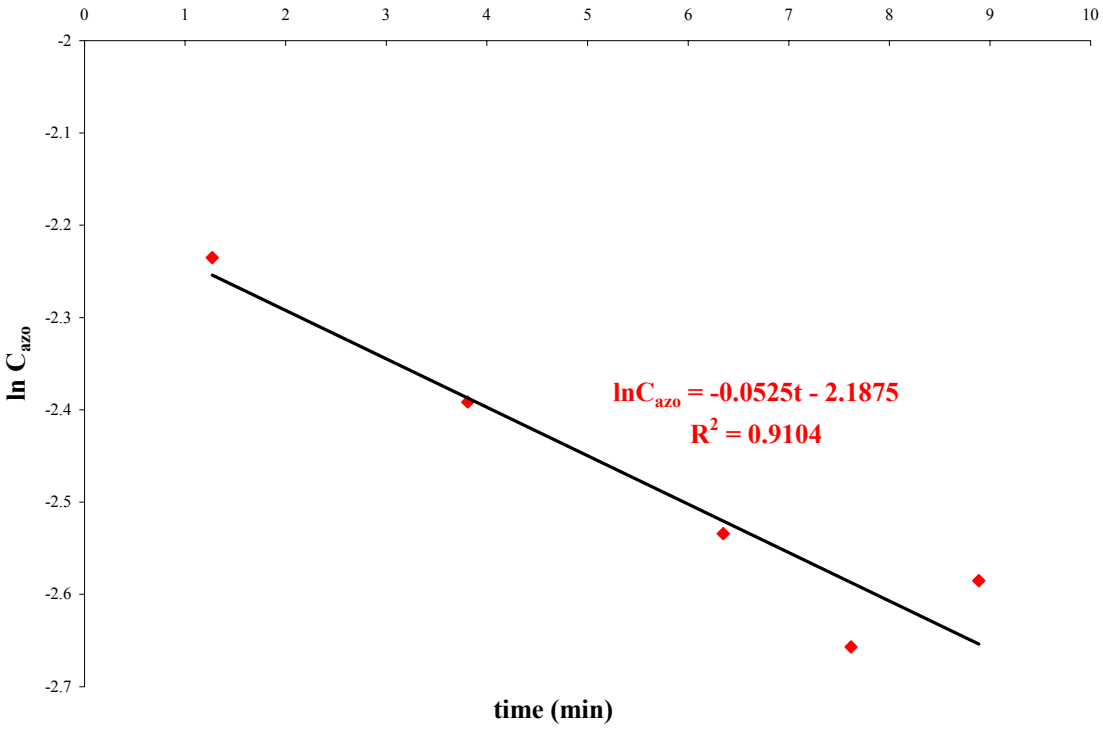

Figure 6.3: First order rate plot of the decomposition of the initiator in the XPS

6.4 Results and Discussion

6.4.1 Photochemical Decomposition

The resulting plot of the azo peak area as a function of DUV (248 nm) exposure dose for initiators A and B is shown in figure 6.4. The decomposition of both initiators follows first order kinetics as indicated by figure 6.5 which shows a linear relationship between the natural logarithm of the fraction of initiator remaining on the surface as a function of dose.

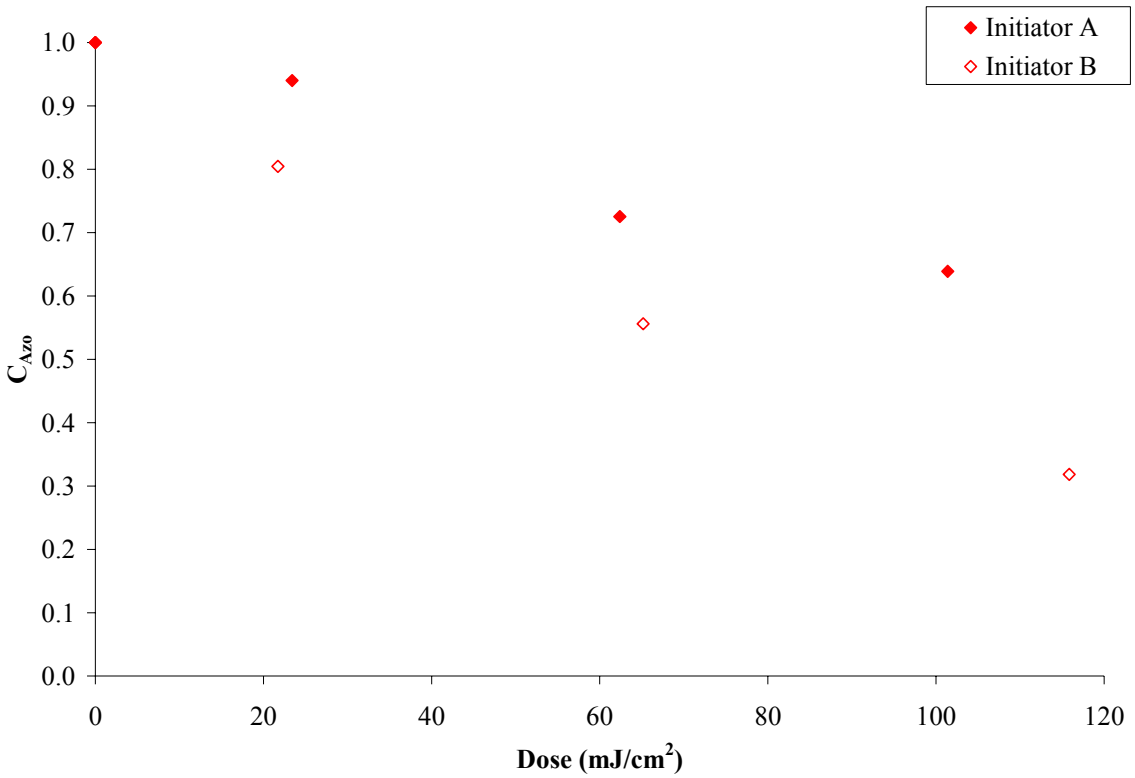

Figure 6.4: Azo concentration versus dose for initiators A & B

Using this slope of the trend line generated by the data, one can derive a simple relation to estimate the dose required (D) to achieve a desired fraction of initiator remaining (X) on the surface as shown in the following equation.

$$D = -\frac{\ln(x)}{slope}$$ **Equation 6.1**

Using this equation, one finds that to achieve 99% conversion of initiator A by exposure to DUV light one must provide an exposure dose of 1 Joule per square centimeter (J/cm^2). The dose required to decompose 99% of initiator B is 475 mJ/cm^2. These doses are lower than those observed by other scientists decomposing self-assembled monolayers on flat surfaces. Ultraviolet doses between 1 and 20 J/cm^2 are usually required to fully decompose straight chain hydrocarbon SAMs to form patterns

on surfaces.[86-89] In one case, a dose of 54 J/cm^2 was required to pattern the SAM.[90] There are only two reports in the literature of SAMs having a greater sensitivity than this. Researchers at the Naval Research Laboratory have been able to decompose phenyl terminated SAMs[91] and amine terminated SAMs[92] at doses of ~ 400 mJ/cm^2 by exposing at a wavelength of 193 nm. At this wavelength, most organic compounds have strong absorbance; therefore, many compounds will show strong ablation phenomena.

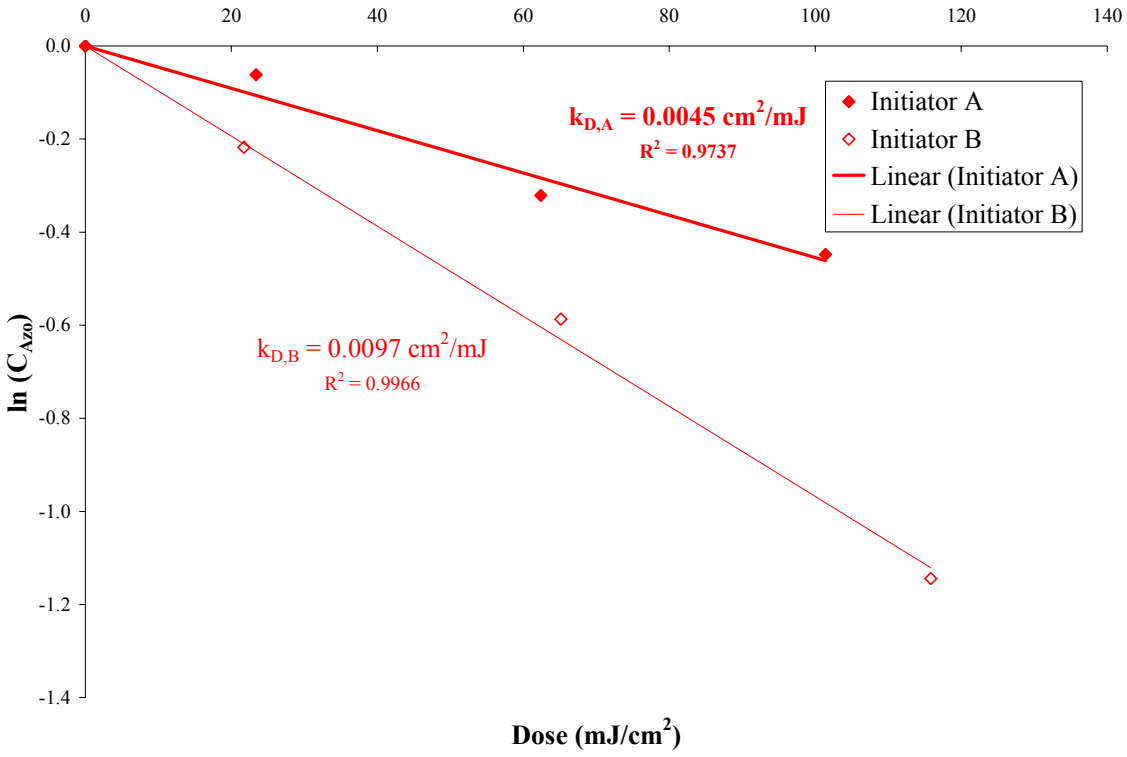

Figure 6.5: First order rate plot of the decomposition of initiators A & B

Though the doses required to decompose these samples are lower than those reported by others, they are unacceptable for an NGL application. The International Technology Roadmap for Semiconductors (ITRS) states that the sensitivities of current and future generation resists should be between 40 and 50 mJ/cm^2; therefore, it is

required to optimize the sensitivity of these initiators for next generation lithography. Initiator B decomposes at twice the rate of initiator A. These rate constants are a product of the molar absorptivity (ε [cm^2/mJ]) and the quantum efficiency (Φ [dimensionless]) of the molecules as shown in equation 6.2.

$$k = \varepsilon\phi$$ **Equation 6.2**

Collecting ultraviolet spectra of the molecules will aid in elucidating which factor is predominant in the difference in their photochemical behavior. Figure 6.6 shows the solution ultraviolet spectra of these materials. The table above the spectra shows the molar absorptivity and the calculated quantum efficiency of these molecules at 248 nm. Initiator A exhibits a molar absorptivity that is 30% higher than that of initiator B at this wavelength; however, the rate constant of photochemical decomposition of initiator B is greater than that of A. The difference in the rate constants is primarily due to the quantum efficiency of each molecule.

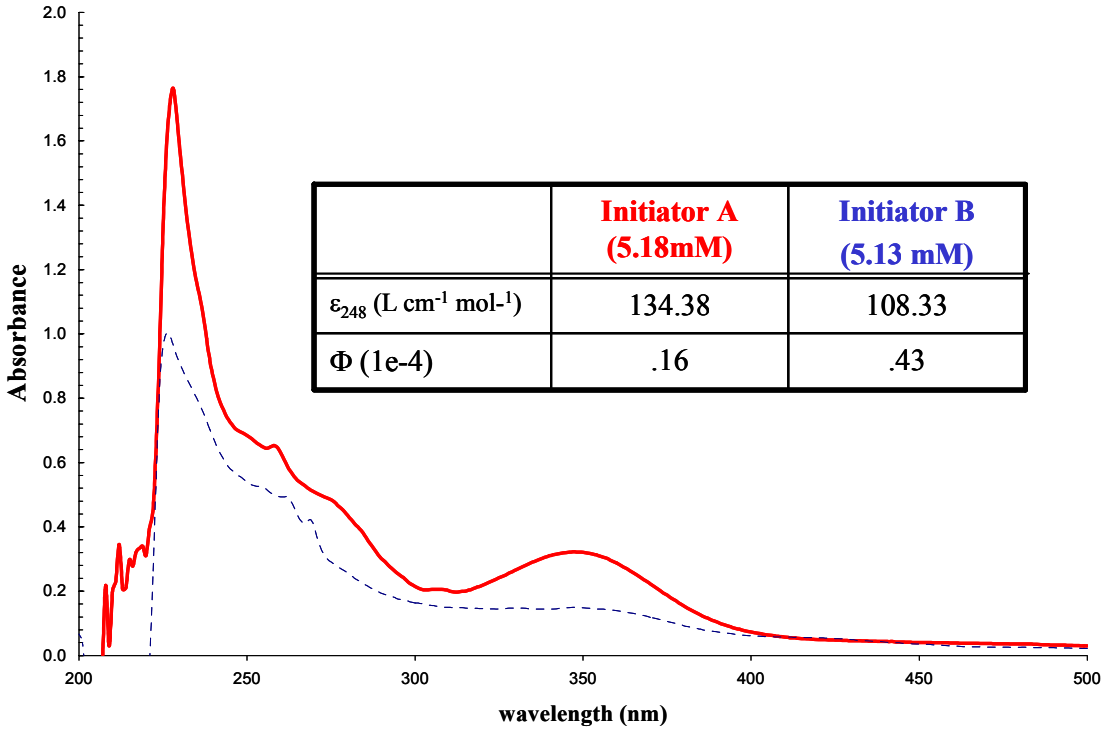

	Initiator A (5.18mM)	Initiator B (5.13 mM)
ε_{248} (L cm^{-1} mol^{-1})	134.38	108.33
Φ (1e-4)	.16	.43

Figure 6.6: Ultraviolet spectrum and table of molar absorptivity and quantum efficiency of initiators A & B. The spectra were obtained in methylene chloride (CH_2Cl_2)

The structure of these molecules can give insight as to why the quantum efficiency of these materials is so different. Both ends of initiator A have the ability to bind to the surface. With both ends of initiator A tethered to the surface, the probability of recombination of the fragments of this molecule is great. Even if only one end group of initiator A is tethered to the surface, the other end is bulky and will not leave the surface easily after the molecule has decomposed. This large molecule will most likely recombine with the fragment on the surface. Initiator B is only singly bound to the surface. As this initiator decomposes, the small non-tethered fragment of the initiator can leave the surface easily and the probability of recombination is minimized. In this experiment, initiator A has a lower rate constant of decomposition because of this phenomenon. A way to test this is to perform these surface decomposition experiments

with bifunctional initiators of different lengths. As the length of the initiator increases, the rate constant of decomposition should decrease. Synthesizing bifunctional initiators of different lengths is simple. It simply requires using altering the material used in the second step of the synthesis.[93] Another way to test this is to perform liquid phase decomposition experiments. In the liquid phase, there should be no difference in volatility of the fragments created during decomposition. All fragments will be in solvent. The vapor pressure of both initiators and initiator fragments in solution will be the same. (The vapor pressure will be that of the solvent.) Both of these molecules, therefore, should exhibit the same decomposition phenomena.

Initiator C (shown in figure 6.7) was synthesized[94], and exhibited a molar absorptivity an order of magnitude greater than initiator B. This molecule exhibits a molar absorptivity approximately an order of magnitude greater than that of initiator B at wavelengths below 275 nm.[95] Assuming that the quantum efficiency of this molecule is similar to that of initiator B (This assumption is based on the similarity in structure of the two molecules.), the rate constant of decomposition of the molecule should be an order of magnitude greater than that of initiator B. A dose of 50 mJ/cm^2 should therefore be required to decompose 99% of this initiator. Invoking this assumption, a plot of the concentration of this initiator on the surface during exposure was generated and is shown in figure 6.7. This initiator would decompose very rapidly. XPS data of the decomposition of this initiator are shown along with this ideal decomposition plot. (Note that this data is not repeated; therefore, there may be significant error in the data.) It appears as if the assumptions made can accurately describe the data; therefore, using this

initiator for processing would bring the sensitivity of the photochemical decomposition to a value that is acceptable for next generation lithography.

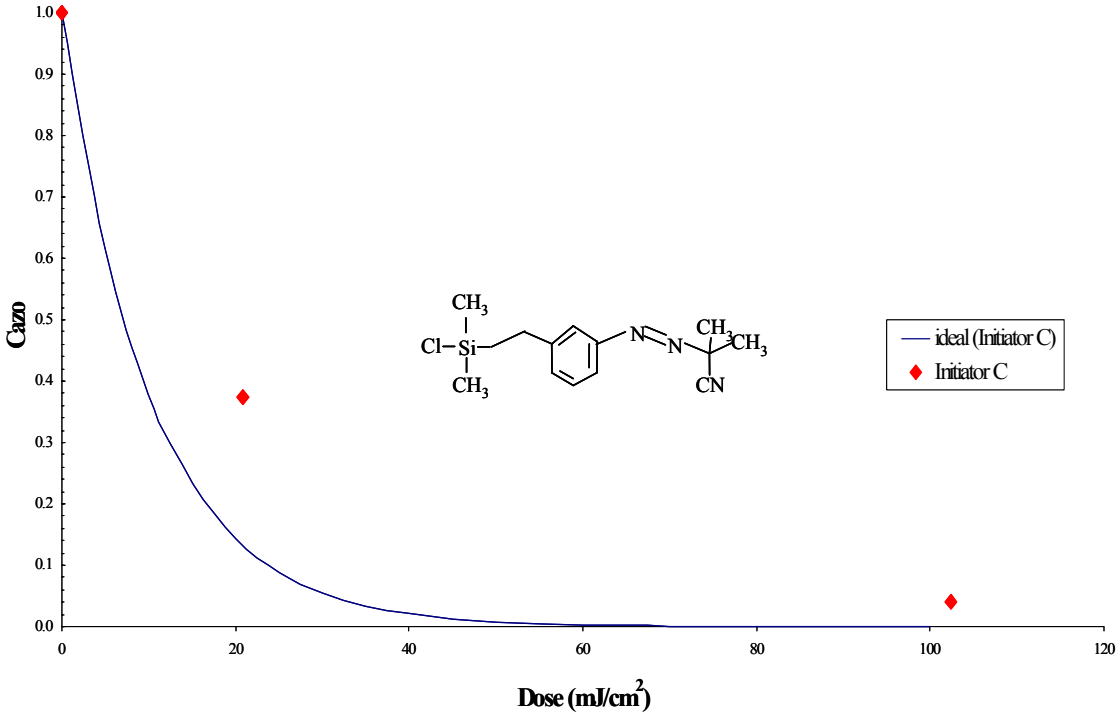

Figure 6.7: Initiator C and its photochemical decomposition. The solid line depicts the ideal decomposition of this material (assuming that the quantum efficiency of this molecule is similar to that of B). The dots depict preliminary photochemical decomposition data of a monolayer of this material

6.5 Conclusion

The rates of decomposition in the deep UV (248 nm) of two self-assembled azo compounds on SiO_2 surfaces have been examined via x-ray photoelectron spectroscopy (XPS). At this wavelength, these molecules decompose via first order processes with rate constants of 9.7 x 10^{-3} cm^2/mJ and 4.5 x 10^{-3} cm^2/mJ. These rates of decomposition are faster than those seen by other observers; however, if it is required that the initiators should be decomposed at 99% to produce high fidelity patterns, these rates are too slow for next generation lithography. The difference in reactivity of these two azo molecules

is due to the differences predominantly in their quantum efficiency. An initiator was synthesized in which exhibited an order of magnitude greater molar absorptivity than the two examined, and it appears that this initiator will provide a rate constant sufficient for NGL processing.

CHAPTER 7

PROPERTIES OF THERMALLY GROWN FILMS AND ISSUES IN PATTERNING

7.1 Introduction

The third step in this SMIP process is to grow a polymer film thermally from the remaining protected initiator sites on the surface. Growing films via this process has proven to be a formidable task. After developing processes to clean the solvents, substrates, and glass cells used in this process, growing uniform films has proven futile; therefore optical thicknesses of these films could not be measured. After analyzing the thickness variation of these films via AFM, it was noticed that there was a correlation between the roughness of the films and the time for which the films had been grown. It was speculated that this roughness was also dependent upon the temperature at which the polymer was grown. The first part of this chapter serves as a means to explain these phenomena. A theory that explains the deviation in roughness of these polymer films is presented and validated with experimental data. Patterning via this positive-toned SMIP method has also proven to be an even greater challenge. It has proven nearly impossible to create smooth, high resolution patterns on the order of microns. The latter part of this chapter explains why patterning has been such a difficult task. The chapter concludes with a recommendation for future work.

7.2 Results

The initial films produced via this SMIP process exhibited a significant amount of roughness during processing. Figure 7.1 below shows pictures of styrene films produced by this SMIP process. All four pictures show that these films exhibit some roughness. A pattern is also present in the progression of the roughness of these films. This pattern in roughness seems to correlate with the amount of time that the material has polymerized. There appears to be a conversion at which the roughness is minimized. Unfortunately during these experiments, the temperature of the heating bath was not precisely controlled, so the exact initiator conversion at which the roughness was minimized could not be found.

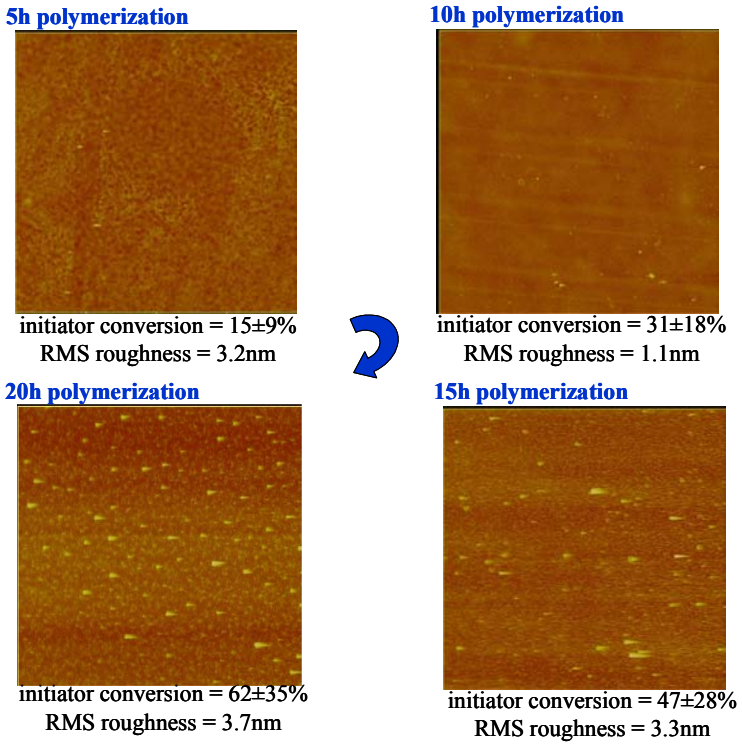

Figure 7.1: Roughness evolution in films created by SMIP process. Each box represents a scan from a 5μm (width) x 5.1μm (length) area

7.2.1 Roughness versus Conversion

When repeating these experiments (each data point is an experiment) polymerizing methyl methacrylate at 80˚C, the same phenomenon occurred. The roughness of the polymer film reached a minimum at a specific conversion of the decomposition of initiator. The plot of roughness versus conversion of thermal decomposition of initiator is shown in figure 7.2. (The thermal conversion of the initiator is calculated from the work of Prucker et al.[40])

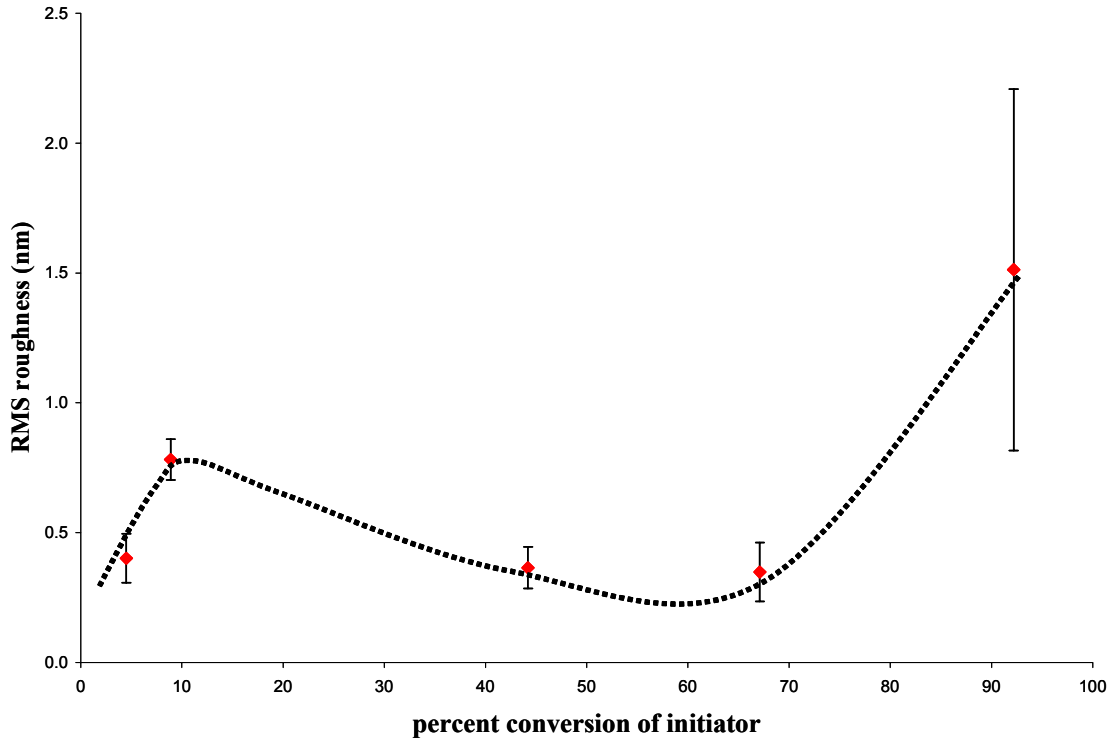

Figure 7.2: Roughness versus percent of thermal decomposition of the initiator. The solid line is drawn to explain the phenomenon that the author feels is occurring. Polymerization of methyl methacrylate (1.74M in n-butanol) at 80˚C

The graph shows that the roughness is low at low conversion. The roughness then increases at 10% conversion and decreases again between 40% and 70% conversion. The roughness then spikes to a high value at high conversion.

There are two phenomena occurring simultaneously while polymerizing these SMIP films. The first phenomenon is exhibited in figure 7.3 below. The initiator layer is decomposing on the surface. As the initiator continues to decompose during the thermal polymerization, a percentage of these decomposed chains initiates the growth of a polymer chain (the radical efficiency dictates this). As the initiator decomposition proceeds to higher conversion, more polymers are grown from the surface and the distance between the polymer chains decreases. Estimating a graft density (Γ) of 6 x 10^{14} molecules/cm^2 from the data in chapter 5 and assuming a radical efficiency (f) of 0.35 (obtained from the analysis of Prucker et al[40]), the distance between growing chains is calculated as a function of thermal conversion of the initiator via equation 7.1 below and is depicted in figure 7.3. As the initiator continues to decompose, the distance between growing polymer chains is initially about 10 nm and approaches 0.7 nm.

$$d = \sqrt{\frac{1}{\Gamma f x_d}} \qquad \textbf{Equation 7.1}$$

The second phenomenon occurring during the polymerization is the growth of the polymer chains. According to Prucker et al, the average molecular weight and therefore the size of the polymer increases as the chains grow. A good indicator of the size of the polymer molecule is the radius of gyration. It is defined as the average square distance to the center of gravity of the polymer.[96] Depending on the temperature of polymerization, the radius of gyration of the polymer can range from nanometers to tens of nanometers.

There can, therefore, be a point at which the radius of gyration of the polymer is equal to the spacing between polymer chains. At this critical conversion, a relaxed polymer chain can fill in spaces on the surface. If the polymerization reaction is stopped at that critical conversion, the film grown would become smooth.

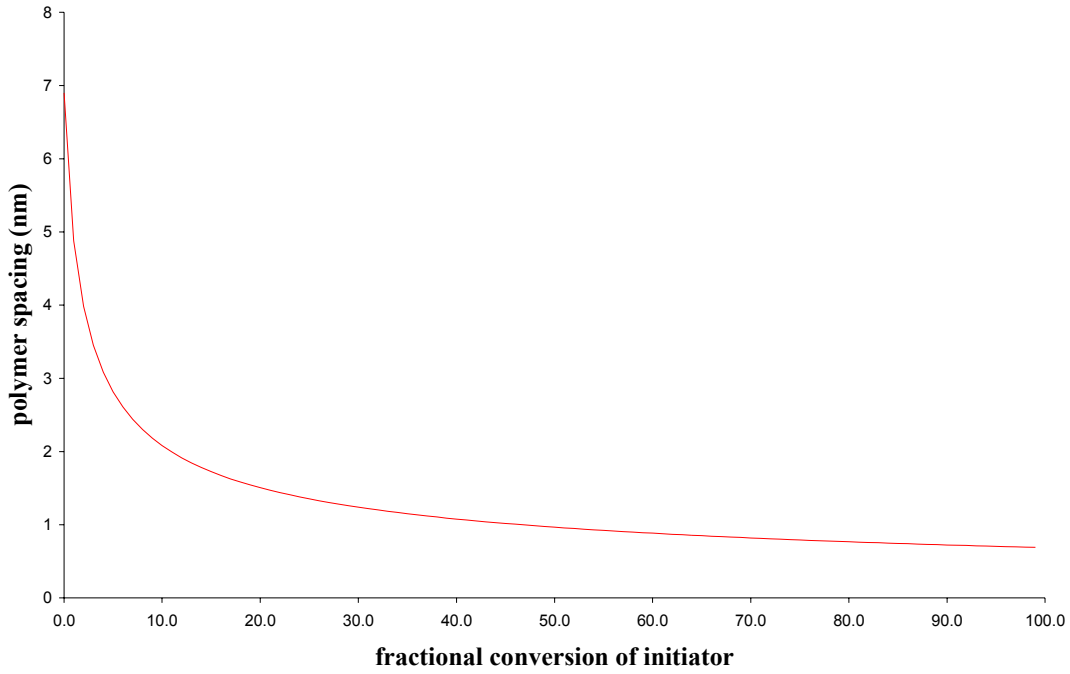

Figure 7.3: Spacing between polymer chains as a function of thermal conversion of the initiator

When the roughness data in figure 7.2 is re-plotted against the spacing between polymer chains (converting percent conversion on the horizontal axis to distance between chains from figure 7.3), the following plot shown in figure 7.4 is obtained. It appears the roughness is minimized at the point at which the polymer chains attain a spacing of about 1nm. According to Prucker et al, at this temperature the polymer chains have a number averaged molecular weight on the order of 10,000. The polydispersity indices of these

films were stated to be between 1.5 and 3; therefore, the weight averaged molecular weight of the polymer chains is approximately the same order of magnitude. The radius of gyration of the polymer chain at that molecular weight is on the order of 1nm.[40] It appears that polymerizing to a conversion at which the radius of gyration of the polymer is approximately equal to the spacing between chains will produce a smooth surface polymerized film.

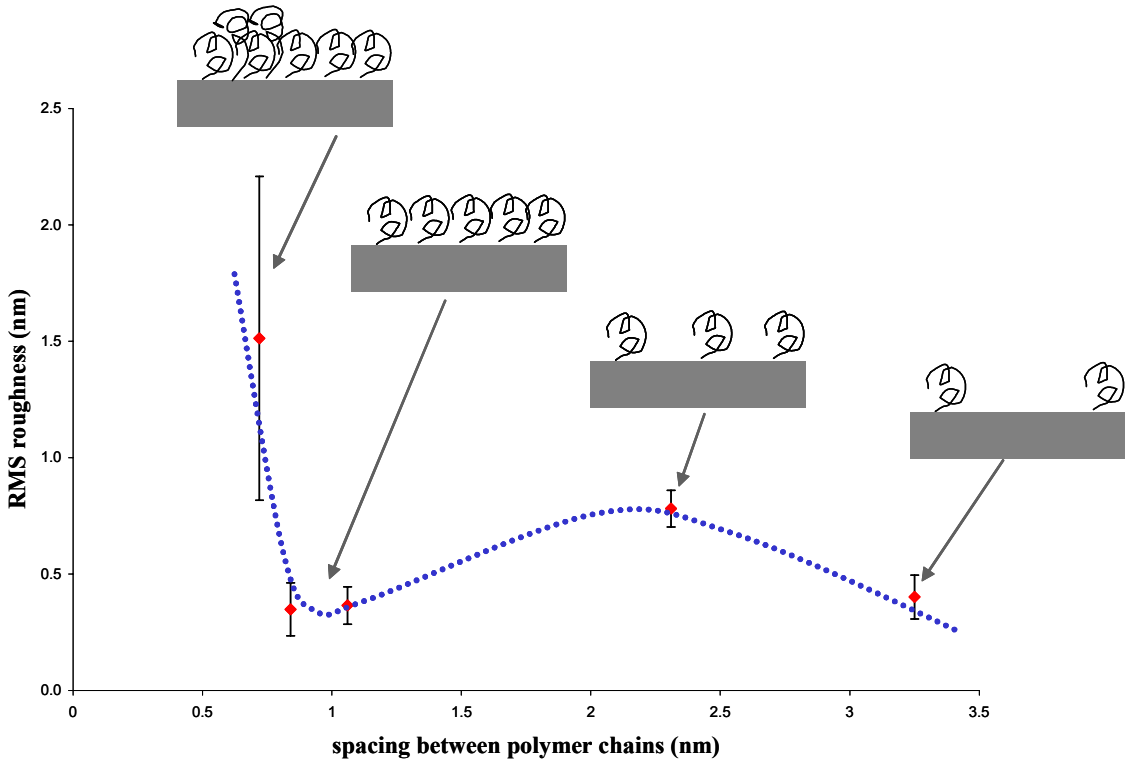

Figure 7.4: Roughness of polymer films versus spacing between polymer chains. The picture shows the physical phenomena occurring as the films are polymerized for different times. Polymerization of methyl methacrylate (1.74M in n-butanol) at 80˚C

7.2.2 Roughness versus Temperature

According to Prucker et al, at a particular conversion of initiator, the molecular weight of the surface polymer grown decreases with an increase in temperature (for

temperatures ranging from 50˚C to 90˚C). If this is true, then the radius of gyration of the polymer should decrease with increasing temperature and the films should become smoother as the temperature of polymerization is increased. The graph on figure 7.5 below shows the roughness of polymer films with respect to the temperature at which the polymer films were grown. A series of polymers were polymerized to 50% conversion (according to Prucker et al's thermal decomposition results) at various temperatures. The roughness of these films was measured, and plotted below.

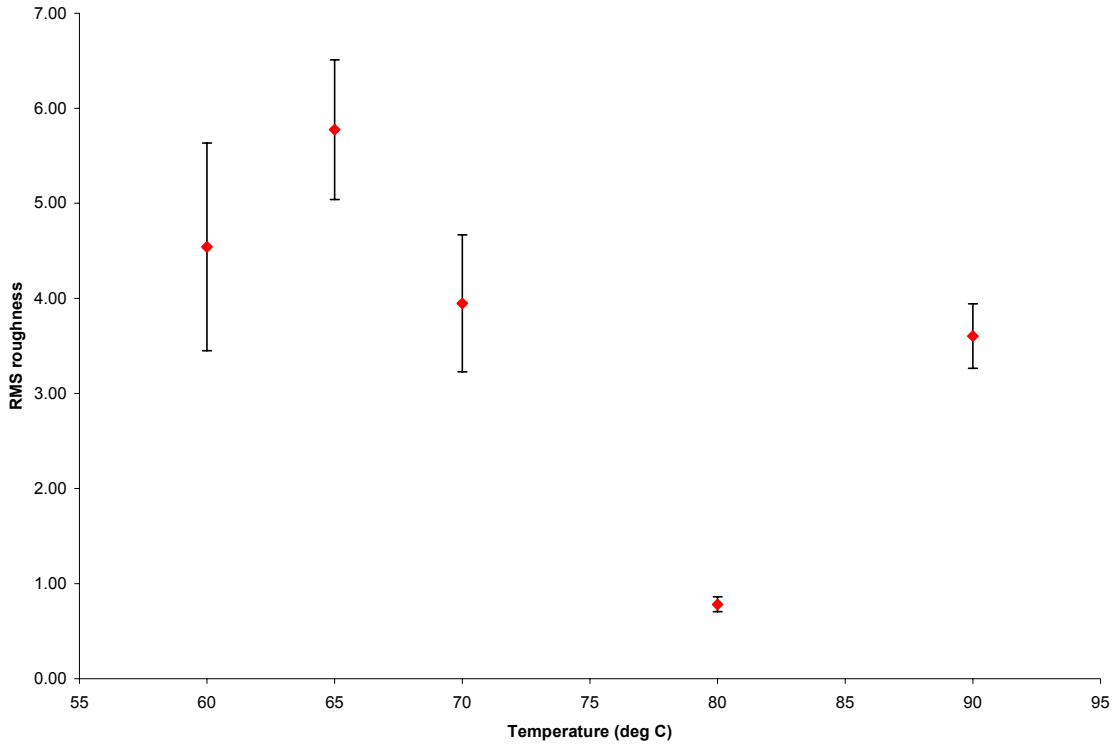

Figure 7.5: Roughness of surface grown polymer films versus temperature. Polymerization of PMMA (1.74M in n-butanol)

There appears to be no trend in the roughness of the films with an increase in temperature. The roughness is essentially constant with the exception of the data point at 80˚C.

7.3 Conclusions Drawn about Surface Roughness

The roughness of polymers grown via the SMIP process was shown to change as the thermal decomposition of the initiator proceeded. The roughness was initially high. Then it decreased until a critical conversion was reached. As the conversion increased past this critical value, the roughness increased. When analyzing the literature written about the molecular weight of the surface polymers grown and converting this molecular weight to a radius of gyration, it becomes apparent that the smoothest films are formed when the radius of gyration of the polymer grown is approximately equal to the spacing between polymer chains. It has been shown that at high conversion (50% or greater), as the temperature at which the polymer is grown increases, the molecular weight of the surface bound polymer decreases. The polymer films, therefore, should become smoother as the temperature at which they are polymerized increases. This phenomenon was not found to occur in this study.

7.4 Perspectives on Patterning

Patterning these materials via this SMIP process has proven to be an impossible task. Attempts were made to pattern the initiator with electron beams and amplify the patterns grown via thermal polymerization. The patterns generated in the first attempt at this process were 2-4x4 arrays of 10μm x 10μm boxes written at doses on the order of milli Coulombs per square centimeter (mC/cm^2). This dose is an order of magnitude greater than the doses normally used for electron beam lithography[97] and writing was intentionally performed at these high doses to insure that patterns were generated. The first attempt at performing this procedure resulted in large blank spaces in the polymer

film that did not resemble the pattern generated. A micrograph of the polymer "pattern" is shown in figure 7.6 below.

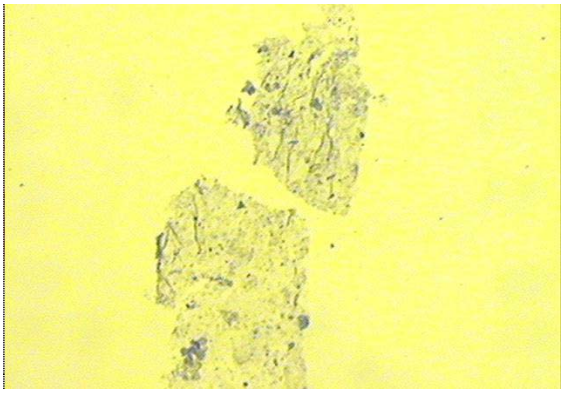

Figure 7.6: Optical micrograph of the "pattern" generated during the first attempt at electron beam patterning. MMA (50 volume % in methanol) was polymerized on the surface at a temperature of between 55˚C and 60˚C for 24 hours.

{It should also be noted that at the temperature and time of polymerization resulted in only 15% thermal decomposition of the initiator (according to Prucker et al).} It was assumed that the energy used to decompose the sample was so great that the pattern spread; therefore, the patterning doses were reduced and further attempts were made to generate patterns in the material to no avail. These later attempts were performed at temperatures ranging from 75˚C to 80˚C for times between 10 and 18 hours. These temperatures and times result in an initiator conversion between 50% and 80%. The simple calculation shown below using data from the photochemical decomposition of the initiator layer on the surface shows why these patterns were not generated via this positive toned SMIP process.

As shown in the previous chapter, doses on the order or 100 mJ/cm^2 are required to photochemically decompose 99% of the initiator. These doses are unacceptable for NGL technology. Previously it was not known if 99% decomposition was needed to

create high fidelity patterns. In order to produce a high fidelity pattern, the remaining protected initiator left on the surface after thermal decomposition must not generate polymer that will destroy the image created; therefore, the spacing between two chains in the photochemically patterned region of the film must be significantly (at least an order of magnitude) greater than the radius of gyration of the polymers grown in the thermal polymerization step. Using the data from the previous chapters, calculating the spacing between two polymer chains in the patterned region of the films is simple. From the data provided in chapter 6, the percent of material decomposed photochemically can be calculated. This number is directly dependent on the rate constant of photochemical decomposition ($k_{D,i}$) and the dose applied (D). It directly affects the initial graft density of initiator sites on the surface before thermal polymerization. Using this information, the spacing between polymer chains in the "dead region" can be easily calculated via equation 7.2 below. If the spacing of the polymer chains at a particular conversion is significantly greater than the radius of gyration of the polymers grown at a specific conversion, then the dose used to photochemically decompose the initiator layer is sufficient for the process.

$$d = \sqrt{\frac{1}{\exp(-k_{D,i}D)\Gamma f x_D}} \qquad \textbf{Equation 7.2}$$

The graph below displays the spacing between polymer chains growing in the "dead" (photochemically decomposed) regions of the film after growth of a polymer film versus the thermal conversion of initiator B described in the previous chapter.

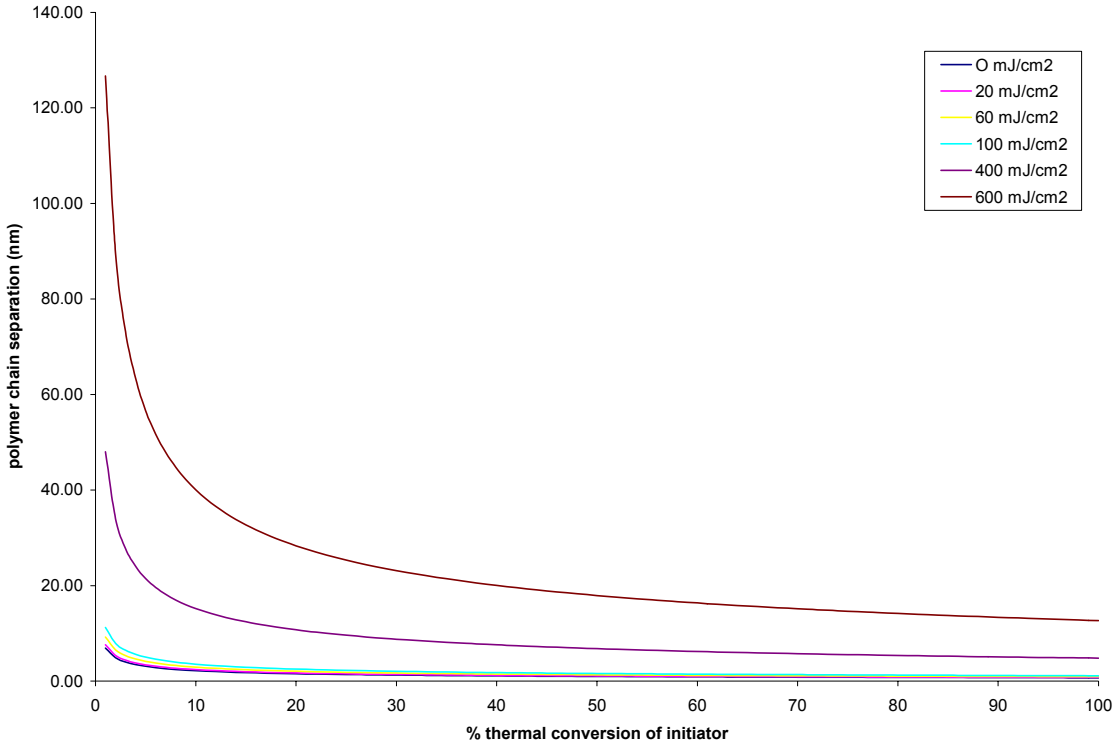

Figure 7.7: Separation between polymer chains grown in the "dead" section of pattern.

As shown in this graph, a dose of at least 400 mJ/cm^2 is needed to separate the polymer chains in the "dead" space by tens of nanometers. If a polymer with a radius of gyration greater than the separation of these polymer chains is grown, the pattern will fill in. For all of these experiments, the radius of gyration of the polymer films grown is at least 10 nm. Therefore, all films fabricated via this process will fill-in. When initially formulating ideas about this process, it was assumed that the pattern in the film would proceed via a mechanism shown at the top of figure 7.8. In the "dead space" of the film essentially no polymerization would occur. An accurate description of the physical phenomena occurring is shown at the bottom of figure 7.8. Polymer is being created in both the dead and protected regions of the film and patterns are not accurately defined.

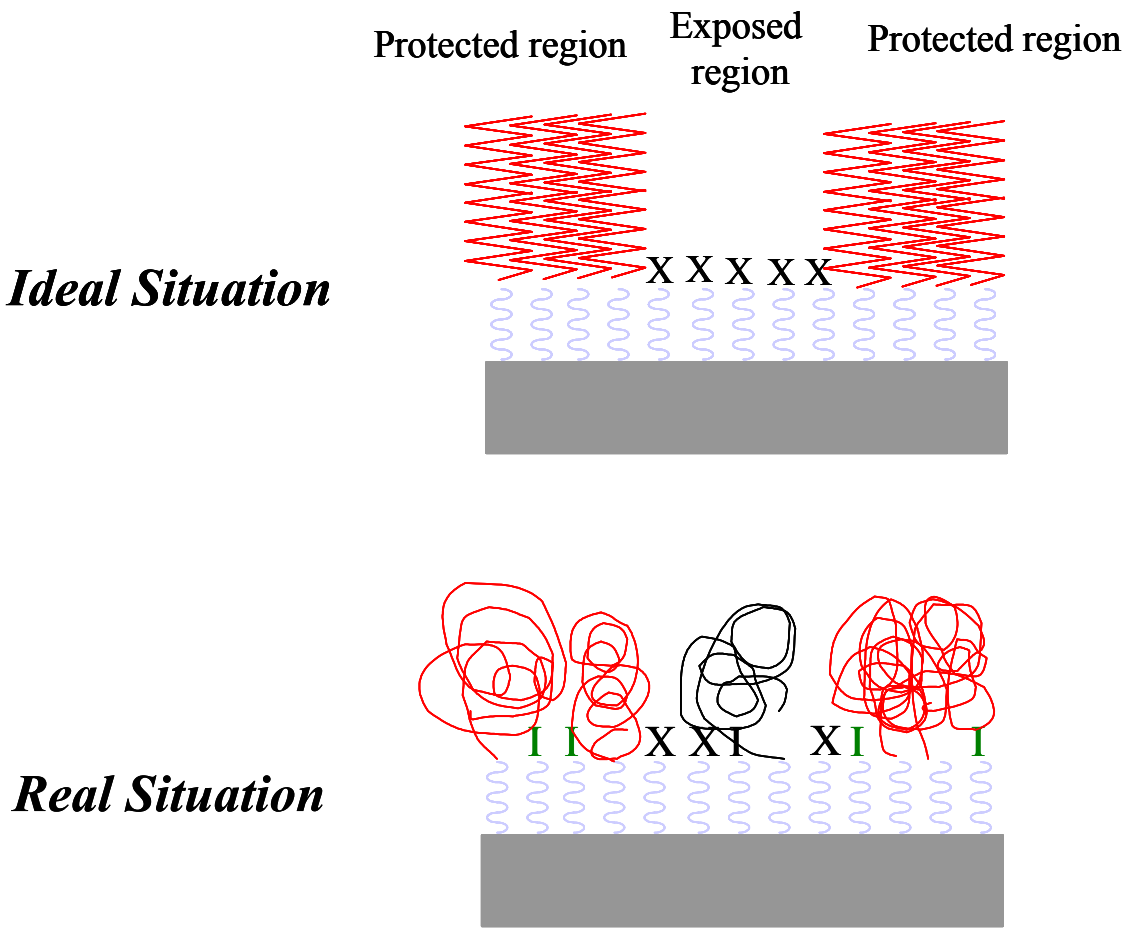

Figure 7.8: Schematic of patterns generated via the positive toned SMIP Process.

The one electron beam imaged pattern that did not fill in was polymerized at such low conversion that the spacing between polymer chains was relatively high. The rate of decomposition of the initiator under the influence of electron beams is not known; therefore, the plot similar to figure 7.7 above for electron beam decomposition cannot be calculated.

This analysis shows that producing positive toned patterns via this SMIP process is not feasible for Next Generation Lithography; therefore, another positive toned process should be explored. In order for this process to be practical, the initiation and polymerization should be performed in two steps; the species that are initiated to

polymerize should have lifetimes that enable the initiation and polymerization to be separate procedures. The general schematic of a process utilizing this scheme is shown below. Designing the initiator such that it generates species that can initiate ionic or living radical polymerization is a means of accomplishing this task.

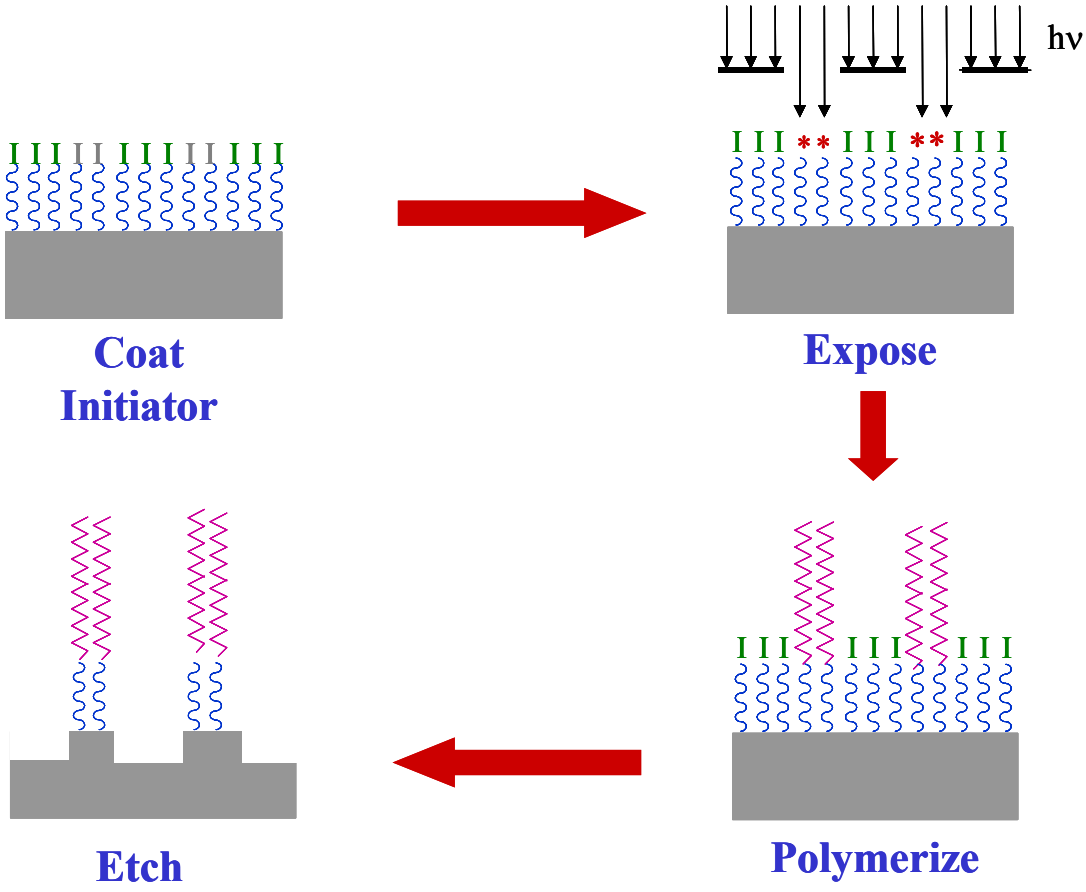

Figure 7.9: Schematic for practically creating negative features via the SMIP process.

Even though it has been shown that the positive toned SMIP process cannot be used as an NGL technology, the ultimate resolution of the negative toned process can still be evaluated. In the previous sections, the radius of gyration of the polymer grown was mentioned as an important factor in determining the roughness of the films. It is also speculated that this radius of gyration will dictate the ultimate resolution of the patterns created via this process. Patterns cannot be created that are smaller than this radius of

gyration, for the polymer pattern will spread past this size. The radius of gyration is a directly related to the molecular weight of the polymer that is grown from the surface. Polymers grown via this free radical mechanism with molecular weights on the order of 10,000 will produce films with a radius of gyration on the order of 1nm.[40] If the molecular weight of polymers grown via this process can be tightly controlled to be on the order of 10,000, then the resolution limit of the process will be about 1nm. According to Prucker et al, to obtain molecular weights on the order of 10,000 one must polymerize at a temperature of at least 70˚C. Another means to control the molecular weight of the growing chains is to perform a more controlled polymerization. Researchers at IBM[51], the University of Delaware[48], and Carnegie Mellon University[49] have investigated surface polymerization via living radical polymerization methods. Polymers grown via these methods exhibit a significant level of control in both the molecular weight and molecular weight distribution. These methods may prove sufficient to tightly control the radius of gyration polymers grown on surfaces. Studies need to be performed to evaluate these living polymerization schemes as alternatives to this SMIP process that undergoes free radical polymerization.

CHAPTER 8

SUMMARY AND FUTURE WORK

8.1 Summary of Findings

The overall goal of this project is to analyze each step in the positive toned SMIP process in the hopes of evaluating the overall process as a viable means to creating high resolution features for Next Generation Lithography. The following is a summary of the findings from each of the investigations.

8.1.1 Surface Preparation

Two means of quantifying the number of hydroxyl groups on the surface were presented. The first method, which was adopted from the heterogeneous catalysis literature, involved reacting vanadium compounds to the surface and quantifying the amount of vanadium reacted to the surface with XPS. In the literature, it was assumed that the vanadium compound formed a monolayer on the surface. From the XPS data, it was clear that a layer thicker than 50Å was on the surface. This vanadium layer was washed off of the surface with water. Because of these problems with treating the surface, this method was not used to characterize the hydroxyl content of the silicon oxide surface. Another method, which involved reacting per-fluorinated self-assembled monolayers onto the surface and analyzing the fluorine content of the surface via XPS, was used to quantify the chemical reactivity of silicon oxide surfaces. It was found that the RCA clean created a silicon oxide with the greatest number of hydroxyl groups.

The effect of the surface treatment on the roughness of the surface was also investigated. It was found that soaking wafers in 1M nitric acid for 2 hours provided the smoothest silicon oxide surface.

8.1.2 Initiator Deposition

Trichlorosilanes deposit onto SiO_2 surfaces quickly and form networks. Depending on the surface treatment, dichlorosilanes form either networks or rigid monolayers on surfaces. The rates of deposition of dichlorosilanes appear to be three times slower than that of trichlorosilanes. Monochlorosilanes deposit in a floppy manner onto surfaces at rates significantly slower than that of dichlorosilanes.

8.1.3 Initiator Decomposition

Initiator layers react with ultraviolet radiation in such a manner that doses on the order of 100 mJ/cm^2 are required to decompose 99% of the initiator layer. This magnitude of dose is unacceptable for a lithographic application.

By altering the chemistry of the initiator such that the ultraviolet absorption of the initiator is increased, the dose required can be reduced to a value on the order of 10 mJ/cm^2.

8.1.4 Polymer Growth

Polymer films exhibited roughness. This roughness reaches a minimum value at a particular conversion of initiator. It was seen that at this critical level of conversion, the spacing of polymer chains that was approximately equivalent to the size of the polymer grown.

The roughness of the polymer films was expected to decrease with increasing temperature at a high conversion. In this study, the roughness did not decrease with increasing temperature.

8.1.5 Patterning

At doses below 500 mJ/cm^2, the separation between polymer chains grown in the "dead" regions (regions that have been photochemically decomposed) is the same order of magnitude as the size of the polymers grown; therefore, patterns generated at these doses fill in.

The resolution of the patterns created via the negative toned process is limited by the size of the polymers grown on the surface. In order for this limit to be on the order of 1 nm, the polymers grown must have molecular weights on the order of 10,000. Polymers of this molecular weight can be grown on the surface by polymerizing at temperatures higher than 70˚C.

8.2 Recommendations for Future Work

8.2.1 Initiator Deposition

A dichlorosilane derivative of the initiator can be synthesized to optimize the rate of deposition of the initiator onto silicon oxide surfaces.

8.2.2 Patterning

A practical means of creating negative toned features on surfaces is highly recommended. This process would involve separate processing steps for imaging the monolayer and polymerizing the pattern. In order to do this, the initiator must create a living species when exposed to light. Examples of these living species are living radicals

(radicals with lifetimes on the order of minutes or hours) or ions. The chemistry of the initiator must be altered to perform this task.

Living polymerization can be used to create polymers of a controlled molecular weight and molecular weight distribution via the negative toned free radical SMIP process. This controlled polymerization may prove to create high resolution patterns.

APPENDIX

A.1 No Transport Phenomena Occurring in QCM-D Studies

Concentration of ODS/OMS/OTS = .005 M

Volume of cell = 100 μL

Total moles of ODS/OMS/OTS in solution = 5e-7 moles

Number of molecules in solution = (5 x 10^{-7} moles)*(6.022 x 10^{23} molecules/mol) = **1.2 x 10^{17} molecules**

Si-O spacing = 1.58 Å

Area occupied by Si-O bond = $\pi(1.58\ Å)^2$

Number of Si-O sites in 1cm^2 = 1e20/1e4 (convert Angstroms to meters to centimeters)/ $\pi(1.58Å)^2$ = **1.25e15**

1.2e17>>>1.2e15

A.2 Summary of Relevant QCM Data

Type of Silane	*Filename*	*Langmuir Absorption*	*Ultimate Frequency Shift (Hz)*	*Surface Treatment*	*D/f Crossover (Hz)*	*D/f < 1/5*
Tri	2km139ots	N/A	66	new	curves upward	no
Di	2km135ods	N/A	22	old	curves upward	no
Di	2km159ods	N/A	32	acid only (old)	curves upward	no
Di	2km170ods	modified	24	plasma and acid (new	16	yes
Mono	2km144oms	neither	20	old	N/A	no
Mono	2km266oms	simple	26	acid only (old)	8	no

Table 0.1: Summary of relevant QCM data

A.3 Cleaning of Quartz Crystals

Used quartz crystals were cleaned in a UV/ozone cleaner for 10 minutes to remove the absorbed monolayers. They were then prepared according to the procedures described in Chapter 3.

A.4 Plots of relevant QCM data

Shifts in the fundamental frequency exhibited a lot of noise, and therefore are not shown in the graphs below. The following are plots of the frequency shifts and D/f plots associated with octadecyltrichlorosilane addition. The file name is 2km139ots.

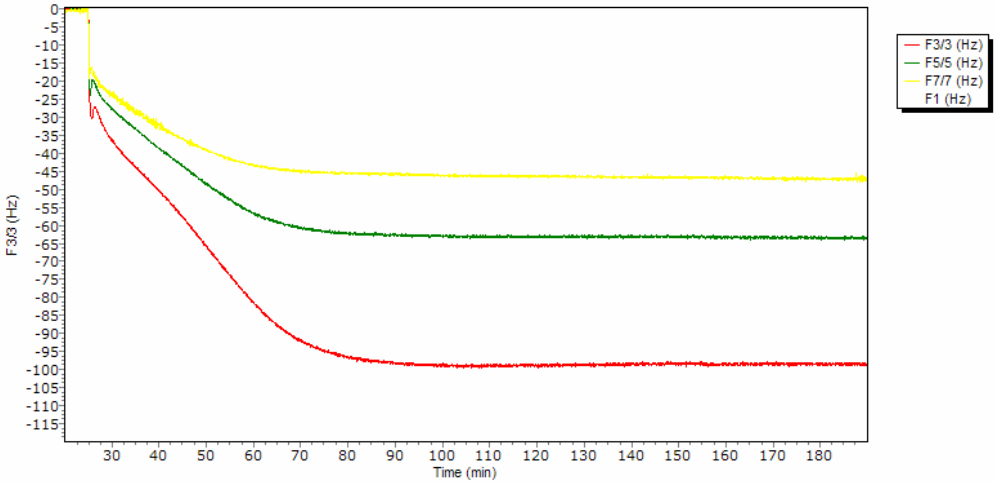

Figure 0.1: Frequency shifts associated with the addition of 5mM (in toluene) of OTS

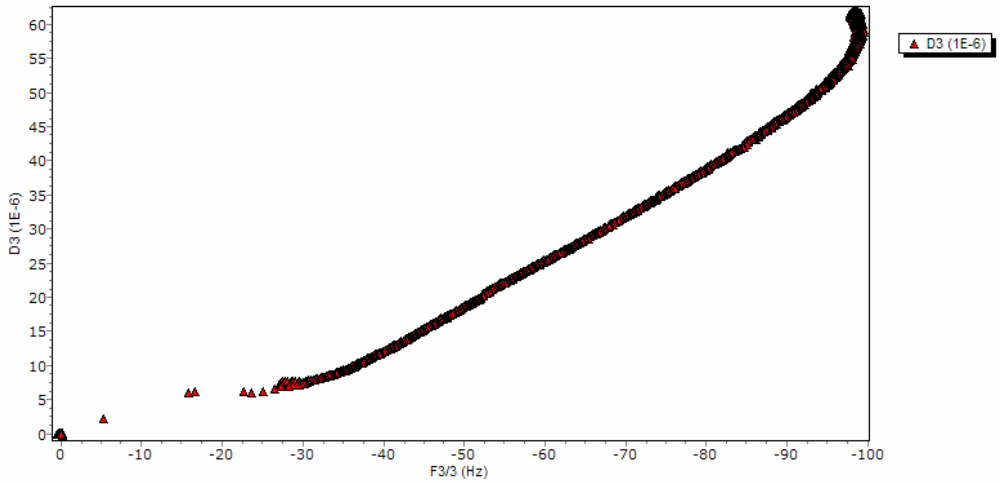

Figure 0.2: D/f plot of the third harmonic frequency and dissipation shifts associated with the addition of 5mM (in toluene) of OTS

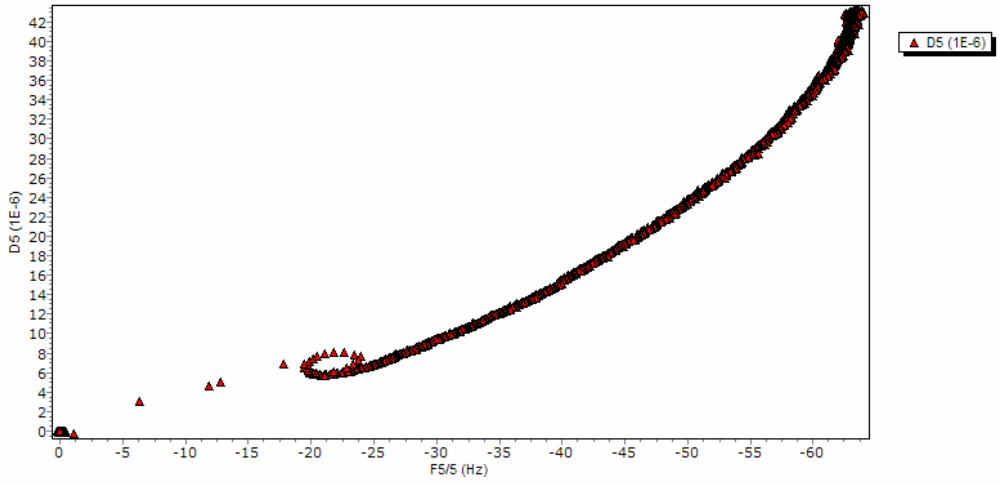

Figure 0.3: D/f plot of the fifth harmonic frequency and dissipation shifts associated with the addition of 5mM (in toluene) of OTS

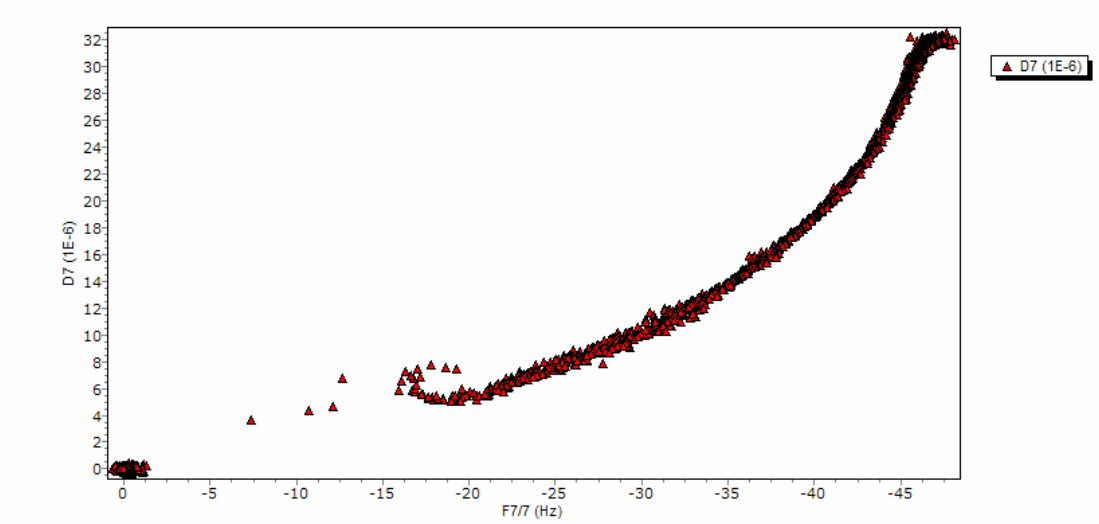

Figure 0.4: D/f plot of the seventh harmonic frequency and dissipation shifts associated with the addition of 5mM (in toluene) of OTS

The following are plots of the frequency shifts and D/f plots associated with octadecylmethyldichlorosilane addition to a QCM crystal that was previously used. The file name is 2km135ods.

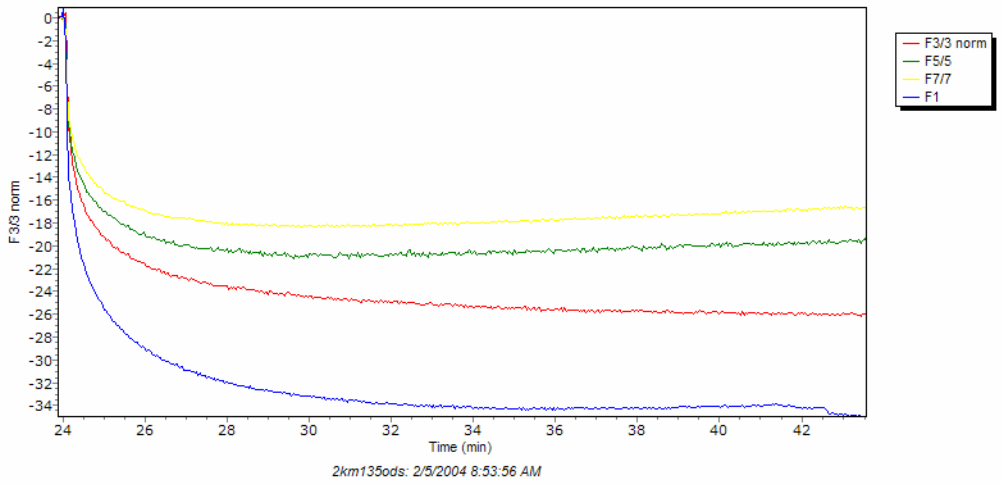

Figure 0.5: Frequency shifts associated with the addition of 5mM (in toluene) of ODS on a previously used crystal

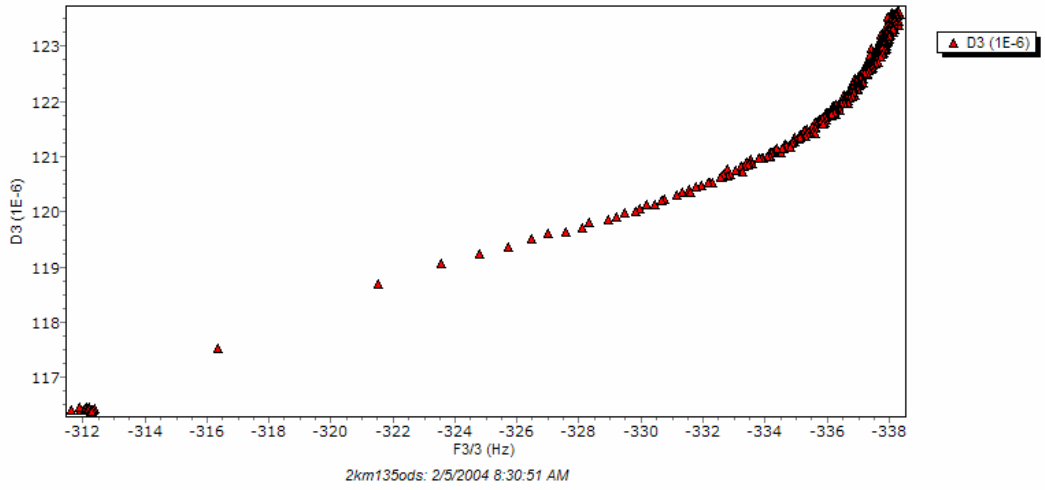

Figure 0.6: D/f plot of the third harmonic frequency and dissipation shifts associated with the addition of 5mM (in toluene) of ODS on a previously used crystal

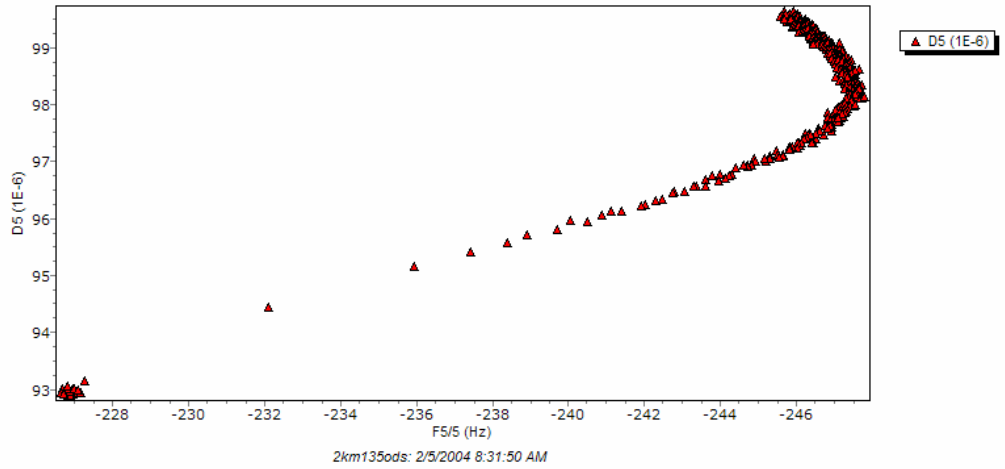

Figure 0.7: D/f plot of the fifth harmonic frequency and dissipation shifts associated with the addition of 5mM (in toluene) of ODS on a previously used crystal

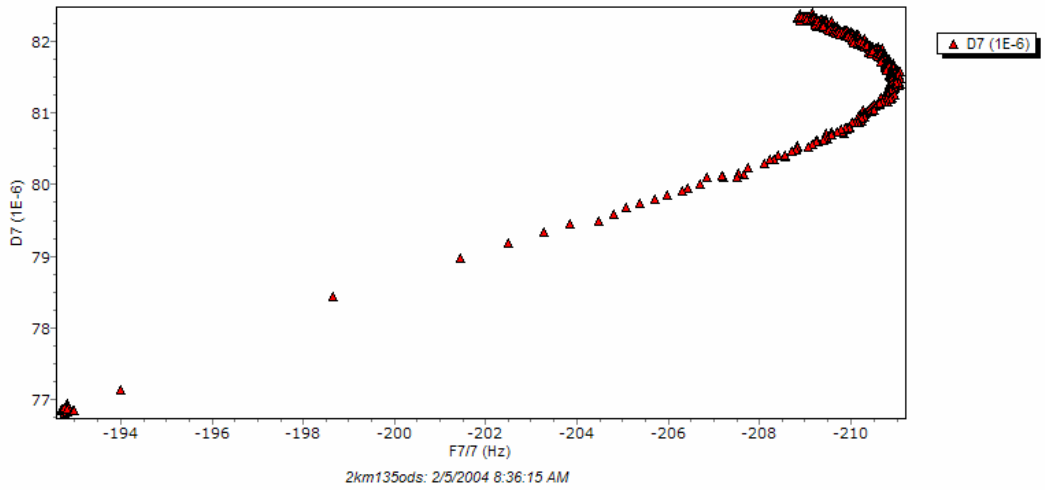

Figure 0.8: D/f plot of the seventh harmonic frequency and dissipation shifts associated with the addition of 5mM (in toluene) of ODS on a previously used crystal

The following are plots of the frequency shifts and D/f plots associated with octadecylmethyldichlorosilane addition to a QCM crystal that was previously used and subsequently treated with acid. The file name is 2km159ods.

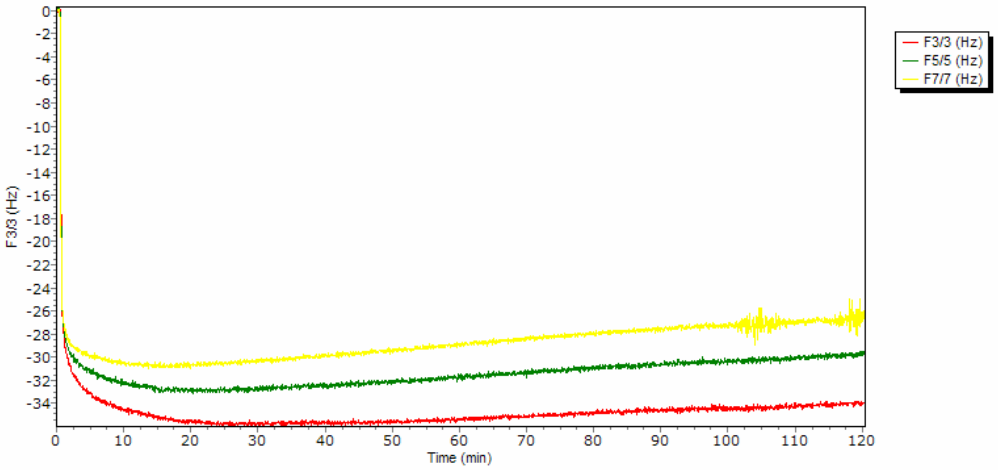

Figure 0.9: Frequency shifts associated with the addition of 5mM (in toluene) of ODS on a previously used crystal that was subsequently acid treated

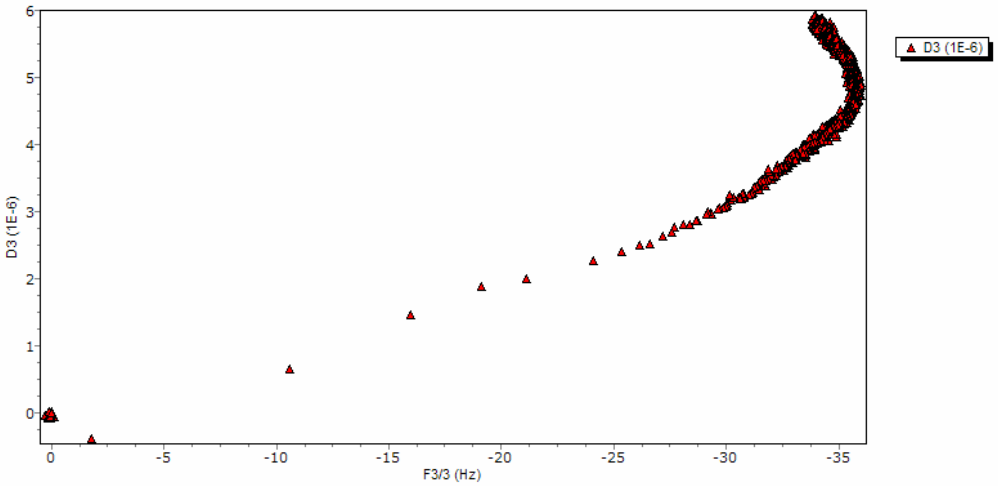

Figure 0.10: D/f plot of the third harmonic frequency and dissipation shifts associated with the addition of 5mM (in toluene) of ODS on a previously used crystal that was subsequently acid treated

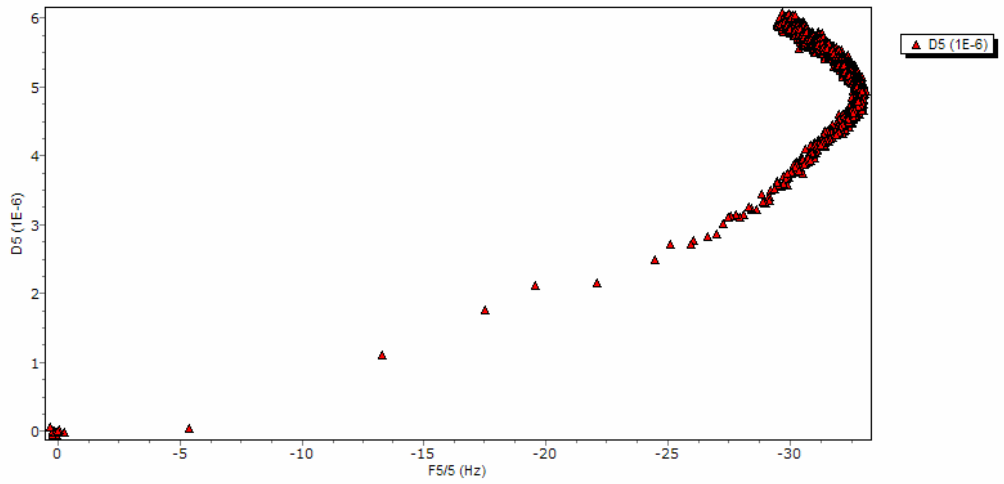

Figure 0.11: D/f plot of the fifth harmonic frequency and dissipation shifts associated with the addition of 5mM (in toluene) of ODS on a previously used crystal and subsequently acid treated

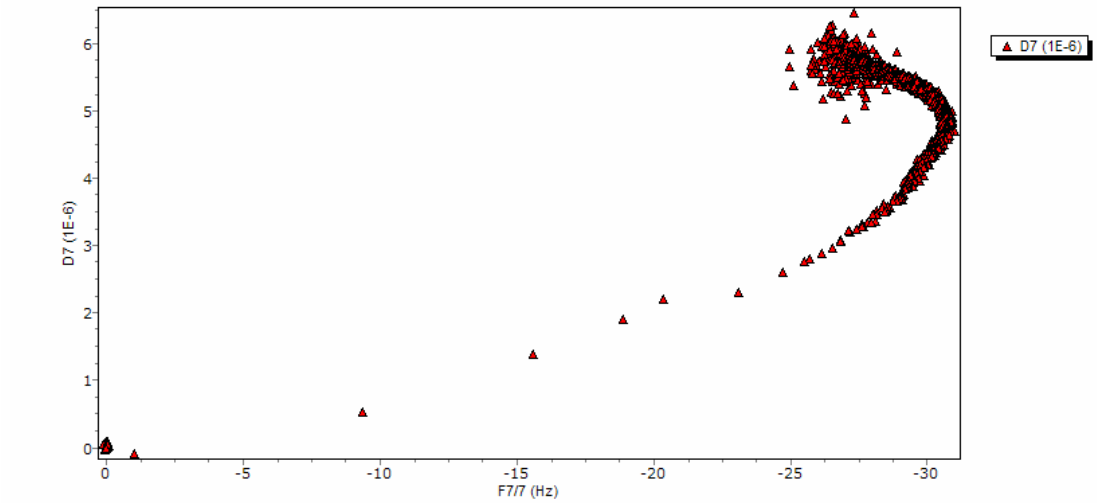

Figure 0.12: D/f plot of the seventh harmonic frequency and dissipation shifts associated with the addition of 5mM (in toluene) of ODS on a previously used crystal and subsequently acid treated

The following are plots of the frequency shifts and D/f plots associated with octadecylmethyldichlorosilane addition to a new QCM crystal that was treated with acid. The file name is 2km170ods.

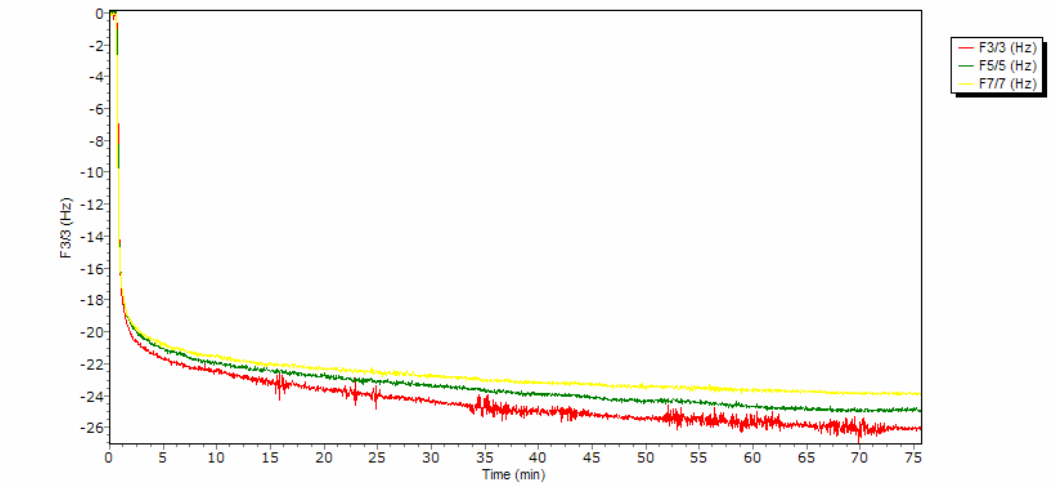

Figure 0.13: Frequency shifts associated with the addition of 5mM (in toluene) of ODS on a new crystal that was subsequently acid treated

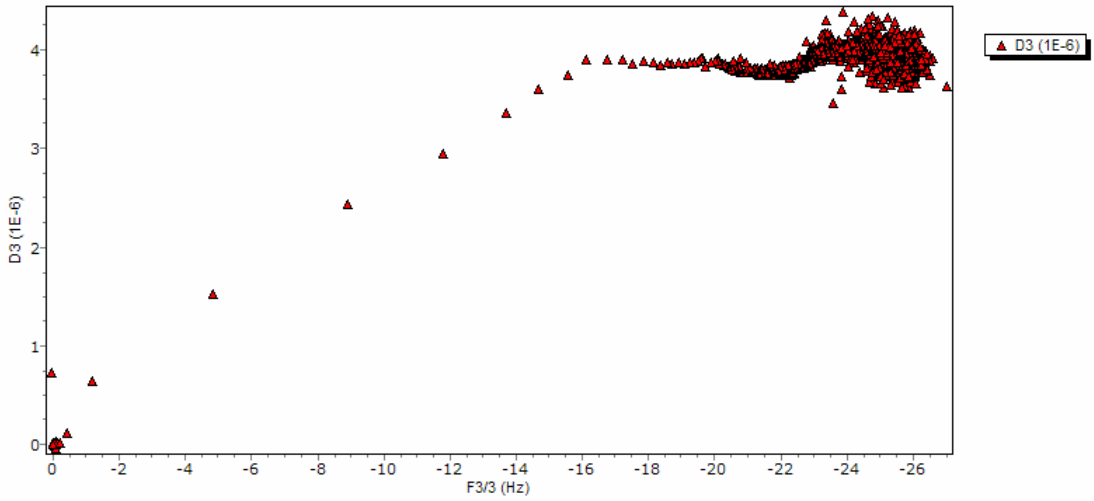

Figure 0.14: D/f plot of the third harmonic frequency and dissipation shifts associated with the addition of 5mM (in toluene) of ODS on a new crystal that was subsequently acid treated

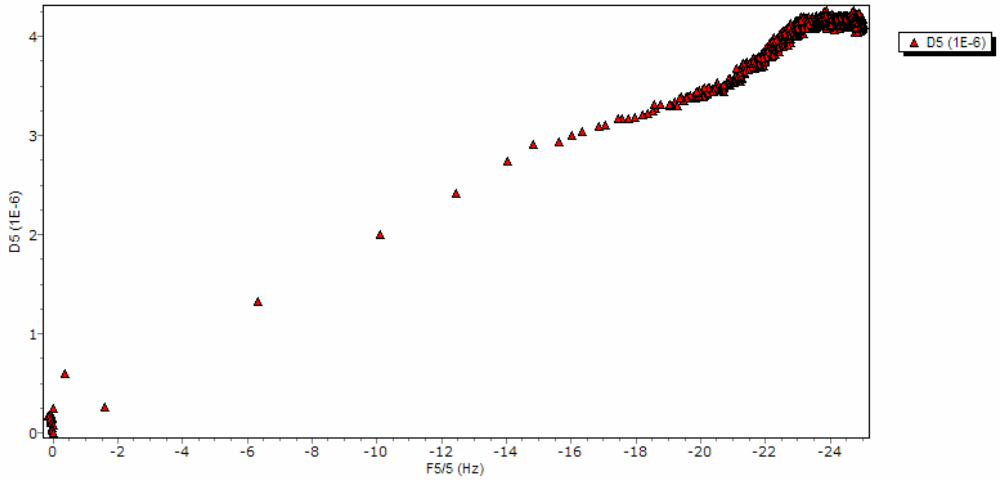

Figure 0.15: D/f plot of the fifth harmonic frequency and dissipation shifts associated with the addition of 5mM (in toluene) of ODS on a new crystal that was subsequently acid treated

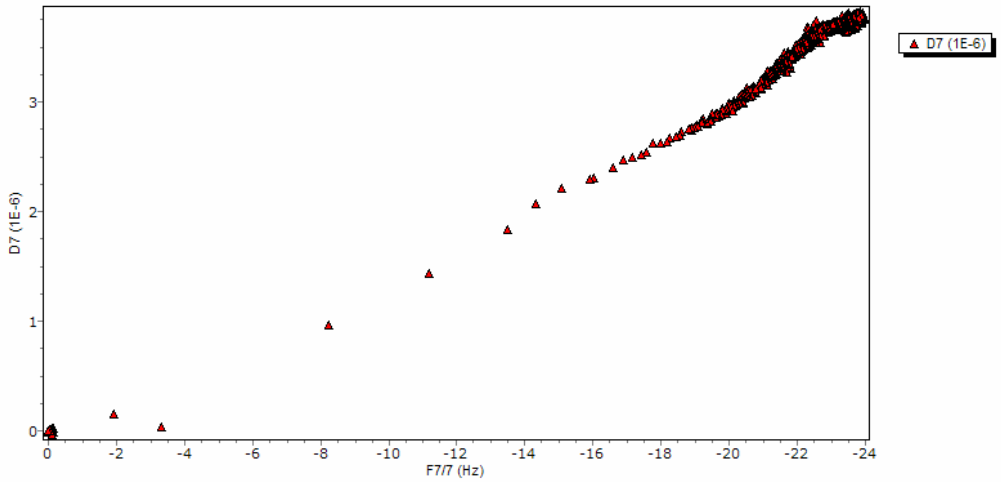

Figure 0.16: D/f plot of the seventh harmonic frequency and dissipation shifts associated with the addition of 5mM (in toluene) of ODS on a new crystal that was subsequently acid treated

The following are plots of the frequency shifts and D/f plots associated with octadecyldimethylchlorosilane addition to a QCM crystal that was previously used. The file name is 2km144oms.

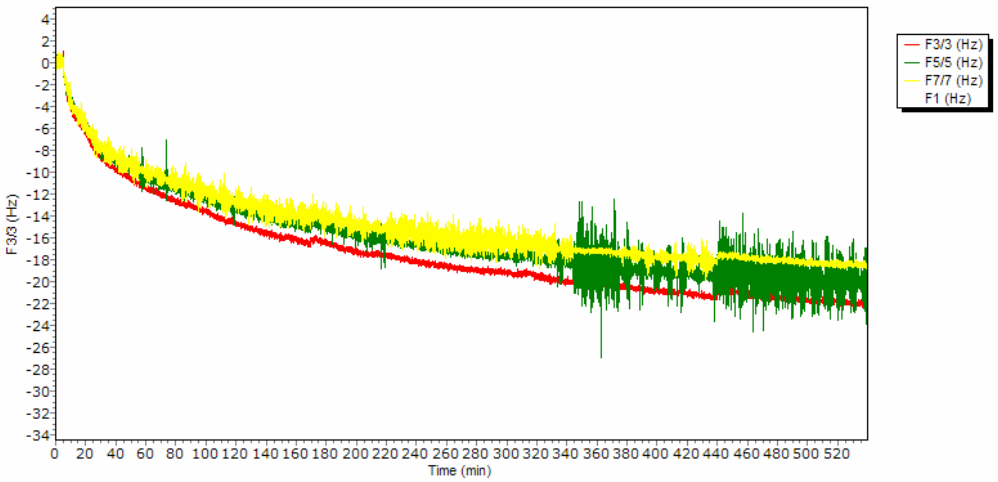

Figure 0.17: Frequency shifts associated with the addition of 5mM (in toluene) of OMS on a previously used crystal

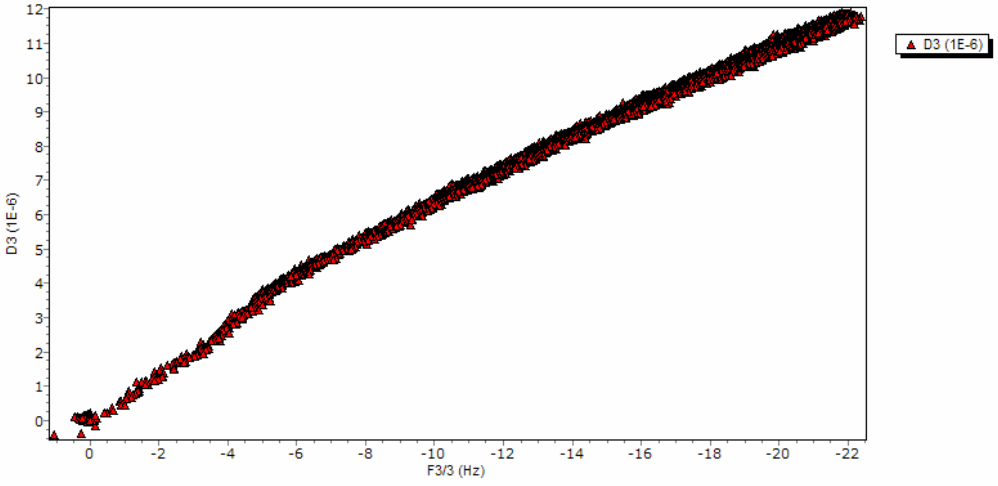

Figure 0.18: D/f plot of the third harmonic frequency and dissipation shifts associated with the addition of 5mM (in toluene) of OMS on a previously used crystal

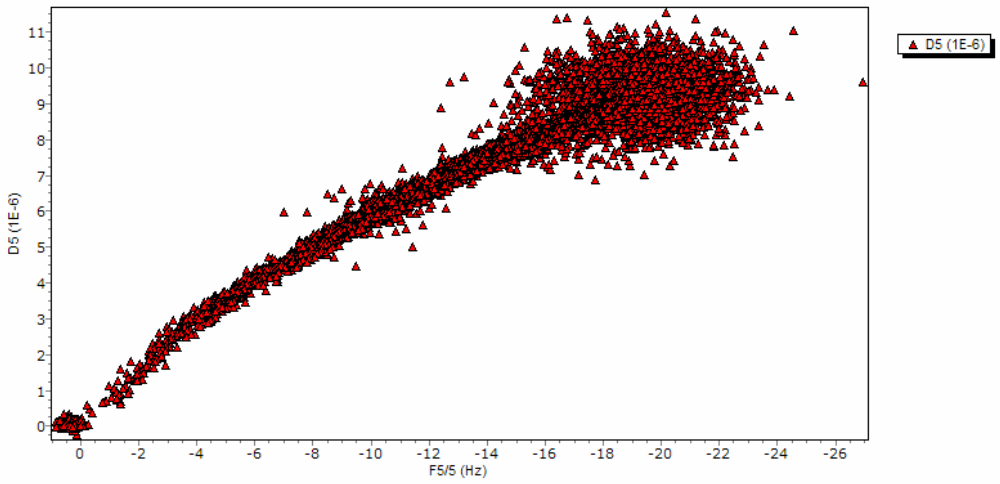

Figure 0.19: D/f plot of the fifth harmonic frequency and dissipation shifts associated with the addition of 5mM (in toluene) of OMS on a previously used crystal

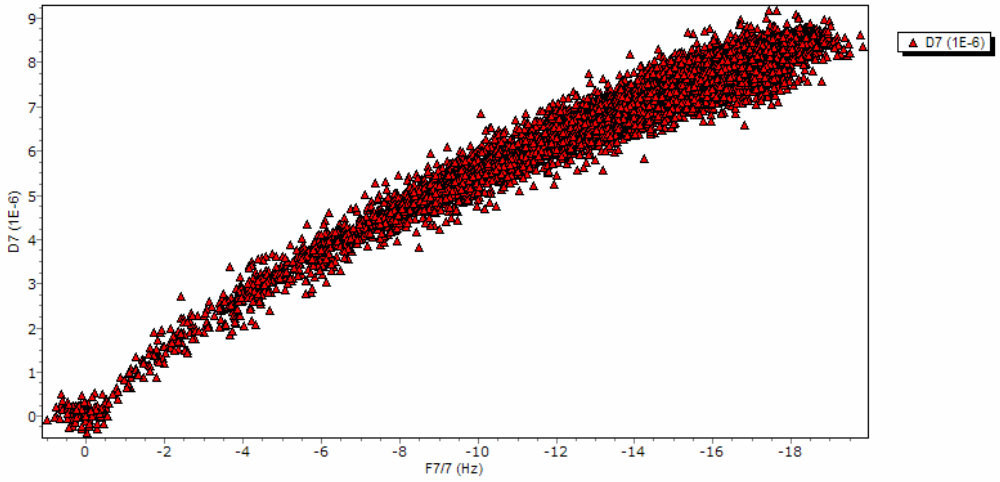

Figure 0.20: D/f plot of the seventh harmonic frequency and dissipation shifts associated with the addition of 5mM (in toluene) of OMS on a previously used crystal

The following are plots of the frequency shifts and D/f plots associated with octadecyldimethylchlorosilane addition to a QCM crystal that was previously used and subsequently treated with acid. The file name is 2km266oms.

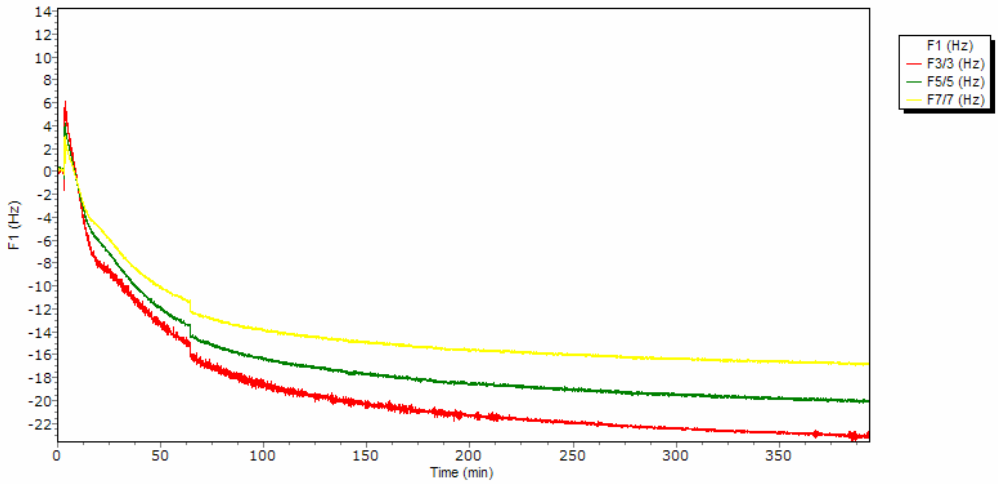

Figure 0.21: Frequency shifts associated with the addition of 5mM (in toluene) of OMS on a previously used crystal that was subsequently acid treated

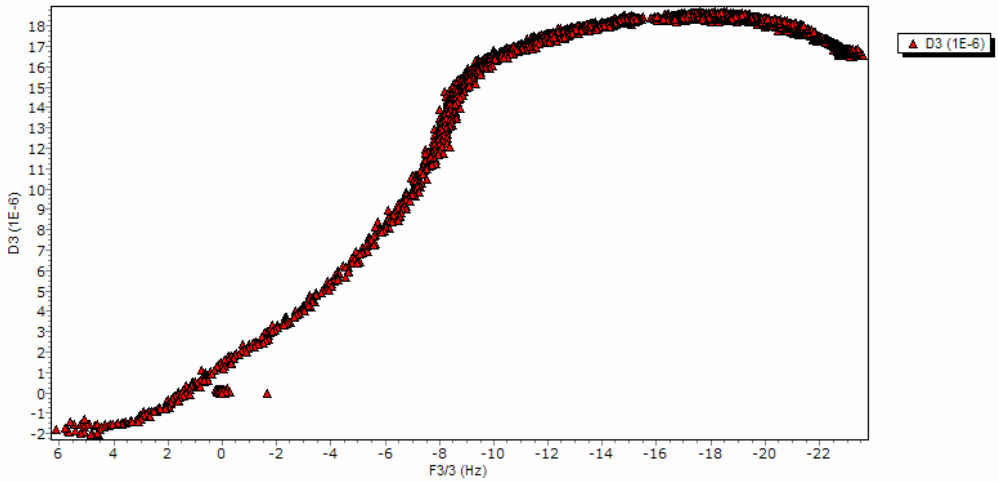

Figure 0.22: D/f plot of the third harmonic frequency and dissipation shifts associated with the addition of 5mM (in toluene) of OMS on a previously used crystal that was subsequently acid treated

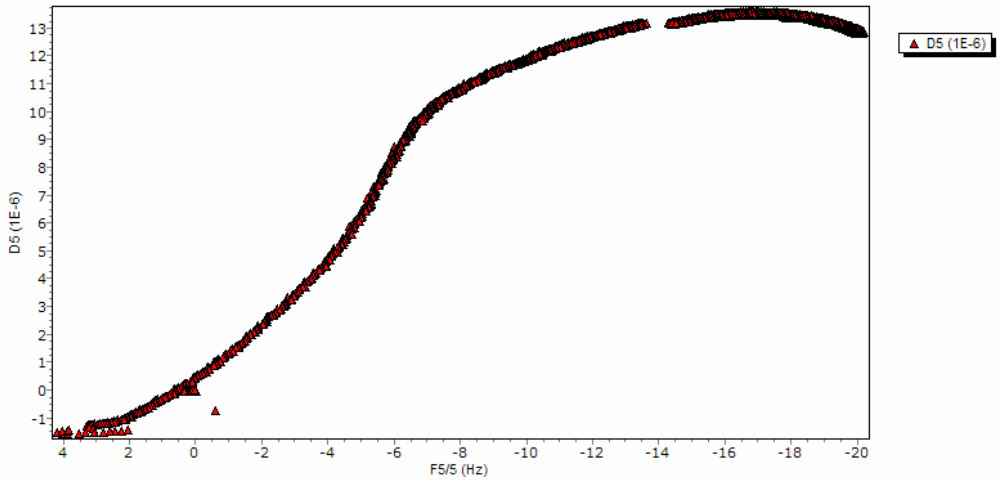

Figure 0.23: D/f plot of the fifth harmonic frequency and dissipation shifts associated with the addition of 5mM (in toluene) of OMS on a previously used crystal that was subsequently acid treated

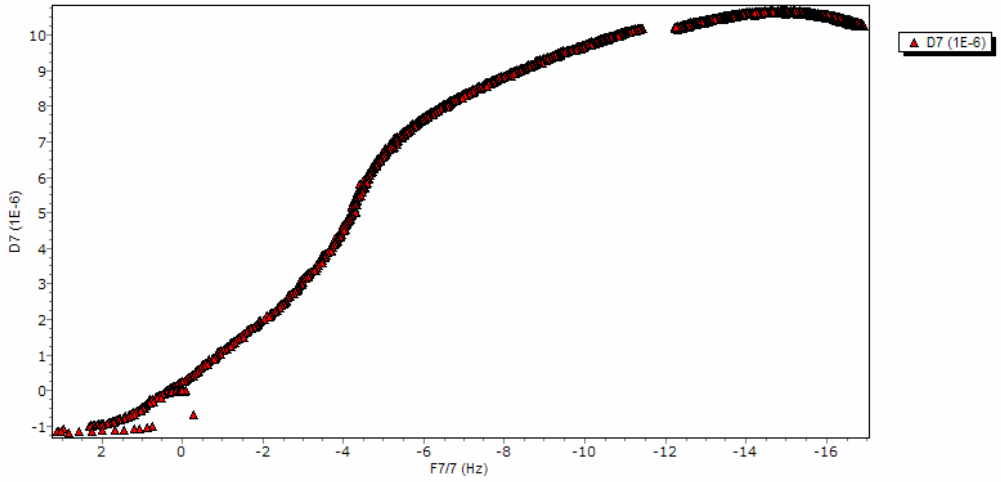

Figure 0.24: D/f plot of the seventh harmonic frequency and dissipation shifts associated with the addition of 5mM (in toluene) of OMS on a previously used crystal that was subsequently acid treated

REFERENCES

[1] J. S. C. Kilby, "Turning Potential into Realities: The Invention of the Integrated Circuit (Nobel Lecture)," *ChemPhysChem*, vol. 2, pp. 482-489, 2001.

[2] S. Lenhert, "Moore's Law," Nanoword.net, 2003.

[3] S. A. Campbell, "An Introduction to Microelectronic Fabrication," in *The Science and Engineering of Microelectronic Fabrication*, *Oxford Series in Electrical Engineering*. New York: Oxford University Press, 1996, pp. 3-9.

[4] "lithography (www.m-w.com)," vol. 2003: Merriam-Webster Incorporated.

[5] D. W. Carr and R. C. Tiberio, "Direct-write electron beam lithography: history and state of the art," *Materials Research Society Symposium Proceedings*, vol. 584, pp. 33-43, 2000.

[6] A. M. Hawryluk, N. M. Ceglio, and D. A. Markle, "EUV Lithography," *Solid State Technology*, vol. 40, pp. 151-152, 154, 156, 159, 1997.

[7] M. C. Peckerar, F. K. Perkins, E. A. Dobisz, and O. J. Glembocki, "Issues in Nanolithography for Quantum Effect Device Manufacture," in *Handbook of Microlithography, Micro machining, and Microfabrication, Volume 1: Microlithography*, vol. 1, *IEEE Materials and Devices Series 12*, P. Rai-Choudhury, Ed., 1 ed. Bellingham, WA: SPIE Optical Engineering Press, 1997, pp. 681-764.

[8] S. Okazaki, "Future of optical lithography," presented at 18th Congress of the International Commission for Optics: Optics for the Next Millennium, San Francisco, CA, 1999.

[9] F. Cerrina, "X-ray Lithography," in *Handbook of Microlithography, Micromaching, and Microfabrication, Volume 1: Microlithography*, vol. 1, *IEEE Materials and Devices Series 12*, P. Rai-Choudhury, Ed., 1 ed. Bellingham, WA: SPIE Optical Engineering Press, 1997, pp. 251-320.

[10] E. A. Dobisz and C. R. K. Marrian, "Scanning tunneling microscope lithography: A solution to electron scattering," *Journal of Vacuum Science and Technology B*, vol. 9, pp. 3024-3027, 1991.

[11] C. G. Willson, "Organic Resist Materials," in *Introduction to Microlithography*, L. F. Thompson, C. G. Willson, and M. J. Bowden, Eds., 2 ed. Washington, DC: American Chemical Society, 1994, pp. 139-268.

[12] R. D. Allen, W. E. Conley, and R. R. Kunz, "Deep-UV Resist Technology," in *Handbook of Microlithography, Micromaching, and Microfabrication, Volume 1: Microlithography*, vol. 1, *IEEE Materials and Devices Series 12*, P. Rai-Choudhury, Ed., 1 ed. Bellingham, WA: SPIE Optical Engineering Press, 1997, pp. 321-376.

[13] C. Brodsky, J. Byers, W. Conley, R. Hung, S. Yamada, K. Patterson, M. Somervell, B. Trinque, H. V. Tran, S. Cho, T. Chiba, S.-H. Lin, A. Jameison, H. Johnson, T. V. Heyden, and C. G. Willson, "157 nm resist materials: Progress report," *Journal of Vacuum Science and Technology B*, vol. 18, pp. 3396-3401, 2000.

[14] W. Conley, B. C. Trinque, D. A. Miller, P. Zimmerman, T. Kudo, R. R. Dammel, A. R. Romano, and C. G. WIllson, "Negative Photoresis for 157-nm lithography; a progress report," *Proceedings of SPIE-The International Society for Optical Engineering*, vol. 4690 (Pt. 1-Advances in Resist Technology and Processing XIX), pp. 94-100, 2002.

[15] W. Conley, D. Miller, C. Chambers, B. C. Trinque, B. Osborn, T. Chiba, P. Zimmerman, R. Dammel, A. Romano, and C. G. Willson, "Dissolution Inhibitors for 157 nm lithography: a progress report," *Journal of Photopolymer Science and Technology*, vol. 15, pp. 613-617, 2002.

[16] R. J.-P. Hung, H. V. Tran, B. C. Trinque, T. Chiba, S. Yamada, D. Sanders, E. F. Connor, R. H. Grubbs, J. M. Klopp, J. M. J. Frechet, B. H. Thomas, G. J. Shafer, D. D. DesMarteau, W. Conley, and C. G. Willson, "Resist Materials for 157 nm microlithography: an update," *Proceedings of SPIE-The International Society for Optical Engineering*, vol. 4345 (Pt. 1, Advances in Resist Technology and Processing XVIII), pp. 385-395, 2001.

[17] L. Singh, P. Ludovice, and C. L. Henderson, "Influence of Molecular Weight and Film Thickness on the Glass Transition Temperature and Coefficient of Thermal Expansion of Supported Ultrathin Polymer Films," *Thin Solid Films*, vol. accepted for publication, 2003.

[18] L. Singh, P. Ludovice, and C. L. Henderson, "Influence of Film Thickness on the Dissolution Rate of Photoresist Polymer Thin Films," to be published.

[19] J. Havas, "High resolution, high temperature lift-off technique," *Electrochemical Society Extended Abstracts*, vol. 2, pp. 742, 1976.

[20] B. J. Lin, "AZ1350J as a deep UV mask material," *Journal of the Electrochemical Society*, vol. 127, pp. 202-205, 1980.

[21] E. Reichmanis and G. Smolinsky, "Deep UV resists for two-level photoresist processes," *Proceedings of SPIE*, vol. 469, pp. 38-44, 1984.

[22] Y. Saotome, H. Gokan, K. Saigo, M. Suzuki, and Y. Ohnishi, "A silicon containing positive photoresist (SIPR) for a bilayer resist system," *Journal of the Electrochemical Society*, vol. 132, pp. 909-913, 1985.

[23] Shipley, "193 nm Bilayer Photoresists," 2003.

[24] R. Sezi, M. Sebald, R. Leushner, H. Ahne, S. Birkle, and H. Borndorfer, "Benefits and prospects of aqueous silylation for novel dry developable high resolution masks," *Proceedings of SPIE*, vol. 1262, pp. 84-93, 1990.

[25] B. J. Lin, "Multi-Layer Resist Systems," in *Introduction to Microlithography*, *ACS Symposium Series*, L. F. Thompson, C. G. Willson, and M. J. Bowden, Eds., 1st ed. Washington, DC: American Chemical Society, 1983, pp. 287-350.

[26] C. Pierrat, S. Tedesco, F. Vinet, M. Lerme, and B. Dal'Zotto, "Positive resist imaging by dry etching: New dry developed positive working system for electron beam and deep ultraviolet lithography," *Journal of Vacuum Science and Technology B*, vol. 7, pp. 1782-1786, 1989.

[27] E. K. Pavelchek, J. F. Bohland, J. W. Thackeray, G. W. Orsula, S. K. Jones, B. W. Dudley, S. M. Bobbio, and P. W. Freeman, "Silylated acid hardened resist process: A deep ultraviolet surface imaging technique," *Journal of Vacuum Science and Technology B*, vol. 8, pp. 1497-1501, 1990.

[28] F. Coopmans, "DESIRE: A novel dry development resist systems," *Proceedings of SPIE*, vol. 631, pp. 34-39, 1986.

[29] F. Coopmans and B. Roland, "DESIRE: A new route to submicron optical lithography," *Solid State Technology*, vol. 30, pp. 93-99, 1987.

[30] M. H. Somervell, D. S. Fryer, B. Osborn, K. Patterson, J. Byers, and C. G. Willson, "Study of the fundamental contributions to line edge roughness in a 193 nm, top surface imaging system," *J. Vac. Sci. Technol. B*, vol. 18, pp. 2551-2559, 2000.

[31] A. Jameison, M. Somervell, H. V. Tran, R. J.-P. Hung, S. A. MacDonald, and C. G. Willson, "Top Surface Imaging at 157nm," *Proceedings of SPIE-The International Society for Optical Engineering*, vol. 4345 (Pt. 1 Advances in Resist Technology and Processing XVIII), pp. 406-416, 2001.

[32] J. B. Ruhe, G; Novotny, V. J.; Street, G. B.; Kuan, S., "Terminal Attachment of Perfluorinated Polymers to Solid Surfaces," *Journal of Applied Polymer Science*, vol. 53, pp. 825-836, 1994.

[33] O. Prucker, C. A. Naumann, J. Ruhe, W. Knoll, and C. W. Frank, "Photochemical Attachment of Polymer Films to Solid Surfaces via Monolayers of Benzophenone Derivatives," *Journal of the American Chemical Society*, vol. 121, pp. 8766-8770, 1999.

[34] C. J. Brodsky and C. G. Willson, "Interfacial cationic graft polymerization lithography," *Polymeric Materials: Science and Engineering*, vol. 81, pp. 83-84, 1999.

[35] C. Brodsky, B. Trinque, H. Johnson, and G. Willson, "Advances in graft polymerization lithography," *Proceedings of SPIE-The International Society for Optical Engineering*, vol. 4343, pp. 415-426, 2001.

[36] H. F. Johnson, S. N. Ozair, A. T. Jameison, B. C. Trinque, C. C. Brodsky, and C. G. Willson, "Cationic Graft Polymerization Lithography," *Proceedings of SPIE-The International Society for Optical Engineering*, vol. 5037, pp. 943-951, 2003.

[37] O. Prucker and J. Ruhe, "Polymer Layers Through Self-Assembled Monolayers of Initiators," *Langmuir*, vol. 14, pp. 6893-6898, 1998.

[38] O. Prucker, M. Schimmel, G. Tovar, W. Knoll, and J. Ruhe, "Microstructuring of Molecularly Thin Polymer Layers by Photolithography," *Advanced Materials*, vol. 10, pp. 1073-1077, 1998.

[39] O. Prucker and J. Ruhe, "Synthesis of Poly(styrene) Monolayers Attached to High Surface Area Silica Gels through Self-Assembled Monolayers of Azo Initiator," *Macromolecules*, vol. 31, pp. 592-601, 1998.

[40] O. Prucker and J. Ruhe, "Mechanism of Radical Chain Polymerizations Initiated by Azo Compounds Covalently Bound to the Surface of Spherical Particles," *Macromolecules*, vol. 31, pp. 602-613, 1998.

[41] O. Prucker, J. Habicht, I.-J. Park, and J. Ruhe, "Photolithographic Structuring of Surface-Attached Polymer Monolayers," *Materials Science and Engineering C*, vol. 8-9, pp. 291-297, 1999.

[42] J. Ruhe, "Polymers Grafted from Solid Surfaces," *Macromol. Symposium*, vol. 126, pp. 215-222, 1997.

[43] N. a. I. Tsubokawa, Hisanori, "Graft Polymerization of Methyl Methacrylate from Silica Initiated by Peroxide Groups Introduced onto the Surface," *Journal of Polymer Science: Part A: Polymer Chemistry*, vol. 30, pp. 2241-2246, 1992.

[44] N. K. Tsubokawa, Masato; Ogasawara, Tomoaki, "Graft Polymerization of vinyl monomers initiated by azo groups introduced onto organic pigment surface," *Progress in Organic Coatings*, vol. 36, pp. 39-44, 1999.

[45] U. Velten, R. Sheldon, W. R. Caseri, U. W. Suter, and Y. Li, "Polymers grafted on mica by radical chain growth from the surface," *Colloids and Surfaces A: Physicochemical and Engineering Aspects*, vol. 154, pp. 87-96, 1999.

[46] X. W. Huang, Mary J., "Surface-Initiated Radical Polymerization on Porous Silica," *Anal. Chem.*, vol. 69, pp. 4577-4580, 1997.

[47] X. D. Huang, Leon J.; Worth, Mary J., "Surface-Confined Living Radical Polymerization for Coatings in Capillary Electrophoresis," *Anal. Chem.*, vol. 70, pp. 4023-4029, 1998.

[48] X. a. W. Huang, M. J., "Surface Initiation of Living Radical Polymerization for Growth of Tethered Chains of Low Polydispersity," *Macromolecules*, vol. 32, pp. 1694-1696, 1999.

[49] K. M. Matyjaszewski, Peter J.; Shukla, Nisha; Immaraporn, Boonchuan; Gelman, ANdrew; Luokala, Barry B.; Siclovan, Tiberiu M.; Kickelbick, Guido; Vallant, Thomas; Hoffman, Helmuth; Pakula, Tadeusz, "Polymers at Interfaces: Using Atom Transfer Radical Polymerization in the Controlled Growth of Homopolymers and Block Copolymers from Silicon Surfaces in the Absence of Untethered Sacrificial Initiator," *Macromolecules*, vol. 32, pp. 8716-8724, 1999.

[50] B. de Boer, H. K. Simon, M. P. L. Werts, E. W. van der Vegte, and G. Hadziioannou, ""Living" Free Radical Photopolymerization Initiated from Surface-Grafted Iniferter Monolayers," *Macromolecules*, vol. 33, pp. 349-356, 2000.

[51] M. Husseman, E. E. Malmstro, M. McNamara, M. Mate, D. Mecerreyes, D. G. Benoit, J. L. Hedrick, P. Mansky, E. Huang, T. P. Russell, and C. J. Hawker, "Controlled Synthesis of Polymer Brushes by “Living” Free Radical Polymerization Techniques," *Macromolecules*, vol. 32, pp. 1424-1431, 1999.

[52] E. C. Peters, F. Svec, J. M. J. Frechet, C. Viklund, and K. Irgum, "Control of Porous Properties and Surface Chemistry in “Molded” Porous Polymer Monoliths Prepared by Polymerization in the Presence of TEMPO," *Macromolecules*, vol. 32, pp. 6377-6379, 1999.

[53] M. Stevens, "Vinyl Polymers," in *Polymer Chemistry: An Introduction*, 2nd ed. New York: Oxford University Press, 1990, pp. 189-233.

[54] X. Chen, D. Hess, L. Tolbert, C. Henderson, and J. Ruhe, "Polymer pattern formation on SiO2 surfaces using surface monolayer initiated polymerization," *Journal of Vacuum Science and Technology B*, vol. 19, pp. 2013-2019, 2001.

[55] A. Khandelwal, H. Niimi, G. Locovsky, and H. H. Lamb, "Low-temperature Ar/N2 remote plasma nitridation of SiO2 thin films," *Journal of Vacuum Science and Technology B*, vol. 20, pp. 1989-1996, 2002.

[56] T. Couteau, M. McBride, D. Riley, and P. Peavy, "Dilute RCA cleaning chemistries," *Semiconductor International*, vol. 21, pp. 95-96, 98, 100, 1998.

[57] K. Prabhakaran, Y. Kobayashi, and T. Ogino, "Chemically prepared oxides on silicon(001): an XPS study," *Surface Science*, vol. 290, pp. 239-244, 1993.

[58] A. Ulman, *Characterization of Organic Thin Films*, vol. 12, 1st ed. Boston: Butterworth-Heinemann, 1995.

[59] D. A. Skoog and J. J. Leary, "Analysis of Surfaces with Electron Beams," in *Principles of Instrumental Analysis*, 4th ed. Fort Worth: Saunders College Publishing, 1992, pp. 383-400.

[60] C. Lu and A. W. Czanderna, *Application of Quartz Crystal Microbalances*, vol. 7, 1st ed. Amsterdam: Elsevier, 1984.

[61] Q-sense Corporation, "QCM-D Technology," Q-sense Corporation AB, 2002.

[62] Q-sense Corporation, "Q-sense Users Manual," Q-sense Corporation AB, 2000.

[63] H.-Q. Li, "Atomic Force Microscopy," 1997.

[64] D. Corporation, "Lateral Force Mode," in *Dimension 3100 User Manual*, 2000.

[65] D. W. Sindorf and G. E. Maciel, "Cross-Polarization/Magic Angle Spinning Silicon-29 Nuclear Magnetic Resonance Study of Silica Gel Using Trimethylsilane Bonding as a Probe of Surface Geometry and Reactivity," *Journal of Physical Chemistry*, vol. 86, pp. 5208-5219, 1982.

[66] D. W. Sindorf and G. E. Maciel, "Solid-state NMR studies of the Reaction of Silica Surfaces with Polyfunctional Chloromethylsilanes and Ethoxymethylsilanes," *Journal of the American Chemical Society*, vol. 105, pp. 3767-3776, 1983.

[67] D. W. Sindorf and G. E. Maciel, "Silicon-29 Nuclear Magnetic Resonance Study of Hydroxyl Sites on Dehydrated Silica Gel Surfaces, Using Silylation as a Probe," *Journal of Physical Chemistry*, vol. 87, pp. 5516-5521, 1983.

[68] S. L. Scott and E. W. Deguns, "Multifunctional Active Sites on Silica Surfaces by Grafting of Metal Complexes," in *Nanostructured Catalysts*, vol. 1, *Nanostructure Science and Technology*, S. L. Scott, C. M. Crudden, and C. W. Jones, Eds. New York: Kluwer Academic/Plenum Publishers, 2003, pp. 1-14.

[69] G. L. Rice and S. L. Scott, "Characterization of Silica-Supported Vanadium(V) Complexes Derived from Molecular Precursors and Their Ligand Exchange Reactions," *Langmuir*, vol. 13, pp. 1545-1551, 1997.

[70] J. Sagiv, "Organized Monolayers by Absorption.1. Formation and Structure of Oleophobic Mixed Monolayers on Solid Surfaces," *Journal of the American Chemical Society*, vol. 102, pp. 92-98, 1980.

[71] L. Boksanyi, O. Liardon, and E. s. Kovats, "Chemically modified silicon dioxide surfaces," *Advances in Colloid and Interface Science*, vol. 6, pp. 95-137, 1976.

[72] C. P. Tripp and M. L. Hair, "An Infrared Study of the Reaction of Octadecyltrichlorosilane with Silica," *Langmuir*, vol. 8, pp. 1120-1126, 1992.

[73] R. Banga and J. Yarwood, "FTIR and AFM studies of the kinetics and self-assembly of alkyltrichlorosilanes and (perfluoroalkyl)trichlorosilanes onto glass and silicon," *Langmuir*, vol. 11, pp. 4393-4399, 1995.

[74] P. Silberzan, L. Leger, D. Ausserre, and J. J. Benattar, "Silanation of Silica Surfaces. A New Method of Constructing Pure or Mixed Monolayers," *Langmuir*, vol. 7, pp. 1647-1651, 1991.

[75] S. Krishnan, "Kinetics of Octadecyltrichlorosilane self-assembly on silicon oxide surfaces: An experimental and numerical study," in *Engineering*. New York: City University of New York, 1999, pp. 127.

[76] T. Balgar, R. Bautista, N. Hartmann, and E. Hasselbrink, "An AFM study of the growth kinetics of the self-assembled octadecylsiloxane monolayer on oxidized silicon," *Surface Science*, vol. 532-535, pp. 963-969, 2003.

[77] M. Goldmann, J. V. Davidovits, and P. Silberzan, "Kinetics of self-assembled silane monolayers at various temperatures: evidence of 2D foam," *Thin Solid Films*, vol. 327-329, pp. 166-171, 1998.

[78] R. Helmy and A. Y. Fadeev, "Self-assembled monolayers supported on TiO_2: Comparison of $C_{18}H_{37}SiX_3$ (X= H, Cl, OCH_3), $C_{18}H_{37}Si(CH_3)_2Cl$, and $C_{18}H_{37}PO(OH)_2$," *Langmuir*, vol. 18, pp. 8925-8928, 2002.

[79] D. L. Angst, "Moisture absorption characteristics of organosiloxane self-assembled monolayers," *Langmuir*, vol. 7, pp. 2236-2242, 1991.

[80] H. Green, "Absorption of SAMs," 2002.

[81] P. Dahlqvist, "Electronic mail: "Re: data analysis"," K. McCoy, Ed. Atlanta, GA, 2003.

[82] P. Dahlqvist and P. Bjoorn, "Analysis of D/f plots," K. McCoy, Ed. Atlanta, 2003.

[83] H. J. Kim, S. Kwak, Y. S. Kim, B. I. Seo, E. R. Kim, and H. Lee, "Adsorption kinetics of alkanethiols studied by quartz crystal microbalance," *Thin Solid Films*, vol. 327-329, pp. 191-194, 1998.

[84] D. R. Jung, D. E. King, and A. W. Czanderna, "Metal overlayers on organic functional groups of self-organized molecular assemblies. II. X-ray photoelectron spectroscopy of interactions of Cu/CN on 12-mercaptododecanenitrile," *Journal of Vacuum Science and Technology A*, vol. 11, pp. 2382-2386, 1993.

[85] F. Tao, W. S. Sim, G. Q. Xu, and M. H. Qiao, "Selective Binding of the Cyano Group in Acrylonitrile Adsorption on Si(100)-2 x 1," *Journal of the American Chemical Society*, vol. 123, pp. 9397-9403, 2001.

[86] H. Sugimura, K. Hayashi, Y. Amano, O. Takai, and A. Hozumi, "Friction force microscopy study on photodegradation of organosilane self-assembled monolayers irradiated with vacuum ultraviolet radiation," *Journal of Vacuum Science and Technology A*, vol. 19, pp. 1261-1265, 2001.

[87] L. Hong, H. Sugimura, T. Furukawa, and O. Takai, "Photoreactivity of alkylsilane self-assembled monolayers on silicon surfaces and its application to preparing micropatterned ternary monolayers," *Langmuir*, vol. 19, pp. 1966-1969, 2003.

[88] N. Saito, K. Hayashi, H. Sugimura, and O. Takai, "The decomposition mechanism of p-chloromethylphenyltrimethoxysiloxane self-assembled monolayers on vacuum ultraviolet irradiation," *Journal of Materials Chemistry*, vol. 12, pp. 2684-2687, 2002.

[89] H. Sugimura, T. Hanji, O. Takai, K. Fukuda, and H. Misawa, "Photo and scanning probe lithography using alkylsilane self-assembled monolayers," *Materials Research Symposium Proceedings*, vol. 584, pp. 163-168, 2000.

[90] D. A. Tryk, X. Yang, K. Hashimoto, and A. Fujishima, "Surface-enhanced raman imaging (SERI) of patterned self-assembled monolayers of various derivitized thiophenols on silver," *Bulletin of the Chemical Society of Japan*, vol. 71, pp. 31-39, 1998.

[91] C. S. Dulcey, J. Jacque H. Georger, V. Krauthamer, D. A. Stenger, T. L. Fare, and J. M. Calvert, "Deep UV Photochemistry of Chemisorbed Monolayers: Patterned Coplanar Molecular Assemblies," *Science*, vol. 252, pp. 551-554, 1991.

[92] W. J. Dressick, C. S. Dulcey, M.-S. Chen, and J. M. Calvert, "Photochemical Studies of (aminoethylaminomethyl)phenethyltrimethoxy silane self-assembled monolayer films," *Thin Solid Films*, vol. 284-285, pp. 568-572, 1996.

[93] O. Prucker and J. Ruhe, "Synthesis of Poly(styrene) Monolayers Attched to High Surface Area Silica Gels through Self-Assembled Monolayers of Azo Initiators," *Macromolecules*, vol. 31, pp. 592-601, 1998.

[94] X. Chen, L. Tolbert, C. Henderson, D. Hess, and J. Ruhe, "Polymer pattern formation on SiO2 surfaces using surface monolayer initiated polymerization," *Journal of Vacuum Science and Technology B*, vol. 19, pp. 2013-2019, 2001.

[95] X. Chen, "Patterning Etch Masks via "Grafting From" Polymerization," in *School of Chemistry and Biochemistry*. Atlanta, GA: Georgia Institute of Technology, 2000, pp. 149.

[96] W. J. Briels, "Radius of Gyration," 2003.

[97] M. A. McCord and M. J. Rooks, "Electron Beam Lithography," in *Handbook of Microlithography, Micro machining, and Microfabrication, Volume 1: Microlithography*, vol. 1, *IEEE Materials and Devices Series 12*, P. Rai-Choudhury, Ed., 1 ed. Bellingham, WA: SPIE Optical Engineering Press, 1997, pp. 139-250.

VITA

Kendra McCoy was born in Washington, DC and grew up in Fort Washington, MD. She graduated from Oxon Hill High school in 1994 and obtained a B.S. in Chemical Engineering in 1998 from Carnegie Mellon University. Kendra is receiving her PhD. in Chemical Engineering from Georgia Tech in 2004, where she had worked with Cliff Henderson in developing novel resists and resist processes for Next Generation Lithography. She will soon begin a postdoctoral assignment at the Naval Research Laboratory in Washington, DC. Eventually, she hopes to be a professor. Kendra's research interests include self-assembled monolayers, polymer-surface interactions, nanoscale patterning, and microfabrication.